RESEARCH
UAC

RESEARCH DEPARTMENT
UNITED AIRCRAFT CORPORATION
EAST HARTFORD, CONNECTICUT

894 300

Copy # 14

UNITED AIRCRAFT CORPORATION

RESEARCH DEPARTMENT

R-1285-11

Turbulent Boundary Layer Characteristics
in Supersonic Streams Having
Adverse Pressure Gradients

UNCLASSIFIED

(UPPER CASE)

by George H. McLafferty and
Robert E. Barber

Department of the Navy
Bureau of Aeronautics
Contract NOa(s) 55-133-c
Lot III of Amendment 7

Approved by _M. Schweiger_

M. Schweiger
Head, Propulsion Section

No. of Pages - 124

Date - September 1959,

R-1285-11

FOREWORD

The efficient application of turbojet engines to the propulsion of aircraft
at high supersonic Mach numbers requires extensive knowledge of the characteristics
of inlets and induction systems. In this connection, the Research Department of
United Aircraft Corporation has been investigating various turbojet inlet design
parameters under Contract NOa(s) 55-133-c with the Power Plant Division of the
Bureau of Aeronautics, Department of the Navy, to provide basic information for the
design of high Mach number inlets. The results of the investigations performed
under Lots I and II of this contract are summarized in Refs. 1 through 6. Additional
investigations performed under Lot III of the same contract pertain to the following
subjects:

1. Performance of a Mach 4.0 variable-geometry axisymmetric inlet having
   external-plus-internal compression.

2. Efficiency of flush oblique nozzles exhausting into supersonic streams
   having Mach numbers up to 4.0.

3. Turbulent boundary layer characteristics in supersonic streams having
   adverse pressure gradients.

This report summarizes the results of the studies of the effect of adverse
pressure gradients on boundary layer characteristics. The investigations which
pertain to the remaining subjects are summarized in Refs. 7 and 8.

Report R-1285-11

Turbulent Boundary Layer Characteristics in Supersonic Streams

Having Adverse Pressure Gradients

TABLE OF CONTENTS

iii

TABLE OF CONTENTS
(Contd.)

Report R-1285-11

Turbulent Boundary Layer Characteristics in Supersonic Streams

Having Adverse Pressure Gradients

SUMMARY

Investigations were conducted to determine the thickness and profile shape
characteristics of turbulent boundary layers in supersonic streams having adverse
pressure gradients similar to those which are encountered in supersonic inlets. The
program included tests conducted at Mach numbers from 2.0 to 3.5 using two-dimensional
and axisymmetric curved-surface models to produce the adverse pressure gradients.
The magnitude of the gradients relative to the boundary layer thickness at the be-
ginning of the gradient was varied by employing models having different radii of
curvature and by changing the boundary layer thickness at the beginning of the
gradient. The over-all pressure rise in most cases was greater than the value which
would cause a turbulent boundary layer to separate if the pressure rise were created
by an oblique shock wave. Some tests were conducted to determine the effect of
boundary layer removal from the curved surfaces on boundary layer growth and on the
pressure gradients which could be realized without separation. An analytical in-
vestigation was also conducted so that the results of the experimental investigation
could be applied to the prediction of cases outside the range of the experiments.

It is shown that the boundary layer momentum thickness can be predicted from the
von Kármán boundary layer momentum equation, but that the measured values of boundary
layer profile shape are in poor agreement with the values computed from procedures
derived by extending conventional methods for predicting profile shape in subsonic
flow. It was found that boundary layers in adverse pressure gradients in supersonic
streams are much less susceptible to separation than is indicated by extension of
conventional procedures developed for subsonic flow; therefore, supersonic inlets can
be made much shorter and lighter than inlets which are designed on the basis of these
conventional procedures. A new procedure for calculating boundary layer profile
shapes, developed in this report, is shown to provide a good correlation between ex-
perimental and calculated values of boundary layer profile shapes in adverse pressure
gradients created by curved surfaces. This new procedure is based on the experimental
observation that the station at which high-energy free-stream flow actually mixes into
a turbulent boundary layer in an adverse pressure gradient is well downstream of the
station at which flow would have to mix in order to maintain a flat-plate profile.

This project was undertaken for the Department of the Navy, Bureau of Aeronautics
under Lot III of Amendment No. 7 to Contract NOa(s) 55-133-c.

1

CONCLUSIONS

1. Boundary layers in adverse pressure gradients in supersonic streams are much less susceptible to separation than is indicated by extension of previously developed procedures for subsonic flow; therefore, supersonic inlets can be made much shorter and lighter than inlets which are designed on the basis of extrapolated subsonic theory.

2. The shape of a turbulent boundary layer in adverse pressure gradients generated by curved surfaces in supersonic flow can be predicted with much greater accuracy by the lag-length procedure developed in this report than by existing procedures based on extrapolation of data from subsonic flow. The lag-length procedure makes use of experimental data which show that high-energy free-stream flow begins to mix with the low-energy boundary layer flow at a station located at a distance (called the lag length) from 0 to 60 boundary layer momentum thicknesses downstream of the station where flow would have to mix to maintain a flat-plate profile.

3. Dimensionless lag lengths obtained by dividing the measured lag lengths by the boundary layer momentum thickness are a function of Reynolds number but are independent of Mach number and pressure gradient for a wide range of Mach numbers, pressure gradients, and Reynolds numbers for curved surfaces in supersonic flow.

4. The momentum thickness of a turbulent boundary layer in adverse pressure gradients generated by curved surfaces in supersonic flow can be calculated from the von Kármán boundary layer momentum equation.

5. The use of boundary layer bleed results in a large increase in the pressure gradient which can be tolerated by a turbulent boundary layer in supersonic flow without separating.

6. The decrease in the momentum thickness of a turbulent boundary layer due to bleed is approximately half that calculated with the assumption that the bleed flow has zero axial velocity.

INTRODUCTION

The characteristics of boundary layers in adverse pressure gradients at super-sonic speeds have a particularly large influence on the performance of supersonic in-lets. The thickness of the boundary layer approaching the normal shock at the throat has a direct influence on the pressure recovery through the normal shock (see Ref. 1). In addition, boundary layer separation can prevent attainment of a low Mach number upstream of the normal shock and, hence, prevent attainment of high inlet pressure recoveries. If the inlet is made longer than the minimum length necessary to prevent separation, unnecessary structural weight will result.

The object of the research described herein was to establish criteria for pre-dicting the characteristics of boundary layers in supersonic streams having adverse pressure gradients to provide a more rational basis for the design of supersonic inlets.

RÉSUMÉ OF PREVIOUS WORK

Most of the data available in the literature (see, for example, Refs. 9 through 19) were obtained from tests in which the pressure rise was created by oblique or normal shock waves (severe adverse pressure gradients) and in which the mixing of flow from the free stream into the boundary layer had little effect on the shape of the boundary layer profile within the severe adverse pressure gradient. The portion of the data from these reports dealing with the maximum pressure rise that can be obtained without separation has been explained in Refs. 20 through 24 on the basis that there is little or no mixing of free-stream flow with the flow in the boundary layer.

The only data which is known to be available on boundary layer characteristics in supersonic streams for adverse pressure gradients more moderate than those created by shock waves is contained in Ref. 25. This NASA memorandum provides separation criteria only and does not include information on the actual shape of the boundary layer within the adverse pressure gradients. Attempts to explain the pressure-rise data presented therein on the basis of the theories of Refs. 20 through 24 were not successful because the theories of these five reports neglect the effect of mixing the free-stream flow with the flow within the boundary layer. The only known theory for the calculation of boundary layer shape in a moderate adverse pressure gradient at supersonic speeds, given in Ref. 26, is an extension of the theory developed in Ref. 27 for subsonic flow. The latter reference presents one of many similar theories (see Refs. 28, 29, and 30) which have been developed for the prediction of boundary layer shape for subsonic flow. It is shown in the present report that the terms in the equations of Ref. 26 which account for the mixing of free-stream flow with flow in the boundary layer severely underestimate the improvement in boundary layer shape

3

due to mixing and, hence, severely underestimate the pressure rise which can be obtained without separation in moderate adverse pressure gradients.

The effect of pressure gradient on boundary layer thickness must be evaluated in supersonic inlets because the total pressure recovery through the normal shock at the throat of the inlet is a function of the thickness of the boundary layer approaching the throat (see Ref. 1). Although some data are available on boundary layer growth in severe adverse pressure gradients (see, for example, Refs. 9, 14, and 19), no data are known to be available on boundary layer growth in moderate adverse pressure gradients. In calculating the thickness of a boundary layer in an adverse pressure gradient, it is usually convenient to employ the boundary layer momentum thickness. Most procedures for calculating boundary layer momentum thickness in adverse pressure gradients are based on the use of the von Kármán boundary layer momentum equation. Two adaptations of the von Kármán boundary layer momentum equation for calculating momentum thickness growth in an adverse pressure gradient at supersonic speeds are given in Refs. 26 and 31.

EXPERIMENTAL INVESTIGATION

Description of Test Equipment

Tunnel

Tests to determine boundary layer characteristics in adverse pressure gradients were conducted in the UAC Research Department 4.5 x 4.5-in. continuous-flow supersonic wind tunnel. Dry air was supplied to the tunnel at a total pressure of approximately one atmosphere and a total temperature of approximately 150 F. The Reynolds number per in. in the tunnel test section varied from 0.27×10^6 at a Mach number of 2.0 to 0.12×10^6 at a Mach number of 3.5. Two test-section configurations were employed, one for tests of two-dimensional models and one for tests of axisymmetric models (a description of the models is given in the following subsection).

A sketch and a photograph of the test-section configuration used in tests of the two-dimensional curved-surface model are presented in Figs. 1 and 2, respectively. A flat surface on the centerline of the tunnel (centerline block) produced the boundary layer approaching the models. The use of this centerline block reduced the height of the test section by one half to the dimensions given in Fig. 1. The use of surface roughness near the tunnel throat, and the injection of air into the boundary layer through the injection holes (see Fig. 1) were employed to trip the boundary layer to insure turbulent flow. The flow-injection system was also utilized as a method of increasing the boundary layer thickness at the upstream end of the curved surface. The flow rate into the plenum and, hence, the thickness of the boundary layer approaching the two-dimensional models was regulated by a valve

4

R-1285-11

vented to atmosphere.

Provision was made for boundary layer bleed from the surface of selected two-dimensional curved-surface models into the bleed plenum shown in Fig. 1. The flow passing through the bleed plenum was ducted through a flow-measurement bellmouth and a control valve to a region of low static pressure in the tunnel downstream of the models.

The test-section configuration employed in tests of the axisymmetric curved-surface models was obtained by replacing the centerline block with a nozzle block which matched the top nozzle block shown in Figs. 1 and 2. The axisymmetric models were mounted in an adjustable support which was attached to the tunnel side wall.

The probe employed to measure the boundary layers (see Figs. 1 and 2) was driven by a mechanism which allowed the probe to traverse at any angle in the vertical plane so that the traverse could be made normal to the model surface. The position of the probe and the magnitude of the probe pitot pressure were measured by electrical transducers and the output from these transducers was recorded on IBM punch cards at selected values of probe position.

Models

Three types of two-dimensional curved-surface models which did not employ boundary layer bleed were utilized: one type was a reference flat plate, the second type had a constant radius of curvature over the entire curved surface (see Figs. 3 and 4), and the third type had two different radii of curvature (see Figs. 5 and 6). The two-radii curved-surface models were formed by the addition of extensions to the single-radius curved-surface model having a radius of curvature of 6 in. and total turning angle of 20 deg. Extensions were available which had radii of 1.5 and 3 in. and which increased the total turning angle to 30 or 35 deg.

Provisions were made for boundary layer bleed through perforations on selected single-radius two-dimensional curved-surface models. These models are shown in Figs. 3 and 4. The perforations, which were 1/16 in. in diameter and located on 1/4-in. centers across the model, were distributed over the entire curved surface of the model. The porosity of the model could be varied by filling the perforations with plastic.

The sides of all models having total turning angles greater than 20 deg were cut back from the walls of the tunnel in order to minimize the effect of tunnel side-wall boundary layer on the flow over the models. The models with modifications to provide this change in geometry are shown in Figs. 3, 4, 5, and 6. A bypass angle, λ, of 5 deg was employed for all models having total turning angles greater than 20 deg. However, in one test with a model having a total turning angle of 20 deg, a check on model performance was made with bypass angles of 0 and 20 deg.

5

A sketch and a photograph of the axisymmetric models are given in Figs. 7 and 8. Single-radius models having radii of curvature of 1.5 and 3 in. and total turning angles of 20 and 30 deg were employed. The grooves and grit shown in Figs. 7 and 8 were employed to promote boundary layer transition and control the boundary layer thickness at the beginning of the curved surface for most of the tests. For one test, however, a perforated section was employed upstream of the curved surface (see photograph, Fig. 8) to increase the boundary layer thickness by bleeding air from inside the model into the boundary layer.

The model configurations and test conditions for which data are reported are listed in Table I.

Data Reduction Procedure

Conventional data reduction procedures employed in the calculation of boundary layer parameters on flat plates cannot be used for calculating parameters on curved surfaces because large static pressure gradients normal to the curved surfaces are required to provide the centripetal force necessary to turn the flow. Examples of the measured and calculated pressure distributions in a boundary layer having a large static pressure gradient normal to the wall are given in Fig. 9. Although the wall static pressure was measured, the static pressure distribution through the boundary layer could not be determined accurately by use of a static pressure probe because of local flow angularity. Therefore, it was necessary to calculate the local static pressure distribution using measured values of pitot pressure, wall static pressure, and free-stream total pressure. The first approximation to the variation of local static pressure (P_{S_f}) with distance from the wall was obtained from the measured local pitot pressures and a total pressure equal to free-stream total pressure. An example of this variation of P_{S_f} (divided by P_{TO}) is shown in Fig. 9. The values shown are equal to the true local static pressure outside the boundary layer where the local total pressure is equal to free-stream total pressure, but are incorrect within the boundary layer where the local total pressures are lower than free-stream total pressure. In the next step of the calculation procedure, it was assumed that the values of P_{S_f} were correct at a value of y equal to y_{MATCH} where y_{MATCH} was determined from an arbitrary constant, K, times the value of y at the maximum value of pitot pressure. The variation of static pressure from y = 0 to y = y_{MATCH} was obtained by fitting a quartic curve between the wall static pressure and the value of P_{S_f} at y = y_{MATCH}. Since a quartic curve is determined by five conditions, three additional conditions over and above the static pressure at the wall and the value of P_{S_f} at y = y_{MATCH} were needed to define it. These three conditions were determined by the requirement that the static pressure gradient at the wall be zero (determined on the basis of a velocity of zero at the wall) and that the first and second derivatives of the static pressure at y = y_{MATCH} be equal to the values determined from the P_{S_f} curve.

6

R-1285-11

The local total pressure in the boundary layer can be calculated from the local static pressure and the measured pitot pressure. An example of the variation of the local total pressure in the boundary layer with distance normal to the surface is given in the upper part of Fig. 9. The boundary layer thickness, δ, is defined as the value of y at which the local total pressure is equal to 95% of the tunnel total pressure. For flow with no static pressure gradient normal to the wall and a Mach number outside the boundary layer of 2.5, this definition of the boundary layer thickness resulted in a velocity at the outside edge of the boundary layer which was 99.4% of the velocity outside the boundary layer.

It is conventional in the calculation of boundary layer parameters on a flat plate, where the conditions outside the boundary layer are uniform, to base the displacement thickness and momentum thickness of the boundary layer on the conditions outside the boundary layer. However, in the tests conducted in this program, the variation of conditions outside the boundary layer with distance from the wall was so large that this method no longer provided a convenient set of reference conditions. Therefore, it was decided to define boundary layer displacement thickness and boundary layer momentum thickness on the basis of conditions calculated from the wall static pressure. The areas represented by the integrals involved in the definition of the boundary layer quantities are shown in Fig. 10.

A value of match ratio, K = 1.3, was chosen for reduction of the data. Calculations showed that an increase of K from 1.2 to 1.5 (a change in y_{MATCH} of 25%) resulted in an increase in boundary layer thickness, δ, of approximately 5% and a decrease in boundary layer displacement thickness, δ^*, and momentum thickness, θ, of only 3%. Therefore, the error introduced by the arbitrary choice of K was not significant in the evaluation of δ, δ^*, or θ.

Reference Flat Plate Studies

The uniformity of the flow in the test region with the reference flat plate installed in the tunnel is illustrated in Fig. 11. Although the Mach number indicated by the wall static pressure at the tangent points for the different models (Station 0) varied from model to model, the tunnel Mach number referred to in presenting data is the nominal test-section Mach number (2.0, 2.5, 3.0, or 3.5). Typical values of boundary layer characteristics along the centerline of the reference flat plate are given in Fig. 12.

The effect of Mach number on the boundary layer shape parameter, H, for a 1/7-power velocity profile is given in Fig. 13. Because of the large variation of H with Mach number for 1/7-power profiles, the absolute numerical value of H in compressible flow loses the significance that it has in incompressible flow, where H for turbulent flow on a flat plate is near 1.3 and where H at separation is usually

7

between 1.8 and 2.6. In order to employ a boundary layer shape parameter whose absolute numerical values retain physical significance in compressible flow, a reduced boundary layer shape parameter, G, was adopted, where

$$G = \frac{H}{H_{N=7}} \tag{1}$$

$H_N = 7$ in the preceding equation was obtained from the tables in Ref. 31 (see Fig. 13). Values of this reduced boundary layer shape parameter calculated from the data given in Fig. 12 are presented in Fig. 14.

As noted in a preceding section, the boundary layer thickness approaching the models was controlled by the pressure in the injection plenum tank shown in Fig. 1. The effects of injection plenum pressure on the boundary layer thicknesses, δ, δ^*, and θ, and on the boundary layer shape parameters, H and G, are shown in Figs. 15 and 16. There was a sudden change in boundary layer characteristics at an injection plenum pressure equal to approximately 5% of the tunnel total pressure because an injection plenum pressure equal to or greater than this value was required to fix boundary layer transition at a point near the injection station. The effect of air injection on the boundary layer velocity profiles for the reference flat plate is shown in Fig. 17. Although air injection resulted in an increase in boundary layer thickness by a factor greater than two (see Fig. 15), it resulted in very little change in the shape of the boundary layer velocity profiles in Fig. 17.

The effect of Reynolds number on the reduced boundary layer shape parameter, G, for the reference flat plate is given in Fig. 18. The line faired through these data points (noted as G_F) is used as a reference value of reduced boundary layer shape parameter for some of the analyses which are discussed in the following sections. The qualitative variation of G with Reynolds number is expected on the basis of the variation of the exponential profile parameter, N, with Reynolds number as given in Ref. 32. However, the absolute values of G shown for any given value of R_θ in Fig. 18 are approximately 0.03 greater than the values of G determined from the tables in Ref. 31 using the values of N given in Ref. 32. The reason for this discrepancy is that the values of N given in Ref. 32 were determined from faired lines which fit the velocities in the outer portion of the boundary layer but did not fit the measured velocities near the wall.

Boundary Layer Characteristics Without Bleed

Thirty-eight runs were made with models having no boundary layer bleed, a run being defined as the set of measurements necessary to determine the variation of boundary layer characteristics with distance along a curved-surface model at one

Mach number and one value of boundary layer thickness approaching the model. Of these 38 runs, 21 were obtained with single-radius two-dimensional models, 11 with two-radii two-dimensional models, and 6 with axisymmetric models. The values of initial boundary layer momentum thickness approaching the models are given in Table I. None of these 38 runs contain data for which separation was indicated at any point along the curved surface. Sample data obtained from the tests are discussed in the following paragraphs.

Typical schlieren photographs obtained during tests of single-radius two-dimensional curved-surface models are presented in Fig. 19. The curved shock waves in the lower portion of these schlieren photographs were formed by coalescence of the Mach waves originating from the two-dimensional curved surfaces. By following streamlines, it was determined that the total pressure loss due to this oblique shock wave near the outside edge of the boundary layer at the downstream end of the model was less than 1% of free-stream total pressure for all models tested.

All models employed in the tests discussed in this report were designed so that a Mach wave emanating from the sidewall of the tunnel at Station 0 and progressing downstream at an angle determined from the Mach number calculated from wall static pressure would not intersect the centerline of the model until a point downstream of the curved surface. This limitation on the maximum model length did not, however, eliminate the possibility of changes in the flow on the centerline of the model due to propagation of end effects through the boundary layer. To investigate this possibility, a series of tests was conducted during the initial portion of the experimental program to determine the influence of the boundary layer on the side walls of the tunnel on the flow over the two-dimensional curved-surface models. The effect of wall boundary layer was altered by changing the bypass angle of the model (see Figs. 3 through 6). During preliminary tests the models having total turning angles of 20 deg functioned satisfactorily with a bypass angle of zero. However, for a bypass angle of zero and total turning angles greater than 20 deg, the flow separated from the models because of the effect of the adverse pressure gradient on the thick wind-tunnel sidewall boundary layer. Although this separation was eliminated by the use of a bypass angle of 20 deg, the static pressures near the downstream end of the models with bypass angles of 20 deg were considerably less than those predicted by theory, and the static pressures on the ends of the model were considerably less than on the model centerline. These results indicated a severe sideways flow of air within the boundary layer for a bypass angle of 20 deg. However, it was possible with a bypass angle of 5 deg to test models with turning angles greater than 20 deg without separation, with static pressure distributions approximately equal to those predicted by theory, and with relatively flat distributions of static pressure across the models. Therefore, a bypass angle of 5 deg was employed for all subsequent tests of models having total turning angles greater than 20 deg.

Typical data showing the variation of wall static pressure with distance across a two-dimensional curved-surface model for three different values of initial

9

boundary layer thickness are shown on the upper part of Fig. 20. During tests of one model which employed a 5-deg bypass angle, measurements of the boundary layer characteristics at several stations across the model near the downstream end of the curved surface indicated that there was no significant change in boundary layer shape or thickness with distance across the model.

Examples of the variation of wall static pressure with distance from the curved-surface tangent point of a two-dimensional curved-surface model are given in the lower part of Fig. 20. The small differences between the measured and theoretical (based on method of characteristics) static pressure distributions shown in the lower plot of Fig. 20 were caused by the increased boundary layer growth as compared to the growth on the reference flat plate and by gradients in the test section (see Fig. 11). The variation of Mach numbers determined from the wall static pressures given in Fig. 20 with distance from the curved-surface tangent point is shown in Fig. 21. Also shown in Fig. 21 are Mach numbers near the outside edge of the boundary layer determined from the boundary layer reduction procedure outlined in Figs. 9 and 10. The difference between the Mach number indicated by the wall static pressure and the Mach number at the outside edge of the boundary layer is a measure of the difference in static pressure required to provide the centripetal force necessary to turn the flow.

Typical boundary layer velocity profiles for different stations along a model are given in Fig. 22. The velocities given in the figure are referenced to the nominal tunnel velocity because of the variation of velocity with distance from the wall outside the boundary layer. It is shown in this figure that the velocity of the flow near the wall decreased rapidly with increasing distance along the model for values of local surface angle, α_s, between 0 and 18 deg. However, the velocities near the wall decreased very little between values of α_s of 18 and 30 deg because of increased mixing of the flow into the inner portion of the boundary layer.

The effect of changes in the boundary layer thickness at Station 0 on boundary layer profiles at the downstream end of the curved-surface portion of the models is given in Fig. 23. An increase in boundary layer thickness at Station 0 resulted in an increase in boundary layer thickness and a distortion of profile shape at the downstream end of the model. Two of the profiles shown in Fig. 23 were obtained during tests in which the boundary layer was separated from the surface of the model near the station where the local model surface angle was 15 deg. These two profiles were not included in the series of 38 zero-bleed runs listed in Table I.

The variations of boundary layer displacement thickness, δ^*, boundary layer momentum thickness, θ, and reduced boundary layer shape parameter, G, with distance from the curved-surface tangent point are shown in Fig. 24 for three different values of initial boundary layer thickness. The reduced boundary layer shape parameter, G,

increased with increasing distance along the wall for values of local surface angle, a_s, between approximately 0 and 15 deg (approximately the same range of a_s for which the velocities near the wall decreased in Fig. 22) and decreased for values of a_s greater than approximately 15 deg (where the velocities near the wall in Fig. 22 were relatively uninfluenced by distance along the curved surface). The significance of this observation is discussed in a following section.

Typical schlieren photographs obtained during tests of the two-radii two-dimensional curved-surface models are shown in Fig. 25. The variations of Mach number, boundary layer momentum thickness, θ, and reduced boundary layer shape parameter, G, with distance along the wall of the two-radii models are given in Fig. 26.

A schlieren photograph obtained during tests of the axisymmetric curved-surface models is shown in Fig. 27. The wave patterns are similar to those shown in Figs. 19 and 25 for the two-dimensional models. The variations of wall static pressure and Mach number with distance from the curved-surface tangent point of a typical axisymmetric curved-surface model are given in Fig. 28. The theoretical variations of static pressure and Mach number with distance shown therein were obtained from a method-of-characteristics solution of the axisymmetric inviscid flow over the model. The variations of boundary layer displacement thickness, δ^*, boundary layer momentum thickness, θ, and reduced boundary layer shape parameter, G, with distance from the curved-surface tangent point of an axisymmetric curved-surface model are shown in Fig. 29. The increase in local radius (in a plane normal to the axis of symmetry) with distance along the axisymmetric curved-surface models should result in a thinning out of the boundary layer on the curved surface if the boundary layer displacement "area" and momentum "area" are assumed to remain constant. (As noted in the section entitled ANALYTICAL INVESTIGATION, it is possible for boundary layer momentum and displacement thickness areas to decrease in an adverse pressure gradient.) The dashed lines in Fig. 29, which were obtained by multiplying the initial values of momentum thickness and displacement thickness by the ratio of initial radius to local radius, indicate whether the momentum area and displacement area increased or decreased along the length of the model.

Boundary Layer Characteristics With Bleed

A series of tests was conducted to determine the effect of boundary layer removal on the boundary layer characteristics of some of the single-radius two-dimensional curved-surface models. The models employed had radii of 1.5 and 3 in. (see Figs. 3 and 4). Tests were conducted with different values of approach boundary layer thickness (as determined by the pressure in the injection plenum) and with different amounts of bleed (as determined by the number and location of open bleed holes in the model). The number of holes employed in a given test was controlled by filling a fraction of the total number of holes with a plastic compound.

11

R-1285-11

Typical schlieren photographs of the boundary layer bleed models are shown in Fig. 30. These photographs show the flow pattern with no boundary layer bleed (Fig. 30a), the flow pattern with insufficient bleed to prevent separation (Fig. 30b), and the flow pattern with just enough boundary layer bleed to prevent separation (Fig. 30c). The exact combination of values of initial boundary layer thickness and bleed flow which caused incipient separation was determined by observation of the behavior of an oil film which was injected through one of the wall static pressure taps. Incipient separation was indicated by an accumulation of oil on the model surface at the separation point.

The schlieren photograph in Fig. 31 shows the flow pattern when the bleed flow was considerably greater than that necessary to prevent separation. Under these conditions a shock wave originated from each set of bleed holes. No waves were noted in any tests in which the bleed flow was equal to or less than that for incipient separation.

Preliminary tests indicated that the amount of bleed flow required to prevent separation was less if the bleed holes were located between local surface angles of 12 and 24 deg than if the bleed holes were located at local surface angles less than 12 deg or more than 24 deg. Therefore, all data with boundary layer bleed presented in this report were obtained with the bleed holes located between local surface angles of 12 and 24 deg.

Typical wall static pressure and Mach number distributions along a two-dimensional curved-surface model employing boundary layer bleed are given in Fig. 32. Typical boundary layer characteristics are shown in Figs. 33 and 34. The data presented in Figs. 32 through 34 were obtained with a bleed rate approximately twice that necessary to prevent separation on this model. It was not possible to obtain boundary layer data at all stations on the model at the incipient-separation condition because the presence of the probe caused local separation of the boundary layer.

The effect on boundary layer velocity profiles of bleeding more boundary layer from the model than the amount required to prevent separation is shown in Fig. 35 for a local surface angle of 24 deg. This figure shows that the use of more boundary layer bleed than that required to prevent separation had very little effect on the values of reduced boundary layer shape parameter, G, at this station.

ANALYTICAL INVESTIGATION

A complete determination of the characteristics of a boundary layer in an adverse pressure gradient requires knowledge of both the absolute thickness of the boundary layer (as measured by the boundary layer momentum thickness, θ) and of the shape of the boundary layer (as measured by the boundary layer shape parameter, H, or the reduced boundary layer shape parameter, G - see Eq. 1). Although the problems of determining θ and G are not independent of each other, they are treated separately in

12

the following two subsections. It is assumed in the discussion on the following pages that the total temperature in the boundary layer is constant. A discussion of the effect of wall temperature on boundary layer characteristics is given in Appendix I.

Calculation of Boundary Layer Momentum Thickness

A conventional form of the von Kármán boundary layer momentum equation is given in Ref. 31 as follows:

$$c_f q = \frac{d}{dx}(\rho V^2 \theta) + \rho V \delta^* \frac{dV}{dx} \tag{2}$$

Rearrangement of this equation leads to the following:

$$d\theta = \frac{c_f}{2} dx - \theta \left[\frac{dq/q}{dM} + H \frac{dV/V}{dM}\right] dM \tag{3}$$

The first term on the right side of the equation represents the change in θ due to a change in distance, whereas the second term on the right side of the equation represents the change in θ due to a change in Mach number. The factors affecting the two right-side terms will be treated separately in the following discussion.

The local skin-friction coefficient in a region of zero Mach number gradient is given in Fig. 36 as a function of Mach number and the Reynolds number based on the momentum thickness of the boundary layer. The variations of local skin-friction coefficient with Mach number and with Reynolds number shown in this figure were obtained by cross plotting the experimental data from Refs. 33 through 36. The curves of friction coefficient shown for the transition region between laminar flow and turbulent flow were drawn arbitrarily through the small number of data points which were available.

For incompressible flow, it is known that the friction coefficient in a region of adverse pressure gradient is considerably less than the friction coefficient on a flat plate at the same Reynolds number because of the decrease in velocity gradient at the wall caused by the adverse pressure gradient. According to Ref. 37, the variation of friction coefficient with H for incompressible flow is as follows:

R-1285-11 is the header.

$$c_f \approx \frac{1}{e^{1.56H}} \tag{4}$$

Rearranging yields

$$c_f \approx \frac{1}{e^{1.56 H_{N=7} G}} = \frac{1}{e^{1.56(1.287)G}} = \frac{1}{e^{2.01G}} \tag{5}$$

To account for the fact that G on a flat plate is usually different from unity (see Fig. 18), Eq. (5) has been changed arbitrarily to the following form:

$$c_f \approx \frac{1}{e^{2.01G/G_F}} \tag{6}$$

This equation is plotted in Fig. 37. The curves in Fig. 37 for Mach numbers other than zero were determined in a comparable manner by the use of the transformation employed in Ref. 26.

As noted in a preceding paragraph, the second term on the right side of Eq. (3) represents the change in θ due to a change in Mach number. This term can be simplified by the introduction of a quantity called the boundary layer deceleration parameter, J, where

$$J = \frac{dq/q}{dM} + H\frac{dV/V}{dM} \tag{7}$$

It can be shown that, for isentropic flow outside the boundary layer,

$$\frac{dq/q}{dM} = \frac{2}{M} - \frac{\gamma M}{1+\frac{\gamma-1}{2}M^2} \tag{8}$$

$$\frac{dV/V}{dM} = \frac{1}{M} - \frac{\frac{\gamma-1}{2}M}{1+\frac{\gamma-1}{2}M^2} \tag{9}$$

Substituting Eqs. (1), (8), and (9) into Eq. (7) yields

$$J = \left(\frac{2}{M} - \frac{\gamma M}{1 + \frac{\gamma-1}{2}M^2}\right) + GH_{N=7}\left(\frac{1}{M} - \frac{\frac{\gamma-1}{2}M}{1 + \frac{\gamma-1}{2}M^2}\right) \tag{10}$$

For a value of the ratio of specific heats, $\gamma = 1.4$, Eq. (10) becomes

$$J = \left(\frac{2}{M} - \frac{1.4M}{1 + 0.2 M^2}\right) + GH_{N=7}\left(\frac{1}{M} - \frac{0.2M}{1 + 0.2M^2}\right) \tag{11}$$

The boundary layer deceleration parameter, J, as evaluated herein, is given in Figs. 38 through 41 as a function of Mach number and the reduced boundary layer shape parameter, G.

Substitution of Eq. (7) in Eq. (3) and conversion from differential to incremental form yields

$$\Delta\theta = \frac{C_f}{2}\Delta x - \theta J \Delta M \tag{12}$$

This equation can be used in a step-wise calculation of the boundary layer growth in an adverse Mach number gradient. However, in evaluating this relation, if the momentum thickness, θ, at the beginning of each step is used rather than an average value of θ during the step, errors are introduced into the calculation. These errors can be avoided by the use of an additional factor which is developed in Appendix II. This additional factor, which is a correction factor for the variation of θ during the step, converts Eq. (12) to the following form:

$$\Delta\theta = \left[\frac{C_f}{2}\Delta x - \theta_1 J \Delta M\right]\left[1 - \frac{J\Delta M}{2}\right] \tag{13}$$

The variation of boundary layer momentum thickness with Mach number for zero wall friction is given in Figs. 42, 43, and 44 for three different values of G (assumed constant during the deceleration processes) and for three different values of initial Mach number. The data shown in these figures were obtained by a step-wise integration using Eq. (13). The results for a value of G of unity were checked by the use of the tables in Ref. 31 neglecting the friction term in that reference. These three figures show that, for zero wall friction and a value of G of unity, a reduction in Mach number results in a decrease in momentum thickness for Mach numbers above 2.5 and an increase in momentum thickness for Mach numbers below 2.5. This same result could be obtained from Fig. 38, where the boundary layer deceleration parameter, J, changes sign at a Mach number of 2.5 for a value of G of unity. Figure 38 shows that an increase in G results in an increase in the Mach number at which J equals zero, i.e., an increase in the Mach number for which a decrease in Mach number results in no change in boundary layer momentum thickness.

Calculation of Boundary Layer Profile Shape

Conventional Procedures

The boundary layer profile shape parameter, H (or the reduced shape parameter, G) must be known for three reasons:

1) H influences the growth of θ in an adverse pressure gradient (see preceding subsection).

2) H, in combination with θ, determines the boundary layer displacement thickness, δ^*, which is needed to evaluate the amount that a wall must be diverged to account for boundary layer growth so that the inviscid flow outside the boundary layer is unchanged by the boundary layer growth.

3) H, relative to H for a flat plate (see Figs. 13 and 18), determines whether or not the boundary layer is close to being separated from the wall.

The boundary layer shape parameters, H and G, are functions of Reynolds number and the history of the wall pressure gradient. The effect of Reynolds number on the value of G for a flat plate with zero pressure gradient is given in Fig. 18.

The effect of adverse pressure gradients on the boundary layer shape parameter, H, for incompressible flow is usually calculated from an equation having the following form:

$$dH = f_1(H)\frac{dV}{V} + f_2(H, R_\theta)\frac{dx}{\theta}$$

(14)

The first term on the right side of Eq. (14) results in an increase in H for a decrease in velocity. The second term on the right side results in a decrease in H for an increase in X (i.e., the second term is usually negative). Different forms of the first and second terms on the right side are recommended by different investigators (see Refs. 27 through 30). The particular forms of Eq. (14) used in Refs. 27 and 30, respectively, for the insulated-wall case follow:

$$dH = -\frac{H(H+1)^2 (H-1)}{2} \frac{dV}{V} - 0.00369 \frac{H(H^2-1)}{e^{1.561 H}} R_\theta^{-0.268} \frac{dx}{\theta} \tag{15}$$

$$dH = -e^{5(H-1.4)} \frac{dV}{V} - 0.0135 e^{5(H-1.4)} (H-1.4) R_\theta^{-\frac{1}{6}} \frac{dx}{\theta} \tag{16}$$

The form of Eq. (14) employed in Ref. 27, Eq. (15), is extended in Ref. 26 to compressible flow by a transformation procedure.

Lag-Length Procedure

The lag-length procedure discussed in the following paragraphs for calculating G in adverse pressure gradients was developed because of difficulties encountered in the use of Eq. (14) - see the following section. Development of this procedure required knowledge of the amount of flow in the boundary layer in the adverse pressure gradient. The variation with Mach number of the total flow within a boundary layer for initial Mach numbers of 3.0, 5.0, and 10.0 is given in Fig. 45 for a constant value of G of unity during the deceleration process. The amount of flow within the boundary layer was evaluated from the values of θ given in Figs. 42 through 44 and from the tables of boundary layer parameters for N = 7 in Ref. 31. The increase of flow in the boundary layer with a decrease in Mach number shown in this figure represents the influx of flow necessary to increase the average total pressure in the boundary layer from the low value associated with a high Mach number G = 1 profile to the high value associated with a low Mach number G = 1 profile. Since the variation of boundary layer momentum thickness, θ, with Mach number in Figs. 42 through 44 was calculated on the basis of zero wall friction, the variation of total flow in the boundary layer with Mach number given in Fig. 45 does not include the influx of flow into the boundary layer necessary to overcome the shear force at the wall.

An example of the actual variation of flow within the boundary layer with distance along the surface of a curved-surface model is given in Fig. 46. Two reference curves as well as the measured curve are given in this figure: one shows the varia-

17

tion of flow within the boundary layer with distance which would be required to maintain a $G = G_F$ profile shape with zero pressure gradient; the second reference curve shows the variation with distance of the flow within the boundary layer which would be required to maintain a $G = G_F$ profile for the measured pressure gradient. This figure shows that the variation of the actual flow within the boundary layer with distance along the curved surface is approximately equal to that expected on a flat plate for values of $(X-X_0)$ between 0 and 1.5 in., and that the amount of flow within the boundary layer increases rapidly only for values of $(X-X_0)$ larger than 1.5 in. It can be seen from Figs. 24 and 46 that the region where the rate of influx of flow into the boundary layer in the latter figure is small, $(X-X_0)$ from 0 to 1.5 in., corresponds to a region of rapidly increasing G in the former figure and that the region in which the influx of flow into the boundary layer in Fig. 46 is large (downstream of $(X-X_0) = 1.5$) corresponds to a region of constant or decreasing G in Fig. 24.

It is possible to explain why the position at which flow actually starts to enter the boundary layer lags behind the position at which flow should come into the boundary layer to maintain a $G = G_F$ profile as follows: the adverse pressure gradient is first felt in the boundary layer as a decrease in velocity near the wall which is greater (percentage-wise) than the decrease in velocity of the flow near the outer edge of the boundary layer (see Fig. 22). It is hypothesized that the resulting change in velocity near the wall from the velocity that would exist in a flat-plate velocity profile induces a turbulence in order to cause the high-energy flow near the outer part of the boundary layer to mix with the low-energy flow near the wall. It is also hypothesized that some distance is required for this increased turbulence to move to the outer edge of the boundary layer and that this distance is equal to 1.5 in. for the data of Fig. 46. Some data to support this hypothesis are given in Ref. 38, where it is shown that the height of the region of high turbulence in the boundary layer of a subsonic diffuser increases relative to the boundary layer thickness as the distance from the entrance of the diffuser is increased.

A tentative assumption, suggested in Ref. 39, is that the rate of mixing of flow into the boundary layer in an adverse pressure gradient is approximately equal to that on a flat plate. It appears from Fig. 46 that this assumption is accurate only near the upstream end of the adverse pressure gradient (corresponding to $(X-X_0)$ between 0 and 1.5 in.) and that this assumption is extremely inaccurate near the downstream end of the adverse pressure gradient.

Additional plots of the flow within the boundary layer, prepared from the experimental data presented in this report, showed the same trend as that shown in Fig. 46 but, in some cases, exhibited considerable scatter because of inaccuracies associated with the definition of the exact edge of the boundary layer. Consequently, an alternate method of consistently defining the flow within the boundary layer was needed which did not require definition of the edge of the boundary layer. It is

possible to obtain a consistent measure of the flow within a boundary layer from δ^* and θ if it is assumed that all boundary layer profiles are members of the same family (it is conventional in theoretical analyses of boundary layers to make the assumption of a common profile family). The profile family adopted in this report is assumed to be made up of profiles similar to the equivalent step profile shown in Fig. 47. As noted therein, the equivalent step profile has the same values of δ^* and θ and, hence, the same values of H and G as the actual boundary layer profile. However, the total boundary layer thickness and the total flow within the equivalent step profile are less than those for the actual boundary layer profile. Values of the ratio of the velocity within equivalent step profiles to the velocity outside the boundary layer are given in Fig. 48 for different values of Mach number outside the boundary layer. The equivalent step profile was employed as a tool in this report because it is easily adaptable to physical reasoning concerning the behavior of boundary layers in adverse pressure gradients. A discussion of the influence of employing a family of profiles other than that for equivalent step profiles is given in the following paragraphs.

It is convenient in the development of the lag-length procedure to first consider the behavior of an equivalent step profile in a Mach number gradient corresponding to the region of $(X-X_0)$ between 0 and 1.5 in. in Fig. 46, i.e., in a region in which the deceleration is so rapid that the rate of mixing of flow into the boundary layer from the free stream is not increased above that which occurs upstream of the adverse pressure gradient. Since the influx of flow into the actual boundary layer in this region is approximately equal to that necessary to overcome the shear force at the wall, it is permissible to assume that there is no influx of flow into the equivalent step profile and no shear force at the wall for the equivalent step profile in this region. This assumption is equivalent to stating that the ratio of the total pressure within the equivalent step profile to the total pressure outside of the equivalent step profile is constant during the deceleration process. However, it can be shown from isentropic flow relations that the ratio of the velocity within the equivalent step profile to the velocity outside the boundary layer decreases rapidly during such a deceleration process. (The velocity in the equivalent step profile approaches zero when the flow has decelerated to the condition where the wall static pressure is equal to the total pressure within the equivalent step profile.)

The variations of the boundary layer shape parameters, H and G, with fractional decrease in velocity for incompressible flow calculated on the basis of a constant ratio of step-profile total pressure to total pressure outside the boundary layer are given by the solid line in Fig. 49. Also shown in this figure are the variations of H and G with fractional decrease in velocity calculated from the first term on the right side of Eqs. (15) and (16). The figure shows that the variations of H and G with fractional decrease in Mach number are of the same general form for the equivalent step profile as those calculated from the first term on the right side of

Eqs. (15) and (16). Therefore, the first term of Eqs. (14), (15), or (16), which is much larger than the second terms of these equations for rapid changes in Mach number (small ΔX), represents the change in boundary layer shape which occurs when the rate of influx of flow into the boundary layer has not been increased above that which would be obtained on a flat plate. The effect of a rapid decrease in Mach number on the reduced boundary layer shape parameter, G, for compressible flow is shown in Fig. 50. The variation of G with fractional decrease in Mach number shown in Figs. 49 and 50 applies only when the decrease in Mach number is so rapid that the mixing which occurs downstream of $(X-X_0)$ of 1.5 in. in Fig. 46 has no influence on the profile.

In order to use the characteristics of equivalent step profiles in regions where there is a large influx of flow into the boundary layer (such as the region downstream of $(X-X_0)$ of 1.5 in. in Fig. 46), a new boundary layer parameter was adopted. This new parameter, called the boundary layer flow thickness, β, is related to the flow within an equivalent step profile by the following equation:

$$W_{esp} = \frac{0.531 P_{T_0} \beta}{\sqrt{T_T}} \tag{17}$$

The total pressure and total temperature in the preceding equation are the total pressure and total temperature outside the boundary layer. Therefore, β represents the height of a sonic nozzle which will pass the flow within an equivalent step profile at free-stream total pressure and total temperature. The variations of dimensionless flow thickness, β/θ, with G for various Mach numbers outside the boundary layer are given in Figs. 51 and 52. The curves on these figures were calculated for a value of γ of 1.4 and a value of total temperature within the step profile equal to the total temperature outside the step profile. The flow within an equivalent step profile (as measured by β) at a given Mach number can be determined from the following equation:

$$\beta = \frac{\beta}{\theta}\, \theta \tag{18}$$

An example of the variation of β with distance from the curved-surface tangent point is given in Fig. 53. (The data employed to construct this figure are the same as those employed for Fig. 46.) The method of determination of β in Fig. 53 is noted on the figure. It can be seen that the relationship between the actual and ideal values of β shown therein is qualitatively the same as that for the corresponding curves in Fig. 46. The displacement of the actual β curve from the ideal β curve,

shown on Fig. 53, is described in this report in terms of the lag length, ℓ. The method of determination of ℓ from the experimental data is noted on the figure. The lines between the actual β and ideal β curves on Fig. 53 are drawn at a slope which is calculated from the rate of change of β on a flat plate at the beginning of the adverse pressure gradient. The values of lag length, ℓ, determined from this construction are shown in the lower part of the figure in a nondimensionalized form. The lag lengths are nondimensionalized by dividing by the momentum thickness at the upstream end of the lag length.

The experimental values of G shown in Fig. 29 can be back-calculated from the lag-length data shown in Fig. 53 by the inverse of the procedure by which the lag lengths were obtained. Therefore, the generalized problem of determining G in an adverse pressure gradient is reduced to one of determining the dimensionless lag length, ℓ/θ.

A simplified procedure for approximating the boundary layer shape parameter, G, in small adverse pressure gradients can also be derived on the basis of lag-length data. This procedure, which is illustrated in Fig. 54, is based on the use of curves such as those presented in Figs. 49 and 50. The value of G at a point such as "b" in Fig. 54 is approximately equal to the value of G which would be obtained by rapid deceleration of the flow from a flat-plate profile at Point "a". The difference in Mach numbers between Points "a" and "b" can then be used in curves such as those presented in Figs. 49 or 50. The difference in axial distance between Points "a" and "b" is given by the lag length.

Although the equivalent step profile shown in Fig. 47 was used extensively in the development of the reasoning behind the lag-length procedure, the only place where the characteristics of the equivalent step profile are actually used in determining lag length is through the curves of β/θ given in Figs. 51 and 52. It is possible to generate curves similar to those shown in Figs. 51 and 52 for a different family of profile shapes and, hence, to generate lag-length data which are different from those shown in Fig. 53. However, if a new family of profile shapes were selected in which β/θ was a constant times the values shown in Figs. 51 and 52, then the lag lengths determined by a procedure similar to that described in Fig. 53 would be identical to those determined from the equivalent step profile because of the method employed to attain lag lengths from the β/θ data (see Fig. 53). Evaluation of the flow within power profiles from the tables of Ref. 31 indicates that the flow within a power profile for a given value of θ (a measure of β/θ) is approximately twice that for an equivalent step profile for a wide range of Mach numbers and for values of N between 5 and 11. Lag lengths different from those determined from an equivalent step profile would result only from the use of different types of variations of β/θ with Mach number and G from those shown in Figs. 51 and 52. Although values of ℓ/θ for the data presented in this report have not been evaluated for any variation of β/θ with Mach number and G other than that given in Figs. 51 and 52 because of the

21

large amount of labor involved, a cursory examination of the use of alternate profile shapes for the evaluation of β/θ has indicated that the scatter of the data on $\mathcal{L}/\theta$ presented in this report would not be reduced significantly by the use of alternate profile shapes for the evaluation of β/θ. It is believed that significant improvements in the correlation of data from the correlation based on β/θ presented in this report can only be made by the use of multi-family profile shapes (such as a multi-step profile with no restriction on the relative values of the velocities in each step). A correlation of data based on the use of multi-family profile shapes would be extremely complicated.

CORRELATION OF EXPERIMENTAL AND ANALYTICAL RESULTS

Boundary Layer Profile Shape

Determination of boundary layer profile shape for an arbitrary configuration by the lag-length procedure discussed in the preceding section requires knowledge of the lag-length characteristics of the boundary layer for the arbitrary configuration. Data on lag length have been obtained from the 38 runs without boundary layer bleed (see Table I) in order to obtain a correlation of lag length which can be used for an arbitrary configuration. Typical values of boundary layer flow thickness from which lag length can be determined (see Fig. 53) and lag length are presented in Figs. 55 and 56 for a single-radius two-dimensional curved-surface model, in Figs. 57 and 58 for a two-radii two-dimensional curved-surface model, and in Fig. 59 for an axisymmetric curved-surface model. Although the scatter in the values of lag length for a given run was large as a result of the scatter in the values of G which were used to determine lag length (see Figs. 24, 26, and 29), it appears from study of the data from all 38 runs that there was relatively little variation of lag length with distance along a curved-surface model for a given run. However, there appeared to be large variations of lag length with Reynolds number based on the initial boundary layer momentum thickness (see Figs. 56 and 58). This change in lag length with initial Reynolds number was particularly evident at low values of initial Reynolds number. It is believed that the low values of lag length at low values of initial Reynolds number are caused by the rapid changes in boundary layer shape in the transition region which occurs at Reynolds numbers based on momentum thickness on the order of 1000. It is hypothesized that the vortices which cause the high mixing rates near the wall to propagate to the outside edge of the boundary layer (see discussion in preceding section) are much larger immediately downstream of transition than they are further downstream where the boundary layer has a fully developed turbulent profile. These large-size vortices would require less lag length than small-size vortices to mix the high-energy flow from outside the boundary layer with the relatively low-energy flow near the wall.

Studies of various methods of correlating the lag-length data have indicated that lag length is primarily a function of the Reynolds number at the beginning of the adverse Mach number gradient (see Figs. 56 and 58). Although no data were obtained in which there was an extremely large variation of local Reynolds number during a test with a single model at a single Mach number and initial boundary layer thickness, it was hypothesized that the influence of initial Reynolds number should be reduced at high values of local Reynolds number. This hypothesis must be true for the hypothetical case in which an infinitesimally small pressure gradient is imposed in the region between transition (low R_θ) and the beginning of a severe adverse pressure gradient at high R_θ. It is obvious that ℓ/θ in the region of the severe adverse pressure gradient should be determined from R_{θ_0} evaluated at the beginning of the severe adverse pressure gradient rather than at transition. Therefore, in fitting a curve through the lag-length data, it was decided to employ an equation in which the effect of initial Reynolds numbers would die out at high values of local Reynolds number. The equation fitted through the lag-length data obtained from the tests described in this report is as follows:

$$\ell/\theta = -22.5 + 49.7 \left[\left(\frac{R_{\theta_0}}{1000} - 1 \right)^{0.2} \left(\frac{1}{1 + \frac{R_\theta - R_{\theta_0}}{1000}} \right)^5 + \left(\frac{R_\theta}{1000} - 1 \right)^{0.2} \left(1 - \left(\frac{1}{1 + \frac{R_\theta - R_{\theta_0}}{1000}} \right)^{0.5} \right) \right] \quad (19)$$

A plot of the preceding equation is given in Fig. 60. The two constants in the equation (-22.5 and +49.7) were determined by a least-squares fit through 149 data points obtained from the 38 runs without bleed during which separation did not occur. The exponent 0.2 in the preceding equation was arbitrarily chosen equal to the exponent which governs the variation of friction coefficient with Reynolds number in turbulent flow. Calculations in which the exponent 0.2 was replaced by smaller and larger values indicated that the accuracy of the curve fit through the data was not changed appreciably for values of this exponent between 0.1 and 0.4. The exponent 0.5 in the preceding equation governs the rate at which the solid curves approach the dashed curve in Fig. 60 and was chosen arbitrarily.

A comparison of lag lengths determined from the data and from the curve in Fig. 60 is given in Fig. 61 in terms of the lag-length residual, ρ_ℓ. As noted in a preceding paragraph, the scatter of the lag-length data was large as a result of the scatter in the values of G employed in determining lag length (see Figs. 24, 26, and 29). The scatter in lag length as indicated by the lag-length residuals in Fig. 61 is a large percentage of the absolute value of lag length at low Reynolds numbers (see Fig. 60). This scatter in lag length at low Reynolds numbers results from the large change in lag length with Reynolds number at low Reynolds number and the difficulty of establishing the exact transition point upstream of an adverse pressure gradient.

A statistical analysis of the data in Fig. 61 was performed to determine if lag length should also be expressed as a function of Mach number, type of model, or dimensionless pressure gradient (as determined by the ratio of average model radius to initial boundary layer momentum thickness). The results of this statistical analysis are given in Table II. The average residual for a given set of data ($\Sigma \rho_\ell / n$ in the table) is a measure of how much the average of this set of data falls above or below the fitted curve given by Eq. (19). The only set for which a large value of average residual was obtained was the data for Mach number 3.5. The large average residual for the Mach number 3.5 data is not believed to be significant because of the small number of data points obtained at this Mach number and because the data obtained at Mach number 3.5 was inconsistent due to difficulties in fixing transition at this Mach number. Since no consistent variation of average lag-length residual with Mach number, model type, or dimensionless pressure gradient is noted in the data shown in Table II, it is concluded that none of these variables need be included in the general expression for lag length given by Eq. (19).

The usefulness of the lag-length fairing as given in Eq. (19) and in Fig. 60 is determined by the accuracy with which the relationship for lag length can be used to calculate the variation of boundary layer shape with distance in an adverse pressure gradient. Although evaluation of G by the lag-length procedure is very laborious by hand calculations, such an evaluation is easily adaptable to high-speed computing machines. Typical comparisons of measured values of reduced boundary layer shape parameter and values of reduced boundary layer shape parameter as machine calculated with Eq. (19) are given in Figs. 62, 63, and 64 for single-radius two-dimensional, two-radii two-dimensional, and axisymmetric curved-surface models, respectively. Also shown in these figures are values of the variation of reduced boundary layer shape parameter with distance along the curved plates as calculated by the method of Ref. 26. The calculations by the method of Ref. 26 produced values of reduced boundary layer shape parameter greater than 10 at an intermediate point in the adverse pressure gradient for all cases given in Figs. 62 through 64. The method of Ref. 26, which is based on Eq. (15), gives poor answers because the second term of Eq. (15) does not account for the large rates of mixing of flow into the boundary layer near the downstream end of an adverse pressure gradient. The agreement between the measured values of G and the values of G calculated from the lag-length procedure are good, particularly in relation to the large differences between the measured values of G and the values of G calculated by the Ref. 26 method.

A summary of the difference between the maximum measured values of G and the maximum values of G calculated by the lag-length procedure for all 38 runs for which boundary layer bleed was not employed is given in Fig. 65. As noted thereon, the average difference between measured and calculated values of maximum G is 0.044 and the root-mean-square difference is 0.094. If the data for Mach number 3.5 were omitted, the average difference would be reduced to 0.024 and the root-mean-square difference would be reduced to 0.058.

The calculated values of reduced boundary layer shape parameter shown in Figs. 62 through 64 were determined on the basis of the measured variation of Mach number with distance from the curved-surface tangent point (see Figs. 21, 26, and 28). The effect of small changes in the Mach number distribution on the calculated variation of the reduced boundary layer shape parameter with distance is shown in Fig. 66. The variation of Mach number with distance given by Curve 1 of this figure was determined from the measured variation of Mach number with distance given in Fig. 21. The variation of Mach number with distance given by Curve 2 in Fig. 66 was determined by the theoretical variation of Mach number with distance given in Fig. 21. The lower plot in Fig. 66 shows that the small difference in Mach number distribution between that given by Curve 1 and that given by Curve 2 results in an appreciable change in the variation of reduced boundary layer shape parameter with distance. However, the difference between the maximum value of reduced boundary layer shape parameter for the two cases is only 0.05. An attempt was made to calculate the difference between the measured and theoretical variations of Mach number with distance shown in Figs. 21 and 66 on the basis of the Mach number distribution on the reference flat plate (Fig. 11) and on the basis of the Mach number changes induced by the variation of boundary layer displacement thickness with distance along the curved surface. The resulting corrected theoretical variation of Mach number with distance was in better agreement with the measured variation of Mach number with distance than the uncorrected theoretical Mach number variation.

Lag-length data were also evaluated from the boundary layer profiles given in Refs. 9 and 14. The boundary layer profiles presented in Ref. 14 were obtained for an incident oblique shock having a turning angle through the shock of 10 deg and a Mach number of 2.97 upstream of the shock. The Reynolds number based on the boundary layer momentum thickness approaching the shock was approximately 7400. The values of $\mathcal{l}/\theta$ determined from Ref. 14 were on the order of 90, which is almost twice the value of lag length for the correlation given in Fig. 60. The difference between the lag lengths determined from Ref. 14 and those of this report might be due to the fact that the Ref. 14 variation of wall static pressure with distance along the plate was caused by shock wave—boundary layer interaction, whereas the present variations of wall static pressure with distance along the curved surface were caused primarily by the local slope of the curved surface.

The data presented in Ref. 9 were obtained for normal shocks with a Mach number upstream of the normal shock of approximately 1.3. The Reynolds numbers based on boundary layer momentum thickness approaching the shock were on the order of 1200 to 2300. The measured values of $\mathcal{l}/\theta$ for these conditions were approximately 90, as compared to values on the order of 15 to 30 predicted from the curve presented in Fig. 60. No satisfactory explanation for this difference in lag length has been devised other than that suggested for the Ref. 14 data discussed in the preceding paragraph.

Boundary Layer Momentum Thickness

According to the boundary layer momentum equation (Eq. 3), the growth of boundary layer momentum thickness in an adverse pressure gradient is a function of the wall friction and the shape of the boundary layer profile during the deceleration process. Five sets of calculations employing different assumptions have been made in order to evaluate the effect of changes in the assumptions regarding wall friction and boundary layer profile shape. The assumptions employed in these five sets of calculations are given in Fig. 67. The results of calculations employing the five sets of assumptions are given in Figs. 68, 69, and 70 for the different types of models tested. The most accurate set of assumptions should be that which results in the calculation of Curve c in Figs. 67 through 70.

A comparison of measured values of θ with values of θ calculated by the assumptions leading to Curve c is given in Fig. 71. The scatter of data in this figure is very large relative to that which is ordinarily obtained from tests of a flat plate. For instance, the root-mean-square scatter of flat-plate data about the faired line in Fig. 15 is only 3% of the average value of momentum thickness for this curve. As noted in Fig. 71, the root-mean-square scatter of data is approximately 11% for points half way along the curved surface and approximately 17% for points at the end of the curved surface. These two values of root-mean-square scatter would be reduced to 9% and 13% if the Mach number 3.5 data were omitted. The average value of the ratio of measured θ to calculated θ is 0.99 at a point half way along the curved surface (upper plot of Fig. 71) and is 1.04 at the downstream end of the curved surface (lower plot of Fig. 71). These average values would be reduced to 0.97 and 1.01 if the Mach number 3.5 data were omitted. The difference between the measured values and a value of unity cannot be considered significant on the basis of the large scatter of the data in Fig. 71.

Momentum thicknesses at the downstream end of the curved surface calculated on the basis of the variation of G with length determined from the lag-length procedure (Curve e in Figs. 67 through 70) are different from those calculated on the basis of the measured variation of G with length (Curve c). The average value of the ratio of momentum thickness corresponding to Curve e to that corresponding to Curve c was 0.98. The root-mean-square difference between the momentum thicknesses calculated by the two different procedures was 4% of the absolute value of the momentum thickness at the end of the curved portion of the plate. If the Mach number 3.5 data were omitted, the average value would be increased to 0.99 and the root-mean-square scatter could be reduced to 3%. Therefore, the error introduced into the calculation of growth of boundary layer momentum thickness by the fact that the variation of G with length calculated by the lag-length procedure is different from the actual variation of G with length does not introduce a significant error into the calcuation of boundary layer momentum thickness.

All the data presented in Figs. 67 through 71 were obtained with zero bleed. On the basis of theoretical considerations, boundary layer bleed should result in a reduction in boundary layer momentum thickness. If the flow between the wall and a station y_b away from the wall is bled off, the resulting change in boundary layer momentum thickness can be found from the following:

$$\Delta \theta_b = \frac{1}{\rho_w V} \int_0^{y_b} \rho V (1 - \frac{u}{V}) \, dy \tag{20}$$

The weight flow which is bled off is given by

$$W_b = \int_0^{y_b} \rho V \, dy \tag{21}$$

The ratio of the change in momentum thickness to the flow which is bled off can be obtained through dividing Eq. (20) by Eq. (21):

$$\frac{\Delta \theta_b}{W_b} = \frac{\frac{1}{\rho_w V} \int_0^{y_b} \rho V (1 - \frac{u}{V}) \, dy}{\int_0^{y_b} \rho V \, dy} \tag{22}$$

Examination of this equation shows that the greatest change in boundary layer momentum thickness for a given amount of bleed occurs if the flow which is bled off has zero velocity, which makes the term within the parenthesis in the preceding equation equal to unity. This maximum change of momentum thickness per unit bleed flow is, therefore, given as follows:

$$\frac{(\Delta \theta_b)_{THEORY}}{W_b} = \frac{1}{\rho_w V} \tag{23}$$

The actual change of boundary layer momentum thickness per unit bleed flow should be less than that given by the preceding equation for two reasons: (1) the flow bled off has a velocity somewhat greater than zero, and (2) the removal of the low-energy flow from the portion of the boundary layer near the wall should result in an increase in wall friction.

The effect of boundary layer bleed on the reduction of boundary layer momentum thickness was determined by the procedure indicated in the top plot of Fig. 72. The theoretical variation of momentum thickness with length for zero bleed given in this sketch was determined by the procedure for Curve c in Fig. 67. The variation of G with distance for this theoretical curve was obtained by fairing between a value of $G = G_F$ at the upstream end of the curved surface and the measured value of G at the downstream end of the bleed region. It was not possible to obtain measured values of G in the bleed region of the model because of local flow angularity caused by the flow entering the perforations. The measured difference in θ due to bleed, $(\Delta \theta_b)_{MEASURED}$ was defined as the difference between this calculated value of θ and the measured value of θ at the end of the bleed region.

The ratio of the measured decrease in θ per unit bleed flow divided by the theoretical value of the same quantity is given in the lower plot of Fig. 72. As noted in a preceding paragraph, the measured decrease in θ due to bleed should be less than the maximum theoretical value of this quantity. The average value of the ratio of the measured to theoretical decrease in θ due to bleed is on the order of 0.5. The relatively large scatter of the small amount of data about this average value results from inaccuracies in the absolute values of momentum thickness (see discussion of scatter in Fig. 71).

Boundary Layer Separation

A large amount of data on the pressure ratio for incipient separation for single-radius two-dimensional curved-surface models is presented in Ref. 25. These data and several data points from the present report are presented in Figs. 73 and 74 as a function of the radius of curvature of the model divided by the boundary layer momentum thickness at the curved-surface tangent point, Station 0. The arrows on the data points obtained from the present report indicate the position at which the points should fall to obtain perfect agreement with the data from Ref. 25. The agreement between the data from the present report and from Ref. 25 is fair. Also shown in these figures are reference curves which will be discussed in following paragraphs. The experimental data presented in Figs. 73 and 74 indicate that the pressure ratio for incipient separation increases with a decrease in Reynolds number or with an increase in R/θ_0 (decrease in dimensionless pressure gradient). The local surface angles and Mach numbers corresponding to the pressure ratios shown on the left side of Figs. 73 and 74 are given on the right side of these figures.

In order to explain the data presented in Figs. 73 and 74 in terms of the lag-length concept developed in this report, a series of calculations were performed with systematic variations of Mach number, initial boundary layer momentum thickness, and Reynolds number based on initial boundary layer momentum thickness. The variation of Mach number with distance along the curved surface was assumed to be that deter-

28

mined from theory (see Fig. 66 for the effect on G of the difference between experimental and theoretical Mach number distributions). An assumption was made that separation would be encountered on models where the local value of reduced boundary layer shape parameter, G, exceeded 1.5. This value of G, which is equal to a value of H of approximately 1.9 in incompressible flow, was selected since separation is usually encountered in incompressible flow for values of H between 1.8 and 2.6. The results of these calculations are presented as dashed lines in Figs. 73 and 74. The sharp break in the calculated curves near values of R/θ_0 of 150 for initial Reynolds numbers of 2000 or greater occurs because the lag length becomes equal to the length of the curved-surface portion of the model at these break points.

The effect of radius of curvature and Reynolds number on the pressure ratio for incipient separation calculated from the lag-length procedure (the dashed lines) is in qualitative agreement with the data obtained from Ref. 25. The reason for the differences between the calculated and measured curves for low values of R/θ_0 can be explained on the basis of the pressure distributions noted in Ref. 25 for such models. For a compression-corner model(R/θ_0 equal to zero), the increase in static pressure due to the corner does not occur in zero length as predicted by inviscid theory but spreads out over a considerable distance along the model. The pressure distribution data in Ref. 25 show that the actual increase in static pressure on compression-corner models occurs over a distance which is considerably greater than the lag length calculated for the conditions at the corner. Therefore, the pressure ratio for incipient separation for low values of R/θ_0 should be plotted at values of R/θ_0 considerably greater than zero. Displacement of these data to the right of the break points on Figs. 73 and 74 would result in considerable improvement in the agreement between the calculated and measured pressure ratios for incipient separation.

The difference between the measured and calculated values of pressure ratio for incipient separation at large values of R/θ_0 can be explained on the basis of the theoretical limiting turning angle for isentropic external-compression inlets. According to Ref. 40, the maximum turning angle which can be employed in external-compression inlets is determined by limitations on the shock structure where the waves from the compression surface coalesce. This limiting turning angle is noted on Figs. 73 and 74. If this turning angle is exceeded, a normal shock will be formed at the point at which the waves from the compression surface coalesce. A normal shock wave was noted for some of the high-turning-angle models on which data were reported in Ref. 25; therefore, the turning angle given for external-compression inlets can be exceeded to some degree in some cases without causing boundary layer separation. It should be noted that pressure ratios considerably greater than those determined on the basis of the limiting-turning-angle criteria could be obtained if the variation of static pressure with distance along the surface were created in a convergent duct instead of on a simple curved surface. For instance, at Mach number 3.5 the pressure ratio for incipient separation would be increased from 12 for the

simple curved surface to approximately 30 for a convergent duct at large values of R/θ_0 according to Fig. 74.

As noted in a preceding section, it is possible with a given model to obtain separation-free flow with much larger values of boundary layer momentum thickness at Station 0 if boundary layer bleed is employed than if boundary layer bleed is not employed. The amount of boundary layer bleed necessary to prevent separation on two single-radius two-dimensional models ($R = 1.5$ and 3.0 in.) is given in the upper plots of Figs. 75 and 76 as a function of the boundary layer momentum thickness at Station 0. The amount of bleed necessary to prevent separation for compression corners ($R = 0$), calculated on the basis of bleeding all of the boundary layer flow which had a total pressure less than the calculated static pressure downstream of the compression corner, is also shown in the upper plots of Figs. 75 and 76.

A cross plot of the data in the upper plots of Figs. 75 and 76 is given on the lower plots in the same figures as a function of dimensionless gradient (as measured by R/θ_0). Although it was not possible to determine any significant effect of Reynolds number based on initial momentum thickness for the Mach 2.5 data shown in Fig. 75, there appeared to be a trend toward increasing the bleed flow required to prevent separation as the Reynolds number was increased at Mach 3.0 (Fig. 76).

LA

REFERENCES

1. McLafferty, G. H., E. L. Krasnoff, E. D. Ranard, W. G. Rose, and R. D. Vergara: Investigation of Turbojet Inlet Design Parameters. UAC Research Department Report R-0790-13, December 1955.

2. Karanian, A. J.: Characteristics of Normal Shock Waves in the Throats of Pre-compression Inlets. UAC Research Department Report R-0955-20, October 1957.

3. Cnossen, J. W.: Studies of Boundary Layer Removal Scoops for High-Performance Supersonic Inlets. UAC Research Department Report R-0955-21, October 1957.

4. Anderson, D. C.: Efficiency of Flush and Protruding Oblique Exhaust Nozzles With and Without External Flow. UAC Research Department Report R-0955-22, October 1957.

5. Vergara, R. D.: Performance of Supersonic Inlets Having Perforated Throats. UAC Research Department Report R-0955-23, October 1957.

6. Kepler, C. E.: Performance of a Variable-Geometry Chin Inlet at Mach Numbers from 1.6 to 3.0. UAC Research Department Report R-0955-24, October 1957. Confidential. (Unclassified Title)

7. Kepler, C. E.: Performance of a Mach 4.0 Variable-Geometry Axisymmetric Inlet Having External-Plus-Internal Compression. UAC Research Department Report R-1285-12, September 1959. Confidential. (Unclassified Title)

8. Cnossen, J. W.: Efficiency of Flush Oblique Nozzles Exhausting Into Supersonic Streams Having Mach Numbers up to 4.0. UAC Research Department Report R-1285-10, September 1959.

9. Ackeret, J., F. Feldmann, and N. Rott: Investigations of Compression Shocks and Boundary Layers in Gases Moving at High Speed. NACA TM 1113, January 1947.

10. Fage, A., and R. E. Sargent: Shock Wave and Boundary Layer Phenomena Near a Flat Surface. Proceedings of The Royal Society, Vol. 190, Series A, No. 1020, June 1947.

11. Liepmann, H. W., A. Roshko, and S. Dhawan: On Reflection of Shock Waves from Boundary Layers. NACA TN 2334, April 1951.

12. Barry, F. W., A. H. Shapiro, and E. P. Neumann: The Interaction of Shock Waves with Boundary Layers on a Flat Surface. Journal of the Aeronautical Sciences, Vol. 18, No. 4, April 1951.

13. Moeckel, W. E.: Flow Separation Ahead of Blunt Bodies at Supersonic Speeds. NACA TN 2418, July 1951.

14. Bogdonoff, S. M., and A. H. Solarski: A Preliminary Investigation of Shockwave-Turbulent Boundary Layer Interaction. Princeton University, Department of Aeronautical Engineering, Report 184, November 1951.

15. Donaldson, Coleman duP., and R. H. Lange: Study of the Pressure Rise Across Shock Waves Required to Separate Laminar and Turbulent Boundary Layers. NACA TN 2770, September 1952.

16. Bogdonoff, S. M., and C. E. Kepler: Separation of a Supersonic Turbulent Boundary Layer. Princeton University, Department of Aeronautical Engineering, Report 249, January 1954.

17. Lange, R. H.: Present Status of Information Relative to the Prediction of Shock-Induced Boundary-Layer Separation. NACA TN 3065, February 1954.

18. Chapman, D. R., D. M. Kuehn, and H. K. Larson: Investigation of Separated Flows in Supersonic and Subsonic Streams with Emphasis on the Effect of Transition. NACA TN 3869, March 1957.

19. Hammitt, A. G., I. E. Vas, and S. Hight: An Analysis of the Effect of Shock Waves on Turbulent Boundary Layers. Princeton University Report No. 396. AFOSR TN 57-297, July 1957.

20. Tyler, R. D., and A. H. Shapiro: Pressure Rise Required for Separation in Inter-action Between Turbulent Boundary Layer and Shock Wave. Journal of the Aero-nautical Sciences, Vol. 20, No. 12, December 1953.

21. Crocco, L., and R. F. Probstein: The Peak Pressure Rise Across an Oblique Shock Emerging from a Turbulent Boundary Layer Over a Plane Surface. Princeton University, Report No. 254, March 1954 (Contract N6onr-270, Task Order 6, Project No. NR-061-049).

22. Mager, A.: Prediction of Shock-Induced Turbulent Boundary Layer Separation. Journal of the Aeronautical Sciences, Vol. 22, No. 3, March 1955.

23. Reshotko, E., and M. Tucker: Effect of a Discontinuity on Turbulent Boundary-Layer-Thickness Parameters with Application to Shock-Induced Separation. NACA TN 3454, May 1955.

24. Hammitt, A. G.: An Approximate Theory of Turbulent Boundary Layer Shock Wave Interaction. Princeton University, Report No. 340, AFOSR TN 56-160, April 1956.

25. Kuehn, D. M.: Experimental Investigation of the Pressure Rise Required for the Incipient Separation of Turbulent Boundary Layers in Two-Dimensional Supersonic Flow. NASA Memo 1-21-59A, February 1959.

26. Reshotko, E., and M. Tucker: Approximate Calculation of the Compressible Turbulent Boundary Layer with Heat Transfer and Arbitrary Pressure Gradient. NACA TN 4154, December 1957.

27. Tetervin, N., and C. C. Lin: A General Integral Form of the Boundary-Layer Equation for Incompressible Flow with an Application to the Calculation of the Separation Point of Turbulent Boundary Layers. NACA Report 1046, 1951 (Supersedes NACA TN 2158).

28. Schlichting, H.: Boundary Layer Theory. McGraw-Hill Book Co., New York, 1955.

29. von Doenhoff, Albert E., and Neal Tetervin: Determination of General Relations for the Behavior of Turbulent Boundary Layers. NACA Report 772, 1943 (Supersedes NACA ACR 3G13).

30. Garner, H. C.: The Development of Turbulent Boundary Layers. British A.R.C. Report and Memo No. 2133, 1944.

31. Tucker, M.: Approximate Calculation of Turbulent Boundary-Layer Development in Compressible Flow. NACA TN 2337, April 1951.

32. Persh, J.: A Theoretical Investigation of Turbulent Boundary Layer Flow with Heat Transfer at Supersonic and Hypersonic Speeds. NAVORD Report 3854, May 1955.

33. Coles, D.: Measurements of Turbulent Friction on a Smooth Flat Plate in Supersonic Flow. Journal of the Aeronautical Sciences, Vol. 21, No. 7, July 1954.

34. Lobb, R. K., E. M. Winkler, and J. Persh: Experimental Investigation of Turbulent Boundary Layers in Hypersonic Flow. Journal of the Aeronautical Sciences, Vol. 22, No. 1, January 1955.

35. Hill, F. K.: Boundary-Layer Measurements in Hypersonic Flow. Journal of the Aeronautical Sciences, Vol. 23, No. 1, January 1956.

36. Korkegi, R. H.: Transition Studies and Skin-Friction Measurements on an Insulated Flat Plate at a Mach Number of 5.8. Journal of the Aeronautical Sciences, Vol. 23, No. 2, February 1956.

37. Ludwieg, H., and W. Tillmann: Investigations of the Wall-Shearing Stress in Turbulent Boundary Layers. NACA TM 1285, May 1950.

38. Sandborn, Virgil A., and Raymond J. Slogar: Study of the Momentum Distribution of Turbulent Boundary Layers in Adverse Pressure Gradients. NACA TN 3264, January 1955.

39. Crocco, L., and L. Lees: A Mixing Theory for the Interaction Between Dissipative Flows and Nearly Isentropic Streams. Journal of the Aeronautical Sciences, Vol. 19, No. 10, October 1952.

40. Connors, James F., and Rudolph C. Meyer: Design Criteria for Axisymmetric and Two-Dimensional Supersonic Inlets and Exits. NACA TN 3589, January 1956.

41. Persh, Jerome, and Roland Lee: Tabulation of Compressible Turbulent Boundary Layer Parameters. NAVORD Report 4282, May 1956.

LIST OF SYMBOLS

c_f Local skin-friction coefficient,
(WALL SHEAR FORCE)$/(\rho_w V^2/2)$(SURFACE AREA)

G Reduced boundary layer shape parameter, $H/H_{N=7}$

G_F Value of G on flat plate, $1.12 \, (R_\theta/1000)^{-0.04}$ (see Fig. 18)

G_O Value of G at upstream end of adverse pressure gradient in theoretical calculations

h Tunnel height for tests of two-dimensional models (see Fig. 1)

H Boundary layer shape parameter, δ^*/θ

$H_{N=7}, H_{N=5}$ Boundary layer shape parameters for 1/7 and 1/5-power velocity profiles, respectively (see Ref. 31)

J Boundary layer deceleration parameter (see Eq. 7)

K Match ratio, value of y_{MATCH}/y_P employed in calculation of P_S (a value of $K = 1.3$ was employed for data reduction - see text)

ℓ Lag length (see Figs. 53 and 60)

L_1 Length to upstream end of two-dimensional curved-surface model from tunnel throat for two-dimensional models (see Fig. 1) or from model leading edge for axisymmetric models (see Fig. 7)

L_2 Length from upstream end of curved-surface model to Station 0 (see Figs. 3, 5, and 7)

L_3 Circumferential length along surface of radius R or R_1 (see Figs. 3, 5, and 7)

L_4 Length of constant-angle surface between two curved portions of the two-radii two-dimensional curved-surface models (see Fig. 5)

L_5 Circumferential length along surface of radius R_2 (see Fig. 5)

L_6 Length along constant-angle surface downstream of curved portion of model (see Figs. 3, 5, and 7)

35

M	Mach number determined from P_{S_W}/P_{T_O}
M_O	Nominal tunnel Mach number (also Mach number at upstream end of adverse pressure gradient in theoretical calculations)
M_δ	Mach number at outside edge of boundary layer
N	Exponential profile parameter in equation $\frac{u}{V} = (\frac{y}{\delta})^{\frac{1}{N}}$
n	Number of data points in sample
P	Pressure
P_{IP}	Injection plenum pressure
P_P	Measured pitot pressure (see Fig. 9)
$P_{P_{MAX}}$	Maximum measured pitot pressure (see Fig. 9)
P_S	Local static pressure calculated from analytical curve fitted through P_{S_W} and P_{S_f} at y_{MATCH} (see text and Fig. 9)
P_{S_f}	Static pressure calculated from measured pitot pressure, P_P, and tunnel total pressure, P_{T_O} (see Fig. 9)
P_{S_O}	Nominal tunnel static pressure
$P_{S_{W_{MAX}}}$	Maximum static pressure measured near downstream end of curved-surface model
P_{S_W}	Wall static pressure
P_T	Local total pressure calculated from P_P and P_S (see Fig. 9)
P_{T_O}	Tunnel total pressure
q	Dynamic pressure, $\frac{\rho V^2}{2}$
r	Radius of axisymmetric curved-surface model in a plane normal to axis (see Fig. 7)

36

r_e — Maximum radius of axisymmetric curved-surface model in a plane normal to axis (see Fig. 7)

r_o — Radius of axisymmetric curved-surface model at Station O in a plane normal to axis (see Fig. 7)

R — Radius of curvature of single-radius models (see Figs. 3 and 7)

$\bar{R}$ — Average radius of curvature; equals R for single-radius models and $(R_1 + R_2)/2$ for two-radii models

R_1 — Initial radius of curvature of two-radii model (see Fig. 5)

R_2 — Second radius of curvature of two-radii model (see Fig. 5)

R_θ — Reynolds number based on boundary layer momentum thickness, $\dfrac{\rho_w V \theta}{\mu}$

R_{θ_O} — Values of R_θ at Station O (also, value of R_θ at upstream end of adverse pressure gradient in theoretical calculations)

T_T — Total temperature - assumed constant throughout flow field except in discussion in Appendix I

u — Local velocity determined from P_S/P_P

u' — Ideal local velocity determined from P_S/P_{T_O}

V — Velocity determined from P_{S_W}/P_{T_O}

V_O — Nominal tunnel velocity (also, velocity at upstream end of adverse pressure gradient in theoretical calculations)

V_{esp} — Velocity within equivalent step profile (see Fig. 47)

W_b — Flow bled from the boundary layer

W_{BL} — Flow within boundary layer, $\int_o^\delta \rho V dy$

W_{BL_O} — Flow within boundary layer at Station O

x — Distance from tunnel nozzle throat

x_O — Distance from tunnel nozzle throat to curved-surface tangent point (Station O)

37

y	Distance normal to surface of model
y_b	Distance normal to surface such that $W_b = \int_\delta^{y_b} \rho V \, dy$
y_{MATCH}	Distance normal to surface where $y = K(y_p)$ (see Fig. 9)
y_P	Distance normal to surface at which P_P is a maximum (see Fig. 9)
Z	Distance across model (measured from centerline of tunnel)
α_S	Local surface angle (relative to surface upstream of Station 0)
α_T	Total turning angle of model (see Figs. 3, 5, and 7)
α_1	Initial turning angle of two-radii model (see Fig. 5)
α_2	Second turning angle of two-radii model (see Fig. 5)
β	Boundary layer flow thickness, defined as height of passage which will pass flow within equivalent step profile at Mach 1.0 and free-stream total pressure and temperature (see Figs. 51 and 52 and Eq. 17)
γ	Ratio of specific heats
δ	Boundary layer thickness, determined as the distance normal to the surface where $P_T/P_{T_O} = 0.95$
δ_O	Boundary layer thickness at curved-surface tangent point (Station 0)
δ^*	Boundary layer displacement thickness (see Fig. 10)
θ	Boundary layer momentum thickness (see Fig. 10)
θ_O	Boundary layer momentum thickness at curved-surface tangent point (Station 0)
$\Delta\theta_b$	Decrease in θ due to bleed (see Eq. 20)
$(\Delta\theta_b)_{MEASURED}$	Measured decrease in θ due to bleed (see Fig. 72)
$(\Delta\theta_b)_{THEORY}$	Theoretical maximum decrease in θ due to bleed (see Fig. 72 and Eq. 23)

R-1285-11

ρ Local density determined from P_S/P_P

ρ_ℓ Lag-length residual, $\left[\left(\frac{\ell}{\theta} \right)_{\text{MEASURED}} - \left(\frac{\ell}{\theta} \right)_{\text{Eq.(19),FIG.60}} \right]$

ρ_w Density determined from P_{S_W}/P_{T_O}

ρ' Ideal density determined from P_S/P_{T_O}

μ Viscosity evaluated from static temperature determined from V

λ Bypass angle (see Figs. 3 and 5)

Subscripts

1   Conditions at beginning of integration step (see Appendix II)

2   Conditions at end of integration step (see Appendix II)

APPENDIX I

Effect of Wall Temperature on Boundary Layer Characteristics

The literature contains a large amount of data which show the effect of wall temperature on boundary layer characteristics in flows having zero pressure gradient. For instance, in Ref. 32 it is shown that a decrease in wall temperature results in an increase in friction coefficient and a decrease in the boundary layer shape parameter, H, relative to the values obtained with an uncooled wall. Data on the effect of wall temperature on friction coefficient and reduced boundary layer shape parameter obtained from the tables in Refs. 32 and 41 are given in Figs. 77 and 78. For Mach numbers greater than zero, the values of G obtained from Refs. 32 and 41 for a ratio of wall temperature to insulated-wall temperature of unity are less than unity (i.e., values of H from Refs. 32 and 41 are less than those obtained from Ref. 31 and plotted in Fig. 13). This difference in G results from the assumption of a recovery factor of 0.9 for the tables in Refs. 32 and 41 as compared to a recovery factor of unity for the tables in Ref. 31.

For the case of a boundary layer flowing over a cooled wall, the energy distribution (total temperature distribution) within the boundary layer is determined by the rate at which energy is transferred to the wall and the rate at which energy is transferred to the boundary layer from the free stream. The rate of transfer of energy from the free stream into the boundary layer is much greater in an adverse pressure gradient than in zero pressure gradient because the rate of transfer of flow from the free stream into the boundary layer is much greater in the former case than in the latter. Therefore, the effect of wall temperature on friction coefficient and reduced boundary layer shape parameter in an adverse pressure gradient should be much less than that shown in Figs. 77 and 78 for zero pressure gradient.

The boundary layer momentum equation (Eq. 3) applies to cooled as well as uncooled boundary layers if actual local densities are employed in evaluating the boundary layer momentum and displacement thicknesses. If the use of a cooled wall has anywhere near as large an effect on G in an adverse pressure gradient as in zero pressure gradient (see Fig. 78), then the boundary layer growth in an adverse pressure gradient with cooling should, according to Figs. 42, 43, and 44 be much less than the boundary layer growth in an adverse pressure gradient without cooling. Therefore, determination of the effect of wall cooling on boundary layer characteristics in an adverse pressure gradient is extremely important.

As noted in the preceding paragraph, the effect of wall temperature on boundary layer characteristics is different in an adverse pressure gradient than in zero

pressure gradient because of the large influx of flow into the boundary layer in an adverse pressure gradient. One method of analyzing the problem of the determination of the effect of wall cooling on boundary layer characteristics in an adverse pressure gradient might be to adopt a step profile in which the total temperature of the step profile was a variable rather than a value assumed equal to free-stream total temperature. The total temperature within the equivalent step profile could then be determined by an energy balance at each station along the surface in the adverse pressure gradient.

R-1285-11

APPENDIX II

Development of Incremental Form of Boundary Layer Growth Equation

The differential form of the boundary layer growth equation, Eq. (12), is as follows:

$$d\theta = \frac{c_f}{2} dx - \theta J dM \tag{24}$$

Rearranging Eq. (24) yields

$$d\theta = \left(\frac{c_f}{2J} \frac{dx}{dM} - \theta \right) J dM \tag{25}$$

This equation is to be integrated over a finite change in Mach number. During this integration, c_f, dx/dM and J are assumed to be constant. Then

$$\frac{d\theta}{\theta - \frac{c_f}{2J} \frac{dx}{dM}} = -J dM \tag{26}$$

Integration of this equation yields

$$\ln \left(\theta - \frac{c_f}{2J} \frac{dx}{dM} \right) \Big|_{\theta_1}^{\theta_2} = -JM \Big|_{M_1}^{M_2} \tag{27}$$

42

$$\ell n \ \frac{\theta_2 - \dfrac{c_f}{2J}\dfrac{dx}{dM}}{\theta_1 - \dfrac{c_f}{2J}\dfrac{dx}{dM}} = -J(M_2 - M_1) = -J\Delta M \tag{28}$$

$$\frac{\theta_2 - \dfrac{c_f}{2J}\dfrac{dx}{dM}}{\theta_1 - \dfrac{c_f}{2J}\dfrac{dx}{dM}} = e^{J\Delta M} \tag{29}$$

Expanding the right side of Eq. (29) in a power series yields:

$$\frac{\theta_2 - \dfrac{c_f}{2J}\dfrac{dx}{dM}}{\theta_1 - \dfrac{c_f}{2J}\dfrac{dx}{dM}} = 1 + (-J\Delta M)\left[1 + \frac{(-J\Delta M)}{2} + \frac{(-J\Delta M)^2}{6} + \cdots\right] \tag{30}$$

$$\theta_2 - \frac{c_f}{2J}\frac{dx}{dM} = \theta_1 - \frac{c_f}{2J}\frac{dx}{dM} + \left(\frac{c_f}{2J}\frac{dx}{dM}(J\Delta M) - \theta_1 J\Delta M\right)\left[1 - \frac{J\Delta M}{2} + \frac{(J\Delta M)^2}{6} + \cdots\right] \tag{31}$$

$$\theta_2 - \theta_1 = \Delta\theta = \left(\frac{c_f}{2} \frac{dx}{dM} \Delta M - \theta_1 J \Delta M \right) \left[1 - \frac{J\Delta M}{2} + \frac{(J\Delta M)^2}{6} + \cdots \right] \qquad (32)$$

Since dx/dM has been assumed constant during a step,

$$\frac{dx}{dM} = \frac{\Delta x}{\Delta M} \qquad (33)$$

Equation (32) then becomes

$$\Delta\theta = \left(\frac{c_f}{2} \Delta x - \theta_1 J \Delta M \right) \left[1 - \frac{J\Delta M}{2} + \frac{(J\Delta M)^2}{6} + \cdots \right] \qquad (34)$$

Equation (34) is similar to Eq. (12) except for the second term on the right side of the equation, which is a term to be used when $\Delta\theta$ is an appreciable fraction of θ_1. For most calculations, Eq. (13), which is a reduced form of Eq. (34), contains enough terms.

$$\Delta\theta = \left(\frac{c_f}{2} \Delta x - \theta_1 J \Delta M \right) \left[1 - \frac{J\Delta M}{2} \right] \qquad (13)$$

44

CURVED-SURFACE MODEL CONFIGURATIONS AND TEST CONDITIONS

TABLE I

BLEED EMPLOYED	MODEL TYPE	NOMINAL TUNNEL MACH NUMBER, M_O	RADIUS OF CURVATURE, R OR R_1 - IN.	INITIAL TURNING OF CURVATURE, ANGLE, α_1 - DEG	SECOND RADIUS OF CURVATURE, R_2 - IN.	TOTAL TURNING ANGLE, α_T - DEG	PROFILES MEASURED AT SEVERAL STATIONS ALONG MODEL FOR FOLLOWING CONDITIONS AT STATION O		INCIPIENT SEPARATION DATA MEASURED FOR FOLLOWING CONDITIONS AT STATION O	
							θ_O - IN.	$R\theta_O$	θ_O - IN.	$R\theta_O$
NO	SINGLE-RADIUS TWO-DIMENSIONAL	2.0	6	—	—	20	0.0210,0.0220,0.0258	5670,5940,6970	—	—
		2.5	3	—	—	20	*0.0162	*3370	—	—
			6	—	—	20	*0.0140	*2915	—	—
			6	—	—	30	0.0143,0.0168,0.0195,0.0235	2980,3500,4060,4890	0.0268	5600
		3.0	3	—	—	20	*0.0136	*2160	—	—
			3	—	—	30			—	—
			6	—	—	20	0.0113,0.0170,0.0233	1797,2710,3720	0.0132	2100
			6	—	—	30	0.0105,0.0136,0.0160, 0.0188,0.0215	1680,2160,2540, 2990,3420	0.0222	3600
		3.5	3	—	—	30	0.0109	1340	—	—
			6	—	—	30	0.0115,0.0155	1410,1900	—	—
NO	TWO-RADII TWO-DIMENSIONAL	2.5	6	20	1.5	30	0.0139	2930	—	—
			6	20	3.0	30	0.0162,0.0198	3370,4120	—	—
		3.0	6	20	3.0	30	0.0173,0.0215,0.0235	2720,3420,3720	—	—
			6	20	1.5	35	0.0125,0.0150	2020,2380	—	—
			6	20	3.0	35	0.0110,0.0180,0.0198	1750,2840,3170	—	—
NO	AXISYMMETRIC	2.5	1.5	—	—	30	*0.0080	*1665	—	—
			3	—	—	20	*0.0098	*2040	—	—
			3	—	—	30	*0.0072,0.0130	*1500,2700	—	—
		3.0	1.5	—	—	30	*0.0056	*900	—	—
			3	—	—	30	*0.0049	*780	—	—
YES	SINGLE-RADIUS TWO-DIMENSIONAL	2.5	1.5	—	—	30	—	—	0.0152,0.0188, 0.020,0.0237	3180,3930, 4200,4950
			3	—	—	30	—	—	0.0200,0.0217, 0.0236	4180,4540, 4930
		3.0	1.5	—	—	30	—	—	0.0117,0.0133, 0.0154,0.0192, 0.0211	1660,2100, 2450,3050, 3350
			3	—	—	30	0.0228	3620	0.0132,0.0179, 0.0203,0.0218, 0.0219,0.0235, 0.0239	2100,2840, 3220,3460, 3480,3740, 3800

*INDICATES BOUNDARY LAYER TRIP BY SURFACE ROUGHNESS AIR TRIP USED FOR RUNS WITHOUT *

45

COMPARISON OF MEASURED VALUES OF LAG LENGTH
WITH VALUES COMPUTED FROM FITTED CURVE

$$\rho_{\ell} = (\ell/\theta)_{\text{MEASURED}} - (\ell/\theta)_{[\text{EQ.(19), FIG.60}]}$$

TYPE OF DATA	NUMBER OF POINTS, n	AVERAGE LAG-LENGTH RESIDUAL, $\Sigma\rho_{\ell}/n$
ALL	149	0
SINGLE-RADIUS TWO-DIMENSIONAL MODELS	82	−2.9
TWO-RADII TWO-DIMENSIONAL MODELS	44	+4.0
AXISYMMETRIC MODELS	23	+2.7
$\bar{R}/\theta_0$ FROM 0 TO 250	40	+3.0
$\bar{R}/\theta_0$ FROM 250 − 300	39	−3.8
$\bar{R}/\theta_0$ FROM 300 − 400	36	−0.8
$\bar{R}/\theta_0$ FROM 400 − 700	34	+1.8
$M_0 = 2.0$	11	−3.3
$M_0 = 2.5$	52	−1.4
$M_0 = 3.0$	74	+3.9
$M_0 = 3.5$	12	−15.3

TEST-SECTION CONFIGURATION WITH TWO-DIMENSIONAL CURVED-SURFACE MODEL INSTALLED

M_0	L_1-IN.	h-IN.
2.0	7.55	2.25
2.5	6.40	2.50
3.0	9.40	2.00
3.5	7.40	2.25

TEST-SECTION WIDTH = 4.5 IN.

MOVABLE PLATES FOR TUNNEL DIFFUSER

BLEED FLOW

BOUNDARY LAYER PROBE

TEST MODEL

BLEED PLENUM

h

NOZZLE BLOCK

L_1

4.31 IN.

150 INJECTION HOLES (0.020-IN. DIA) IN 13 ROWS

INJECTION PLENUM

VALVE FOR CONTROLLING PRESSURE IN INJECTION PLENUM

AIRFLOW

CENTERLINE BLOCK

FIG. 2
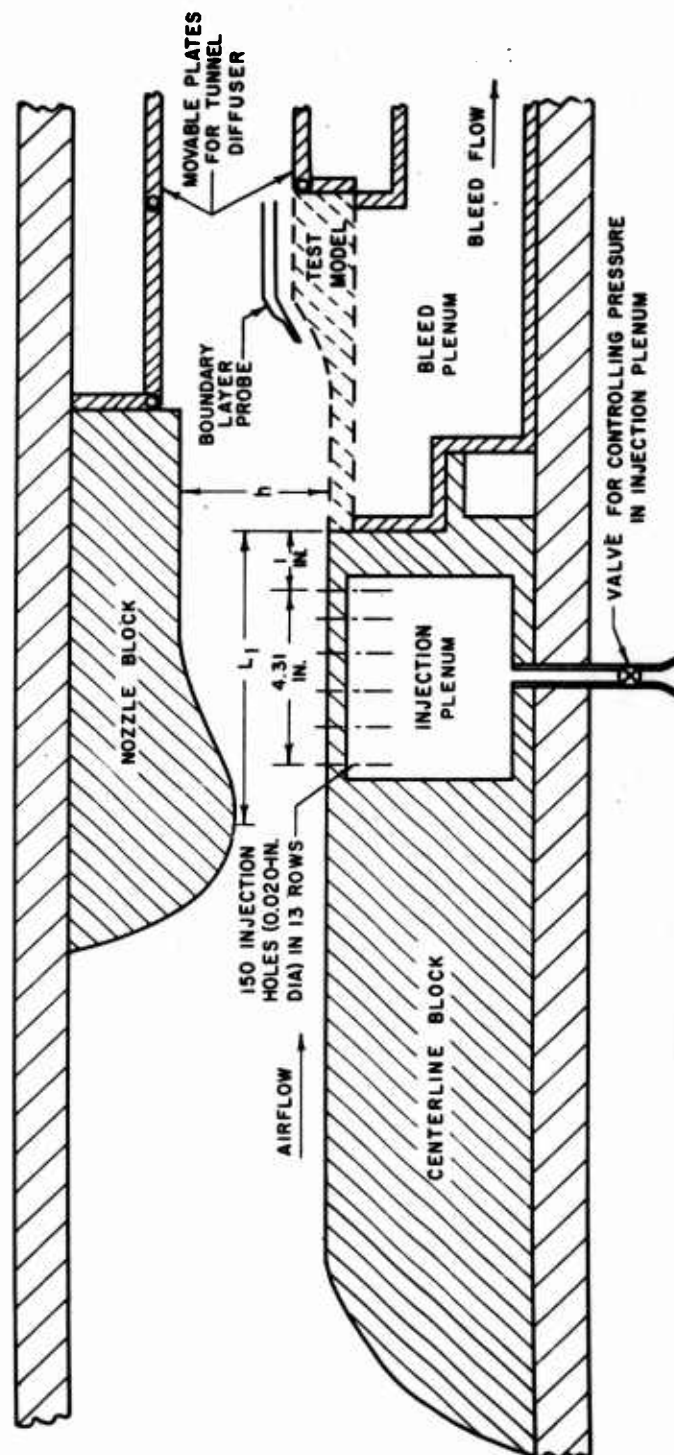
PHOTOGRAPH OF TEST-SECTION CONFIGURATION WITH TWO-DIMENSIONAL
CURVED-SURFACE MODEL INSTALLED
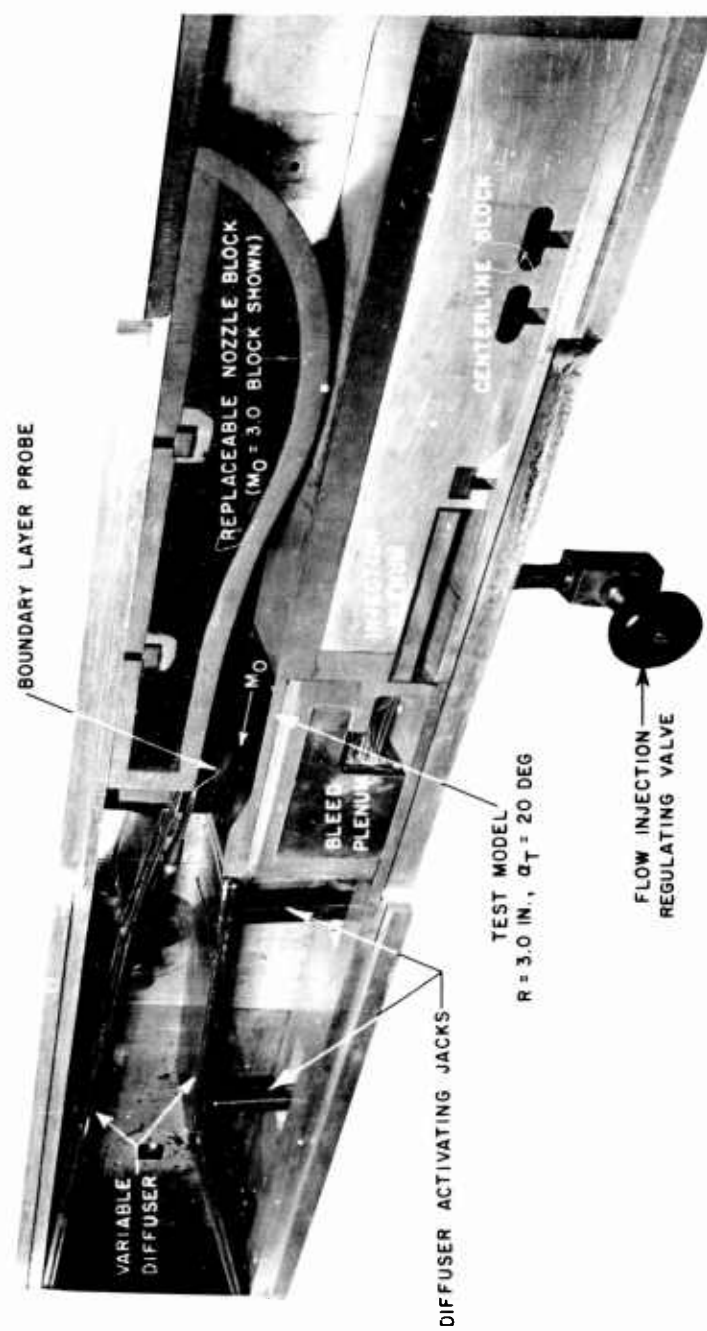
BOUNDARY LAYER PROBE

REPLACEABLE NOZZLE BLOCK
(M_O = 3.0 BLOCK SHOWN)

CENTERLINE BLOCK

M_O

BLEED PLENUM

TEST MODEL
R = 3.0 IN., α_T = 20 DEG

VARIABLE DIFFUSER

DIFFUSER ACTIVATING JACKS

FLOW INJECTION
REGULATING VALVE

SINGLE – RADIUS TWO-DIMENSIONAL CURVED – SURFACE MODELS
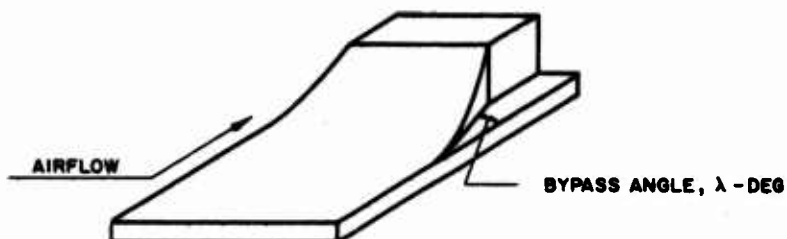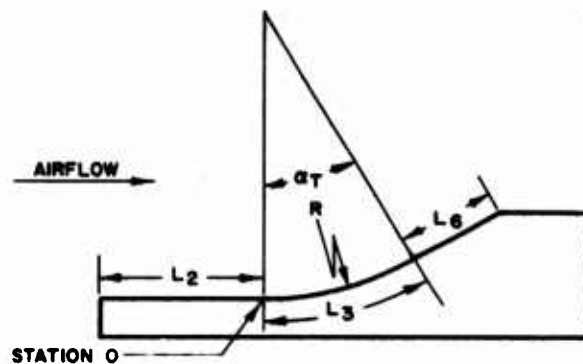
RADIUS OF CURVATURE, R-IN.	TOTAL TURNING ANGLE, α_T-DEG	L_2-IN.	L_3-IN.	L_6-IN.	PROVISIONS FOR BLEED	NUMBER OF ROWS OF BLEED HOLES *	NUMBER OF BLEED HOLES *	VALUE OF BYPASS ANGLE, λ-DEG
1.5	30	5.02	0.78	1.00	YES	10	264	5
3.0	20	4.60	1.05	1.00	NO	—	—	0
3.0	30	4.48	1.57	0.65	YES	21	580	5
6.0	20	4.00	2.09	0.20	NO	—	—	0
6.0	30	3.12	3.14	0.20	NO	—	—	0,5,20

* HOLES PLUGGED FLUSH WITH SURFACE FOR
TESTS WITHOUT BOUNDARY LAYER BLEED

49

FIG. 4

PHOTOGRAPH OF SINGLE-RADIUS TWO-DIMENSIONAL CURVED-SURFACE MODELS

R=6 IN. α_T = 20 DEG

R=6 IN. α_T = 30 DEG

STATIC PRESSURE TAPS

REMOVABLE BYPASS WEDGES

R=3 IN. α_T = 20 DEG

R=3 IN. α_T = 30 DEG

R=1.5 IN. α_T = 30 DEG

BLEED HOLES (SHOWN FILLED)

INCHES
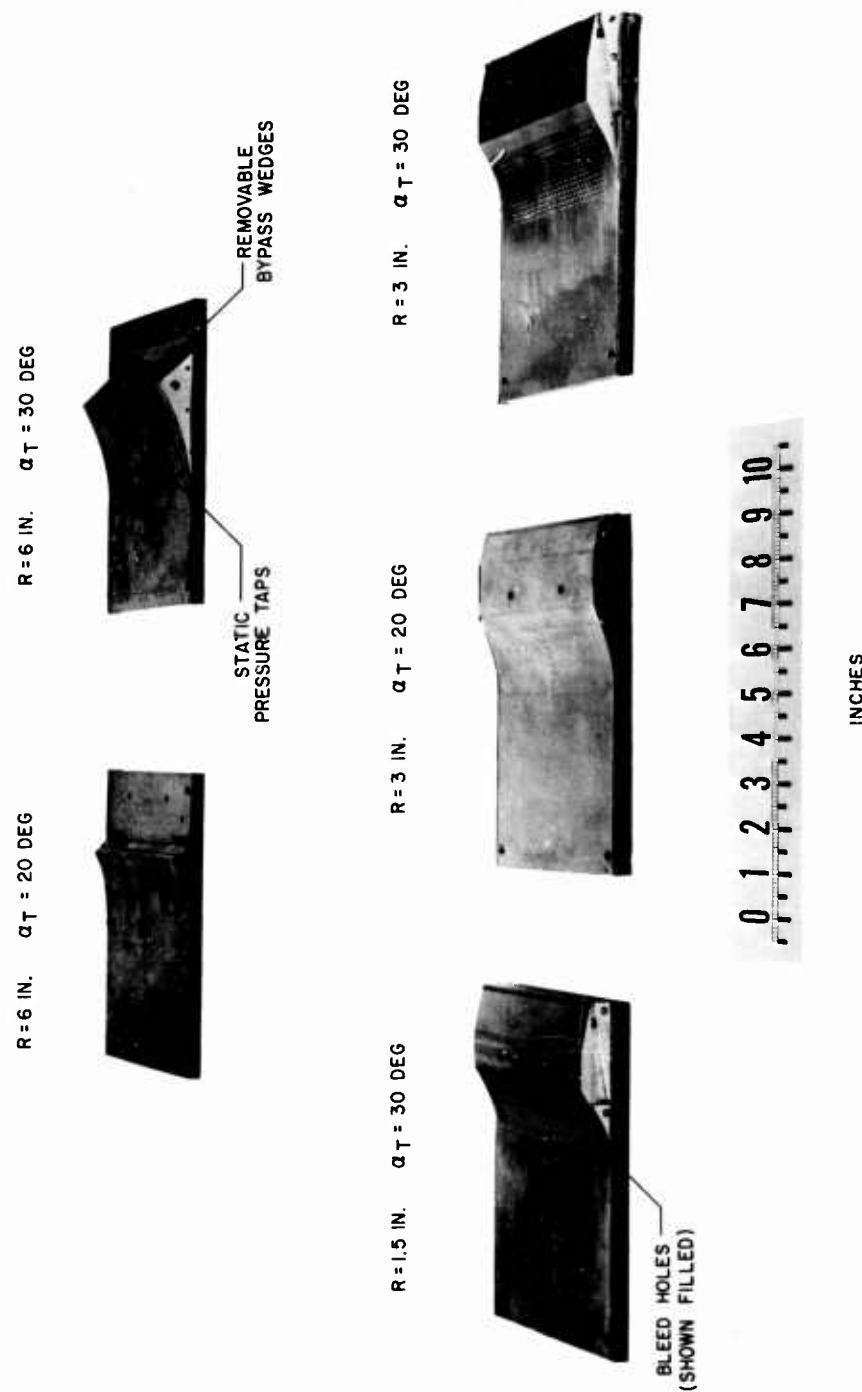
TWO-RADII TWO-DIMENSIONAL CURVED-SURFACE MODELS
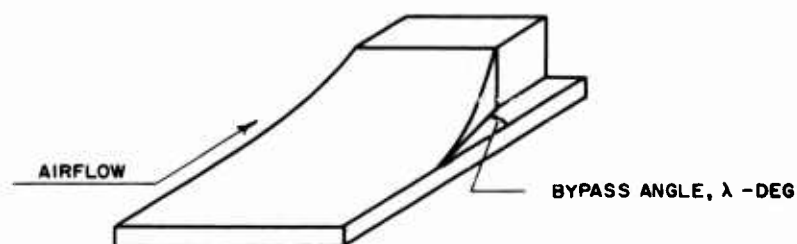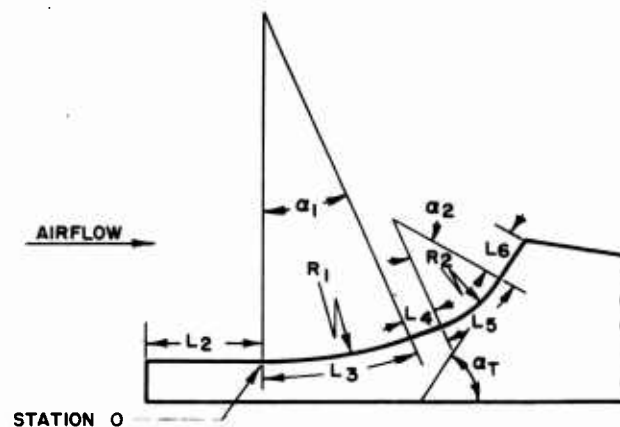
INITIAL RADIUS OF CURVATURE, R_1 – IN.	SECOND RADIUS OF CURVATURE, R_2 – IN.	INITIAL TURNING ANGLE, α_1 – DEG	SECOND TURNING ANGLE, α_2 – DEG	TOTAL TURNING ANGLE, α_T – DEG	L_2 – IN.	L_3 – IN.	L_4 – IN.	L_5 – IN.	L_6 – IN.	VALUE OF BYPASS ANGLE, λ – DEG
6	1.5	20	10	30	4.0	2.09	0.20	0.26	0.70	5
6	1.5	20	15	35	4.0	2.09	0.20	0.39	0.50	5
6	3.0	20	10	30	4.0	2.09	0.20	0.52	0.50	5
6	3.0	20	15	35	4.0	2.09	0.20	0.78	0.30	5

PHOTOGRAPH OF TWO-RADII TWO-DIMENSIONAL CURVED-SURFACE MODELS

EXTENSION PIECE
$R_2 = 1.5$ IN. $\alpha_T = 30$ DEG

TWO-RADII MODEL
$R_1 = 6$ IN. $\alpha_1 = 20$ DEG
$R_2 = 3$ IN. $\alpha_T = 30$ DEG

STATIC PRESSURE
TAP LEADS

0 1 2 3 4 5 6 7 8 9 10

INCHES

AXISYMMETRIC CURVED-SURFACE MODELS
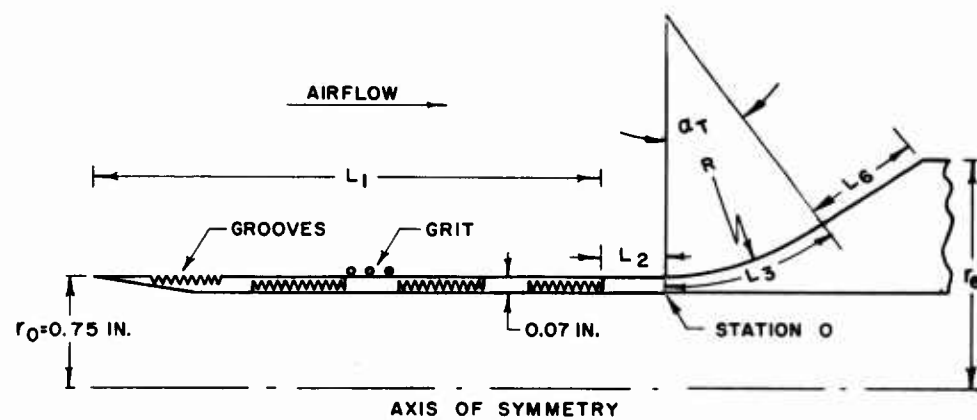
RADIUS OF CURVATURE, R-IN.	TOTAL TURNING ANGLE, α_T-DEG	M_0		L_1-IN.	L_2-IN.	L_3-IN.	L_6-IN.	MAXIMUM RADIUS OF MODEL, r_e-IN.
		2.5	3.0					
1.5	30	3.88	3.88	1.00	0.78	0.46	1.20	
3.0	20	4.38	—	1.00	1.05	0.80	1.20	
3.0	30	3.88,6.38	3.88	1.00	1.57	0.40	1.40	

FIG. 8

PHOTOGRAPH OF AXISYMMETRIC CURVED-SURFACE MODELS

R=3 IN. α_T = 30 DEG

R=3 IN. α_T = 20 DEG

R=1.5 IN. α_T = 30 DEG

STATIC PRESSURE
TAP LEADS

SURFACE ROUGHNESS
BOUNDARY LAYER TRIP

MODEL SUPPORT (ATTACHES
TO TUNNEL SIDE WALL)

SMOOTH LEADING EDGE

PERFORATED FRONT
EXTENSION PIECE

GROOVED LEADING
EDGE
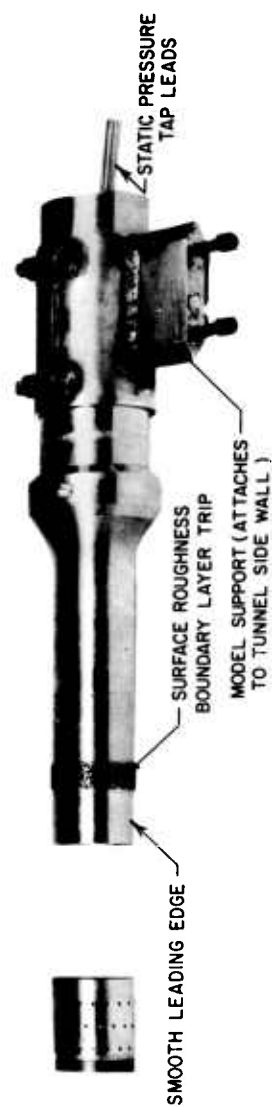
0 1 2 3 4 5 6 7 8 9 10

INCHES

EXAMPLE OF PRESSURE DISTRIBUTION IN SUPERSONIC TURBULENT BOUNDARY LAYER HAVING LARGE STATIC PRESSURE GRADIENT NORMAL TO WALL

ORDER OF DETERMINING PRESSURES

$$\frac{P_P}{P_{T_0}} \rightarrow \frac{P_{S_f}}{P_{T_0}}; \frac{P_{S_f}}{P_{T_0}} \text{ AND } \frac{P_{S_W}}{P_{T_0}} \rightarrow \frac{P_S}{P_{T_0}}; \frac{P_S}{P_{T_0}} \text{ AND } \frac{P_P}{P_{T_0}} \rightarrow \frac{P_T}{P_{T_0}}$$

DISTANCE NORMAL TO SURFACE OF MODEL, y – IN.
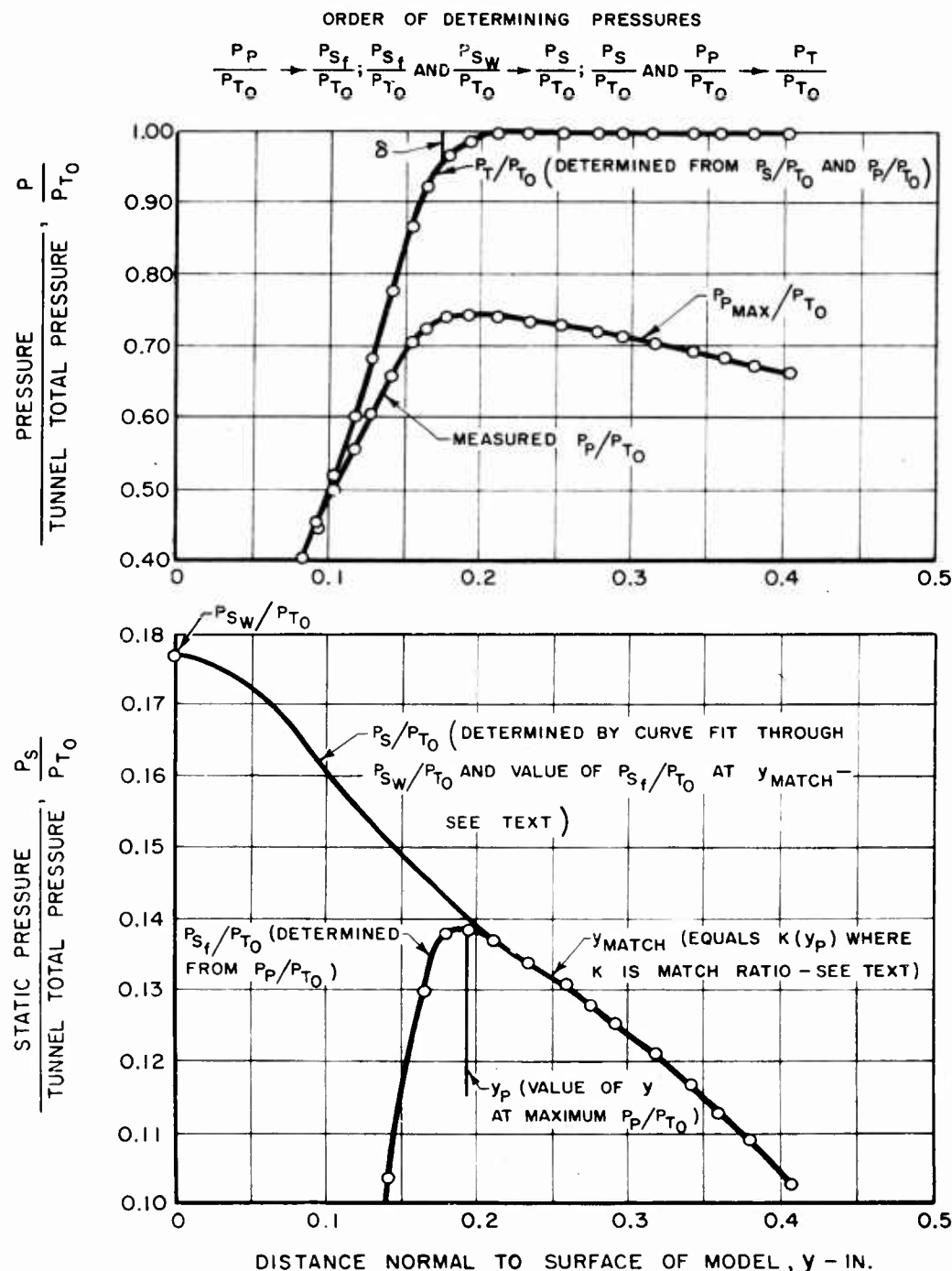
EXAMPLE OF MASS FLOW AND MOMENTUM FUNCTIONS FOR BOUNDARY LAYER HAVING LARGE STATIC PRESSURE GRADIENT NORMAL TO WALL

TOTAL TEMPERATURE ASSUMED CONSTANT THROUGHOUT BOUNDARY LAYER

$\rho' u'$, IDEAL MASS FLOW PER UNIT AREA CALCULATED FROM P_S/P_{T_O}

$\rho_W V$, IDEAL MASS FLOW PER UNIT AREA CALCULATED FROM P_{S_W}/P_{T_O}

δ

y_{MATCH}

ρu, ACTUAL MASS FLOW PER UNIT AREA CALCULATED FROM P_S/P_P

MASS FLOW PER UNIT AREA,

$$\rho_W V \delta^* = \int_0^\delta \rho' u' \, dy - \int_0^\delta \rho u \, dy$$

δ^*

$\rho' u'^2$, IDEAL MOMENTUM PER UNIT AREA CALCULATED FROM P_S/P_{T_O}

$\rho_W V^2$, IDEAL MOMENTUM PER UNIT AREA CALCULATED FROM P_{S_W}/P_{T_O}

$\rho u u'$, ACTUAL MASS FLOW PER UNIT AREA CALCULATED FROM P_{S_L}/P_{P_L} AND MULTIPLIED BY IDEAL VELOCITY CALCULATED FROM P_S/P_{T_O}

δ

y_{MATCH}

ρu^2, ACTUAL MOMENTUM PER UNIT AREA CALCULATED FROM P_S/P_P

MOMENTUM PER UNIT AREA

$$\rho_W V \theta = \int_0^\delta \rho u (u' - u) \, dy$$

θ

DISTANCE NORMAL TO SURFACE OF MODEL, y – IN.

56

TYPICAL WALL STATIC PRESSURE DISTRIBUTIONS
ON REFERENCE FLAT PLATE

$M_0 = 3.0$ $P_{IP}/P_{T_0} = 0.10$ $W_b = 0$

ADDITIONAL DATA FOR THIS MODEL FOUND IN FIGS. 12 AND 14

STATIC PRESSURE DISTRIBUTION ACROSS PLATE, X = 15.6 IN.

LEFT SIDE WALL
LOOKING DOWNSTREAM   DISTANCE ACROSS MODEL, Z-IN.   RIGHT SIDE WALL
LOOKING DOWNSTREAM

WALL STATIC PRESSURE / TUNNEL TOTAL PRESSURE $\dfrac{P_{Sw}}{P_{T_0}}$

CENTERLINE STATIC PRESSURE DISTRIBUTION

RANGE OF TANGENT POINTS (STATION 0) FOR
TWO-DIMENSIONAL CURVED-SURFACE MODELS

DISTANCE FROM TUNNEL NOZZLE THROAT, X-IN.
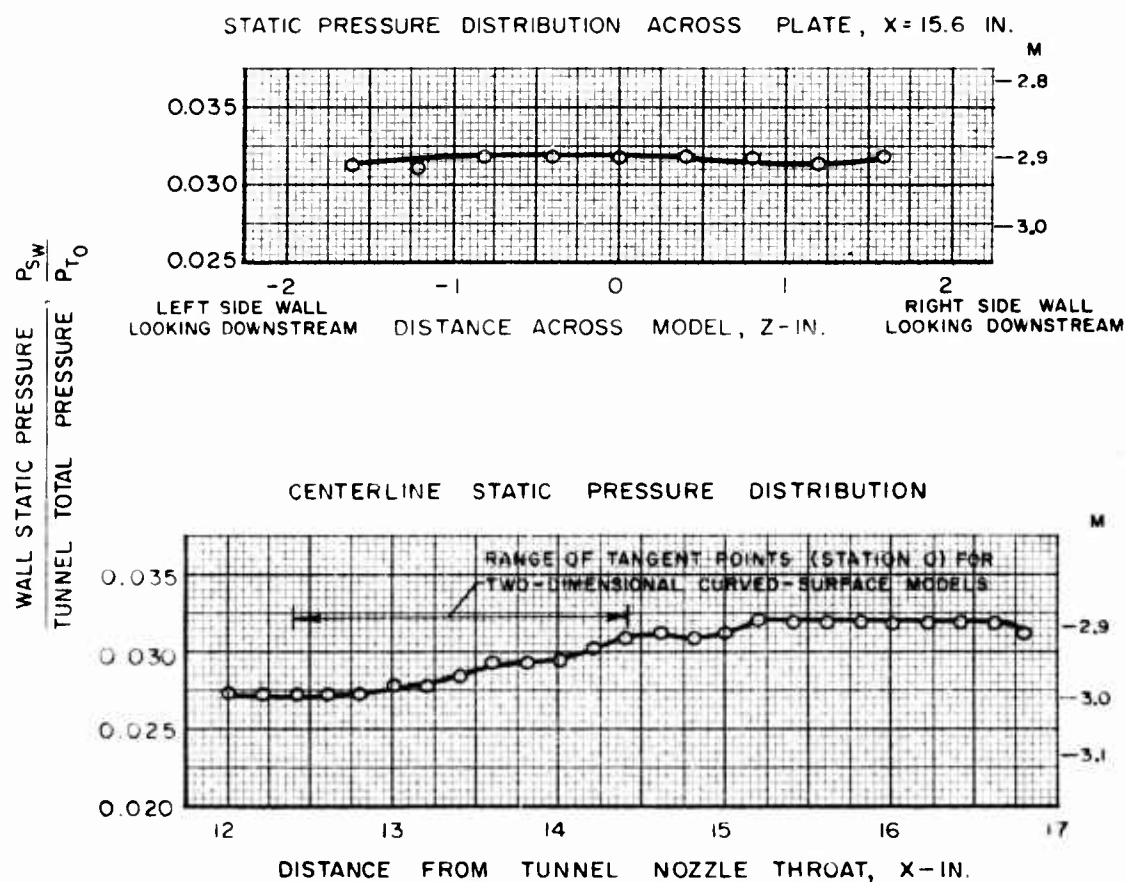
TYPICAL BOUNDARY LAYER CHARACTERISTICS
FOR REFERENCE FLAT PLATE

$M_O = 3.0$ $P_{IP}/P_{TO} = 0.10$

ADDITIONAL DATA FOR THIS MODEL FOUND IN FIGS. II AND I4

BOUNDARY LAYER SHAPE PARAMETER FOR 1/7-POWER PROFILE

TOTAL TEMPERATURE ASSUMED CONSTANT THROUGHOUT BOUNDARY LAYER
DATA FROM REF. 31

$\gamma = 7/5$
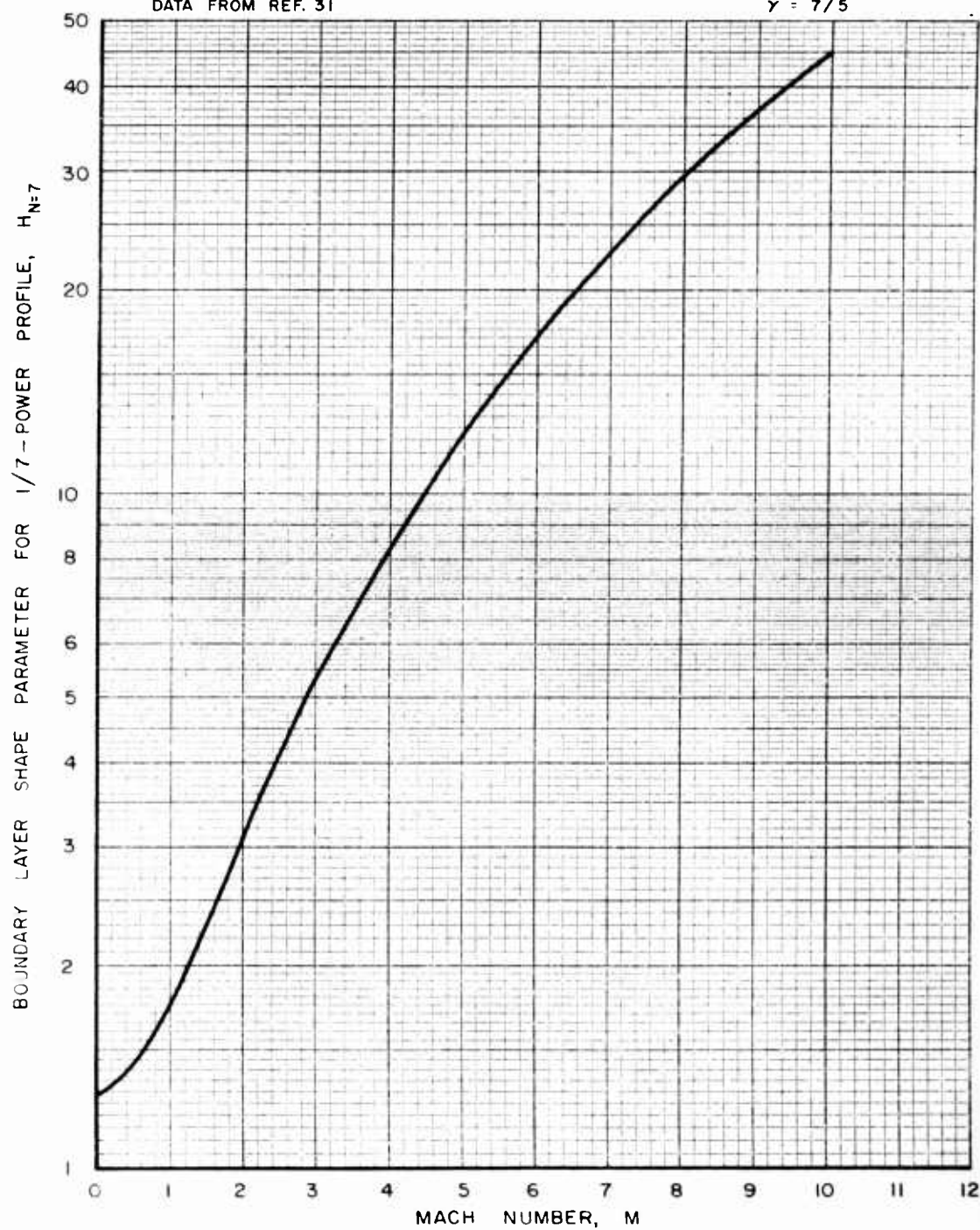
TYPICAL VALUES OF REDUCED BOUNDARY LAYER
SHAPE PARAMETER FOR REFERENCE FLAT PLATE

$M_0 = 3.0$ $P_{IP}/P_{T_0} = 0.10$

ADDITIONAL DATA FOR THIS MODEL FOUND IN FIGS. 11 AND 12

FIG. 15
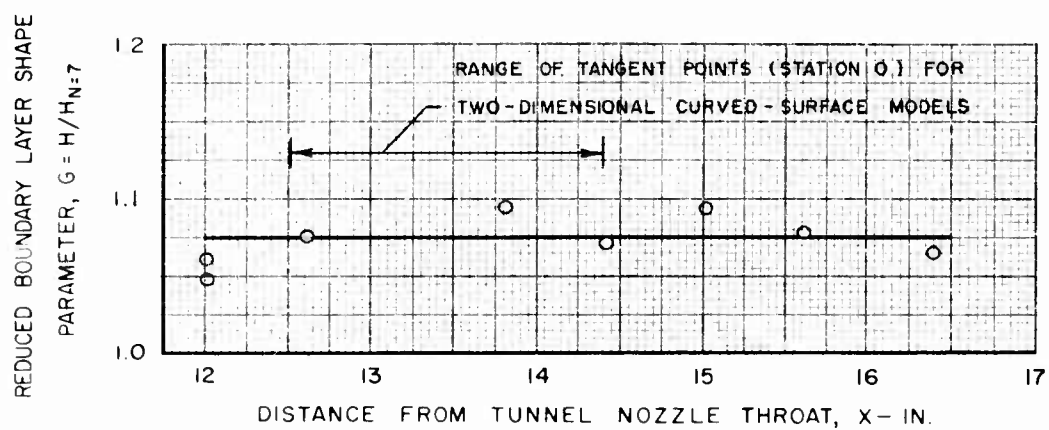
EFFECT OF AIR INJECTION ON BOUNDARY LAYER THICKNESS FOR REFERENCE FLAT PLATE
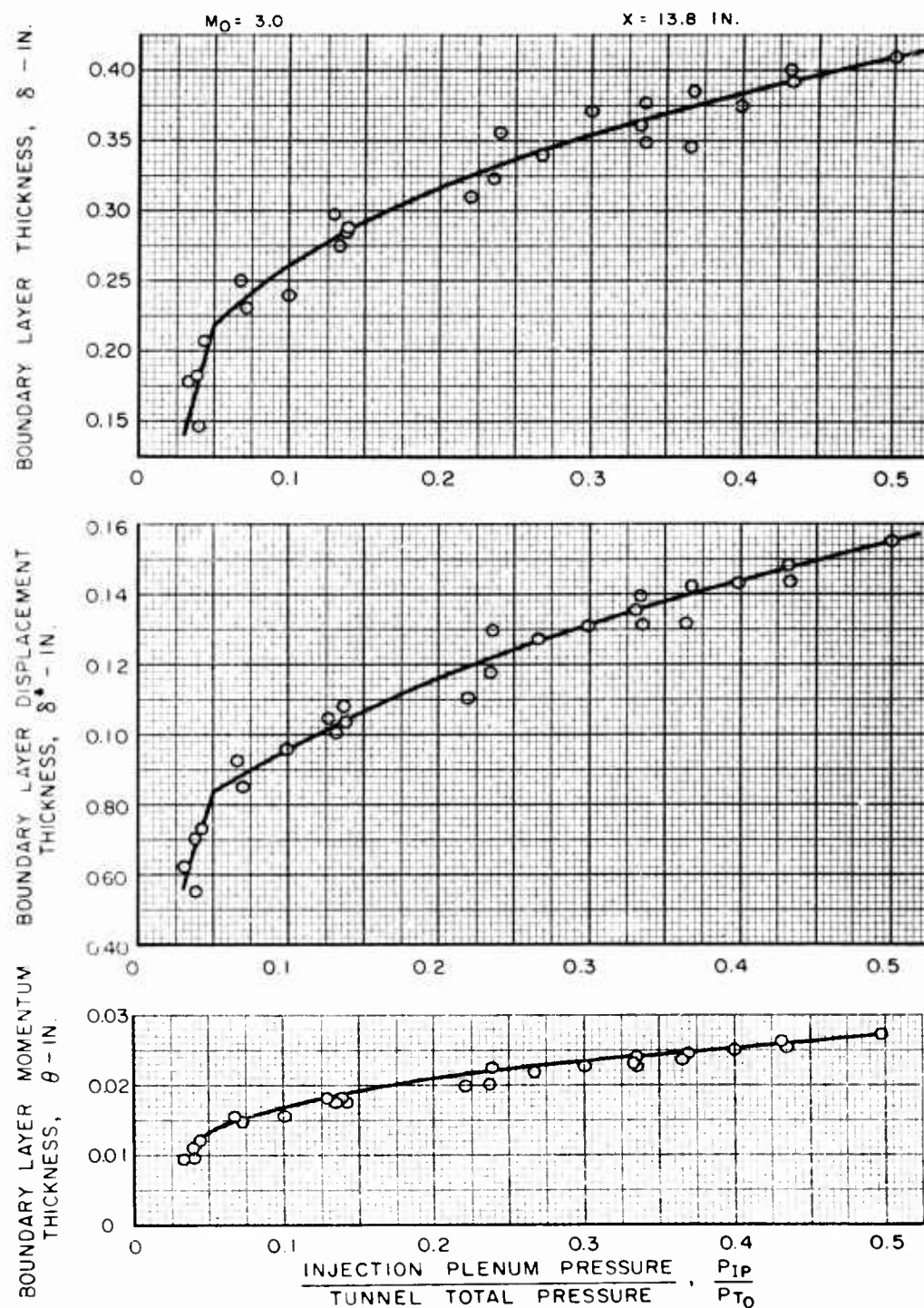
EFFECT OF AIR INJECTION ON BOUNDARY LAYER
SHAPE PARAMETER FOR REFERENCE FLAT PLATE

$M_O = 3.0$ $X = 13.8$ IN.

FIG.17
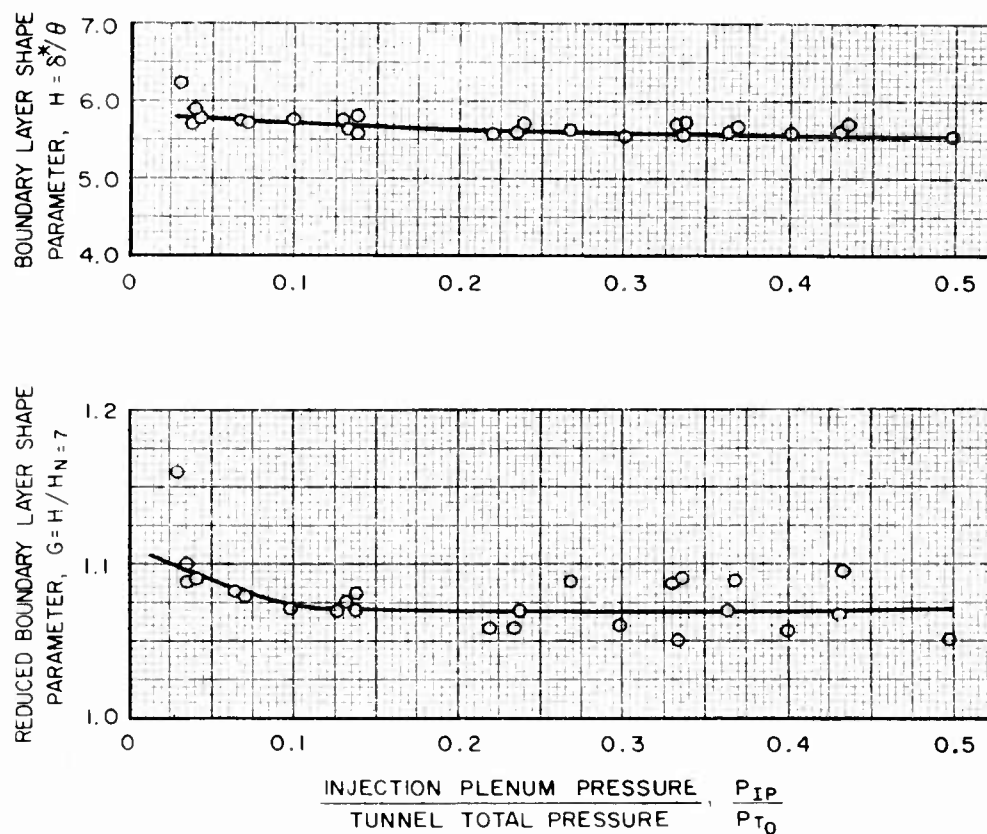
EFFECT OF AIR INJECTION ON BOUNDARY LAYER VELOCITY PROFILES FOR REFERENCE FLAT PLATE

$M_O = 3.0$ $X = 12.5$ IN.

SYMBOL	P_{IP}/P_{TO}	θ_O – IN.	δ_O – IN.	H	G	$R_{\theta O}$
O	0.038	0.0105	0.17	5.877	1.113	1680
□	0.137	0.0160	0.30	5.690	1.076	2540
◇	0.235	0.0188	0.31	5.644	1.092	2990
△	0.333	0.0215	0.33	5.671	1.084	3420
D	0.398	0.0244	0.37	5.662	1.089	3880
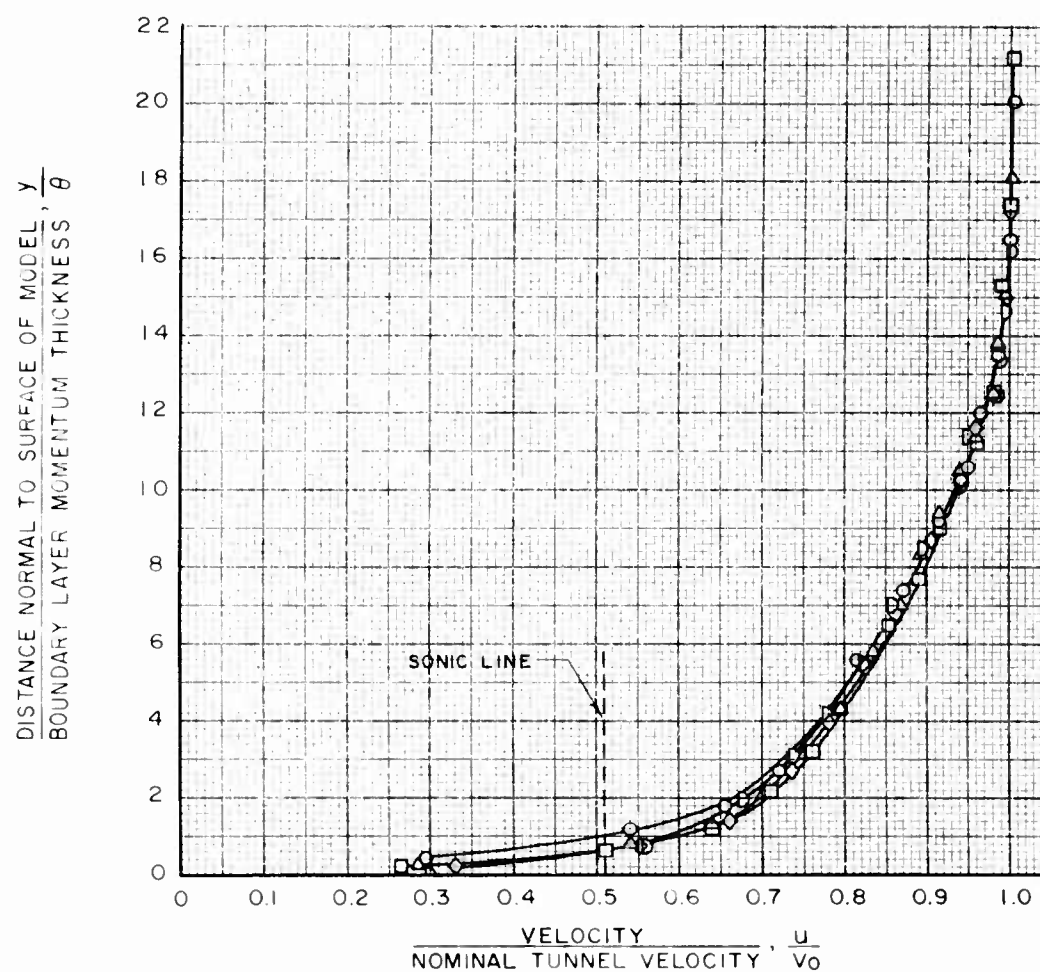
FIG.18

EFFECT OF REYNOLDS NUMBER ON REDUCED BOUNDARY LAYER SHAPE PARAMETER FOR REFERENCE FLAT PLATE

FIG. 19
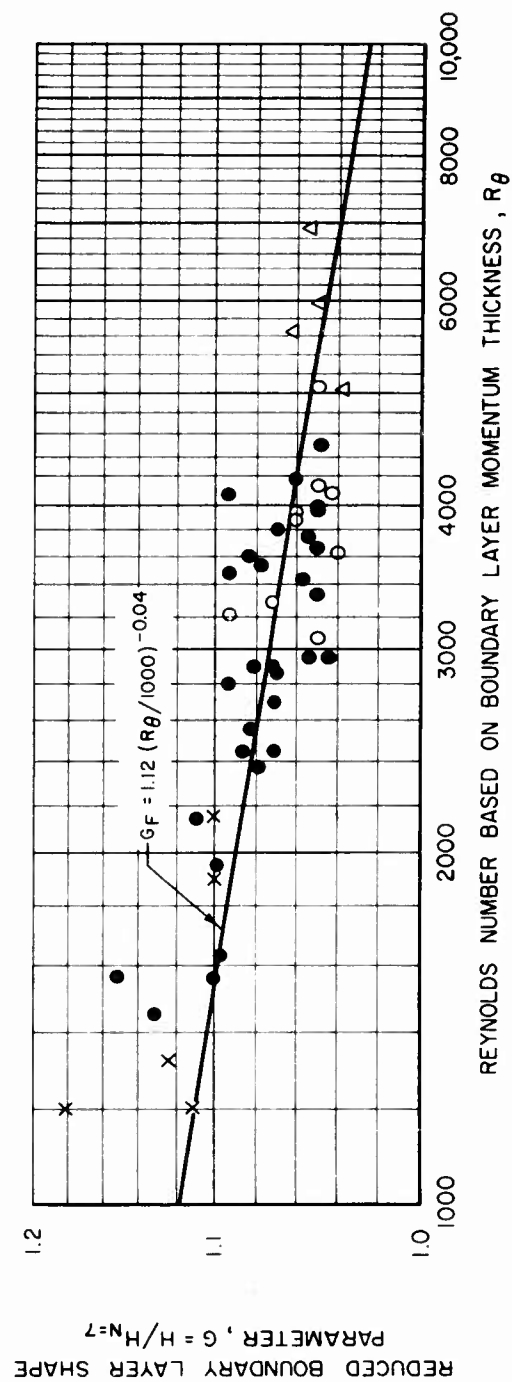
TYPICAL SCHLIEREN PHOTOGRAPHS OF SINGLE – RADIUS
TWO – DIMENSIONAL CURVED – SURFACE MODEL

$M_O = 3$ $R = 6$ IN. $a_T = 30$ DEG $W_b = 0$

$\theta_O = 0.0096$ IN. $R_{\theta_O} = 1530$ $\delta_O = 0.17$ IN.
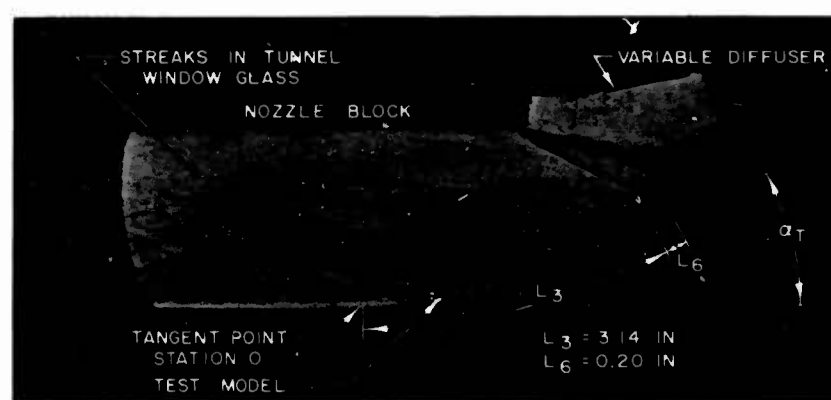
$\theta_O = 0.0205$ IN. $R_{\theta_O} = 3260$ $\delta_O = 0.35$ IN.

TYPICAL WALL STATIC PRESSURE DISTRIBUTIONS
ON SINGLE-RADIUS TWO-DIMENSIONAL
CURVED-SURFACE MODEL

$M_O = 3.0$ $R = 6$ IN. $\alpha_T = 30$ DEG $W_b = 0$

ADDITIONAL DATA FOR THIS MODEL FOUND IN FIGS. 21,22,23,24,46,53,55,62, AND 68
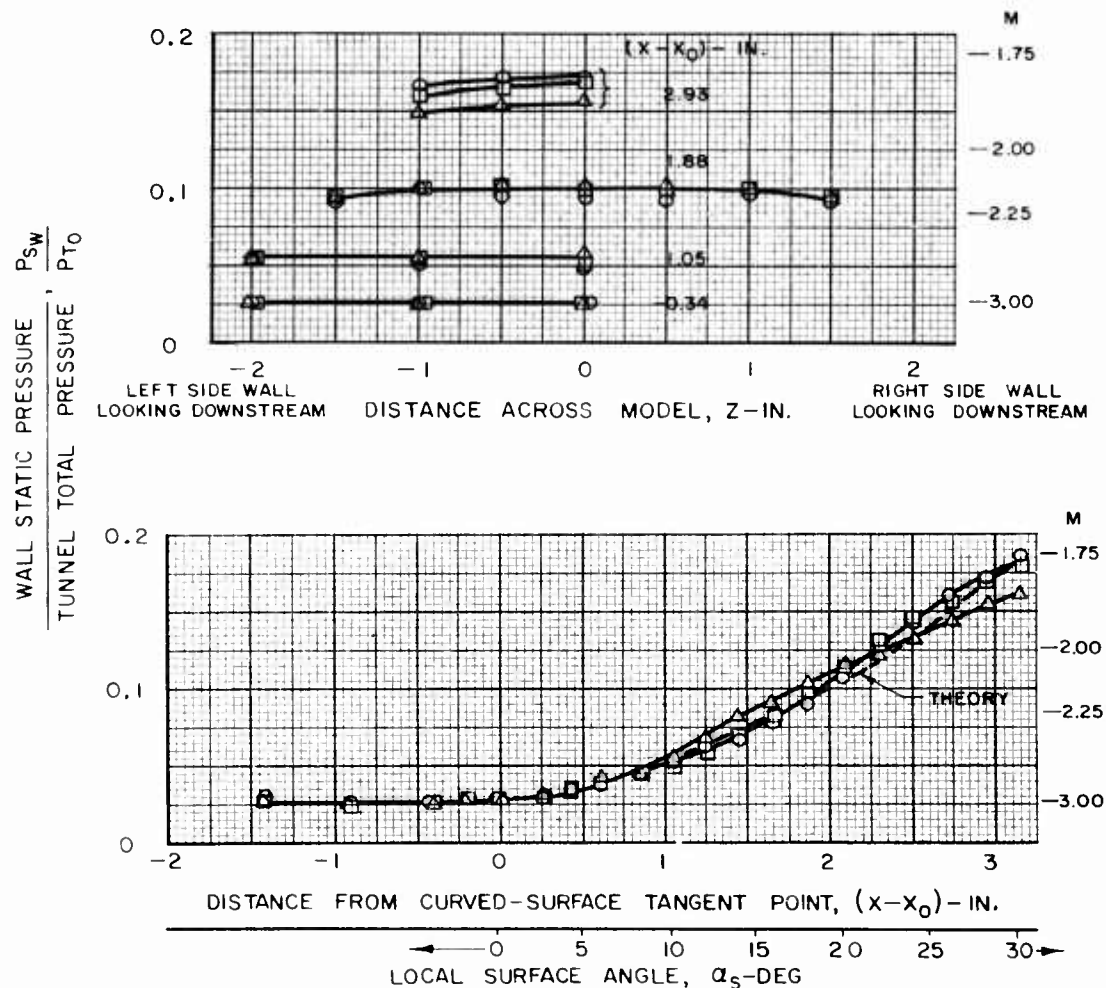
SYMBOL	θ_O-IN.	δ_O-IN.	R_{θ_O}
O	0.0105	0.17	1680
□	0.0160	0.30	2540
△	0.0215	0.33	3420

TYPICAL VARIATION OF MACH NUMBER WITH DISTANCE ALONG SINGLE–RADIUS TWO–DIMENSIONAL CURVED–SURFACE MODEL

$M_O = 3.0$ $R = 6$ IN. $\alpha_T = 30$ DEG $W_b = 0$

ADDITIONAL DATA FOR THIS MODEL FOUND IN FIGS. 20, 22, 23, 24, 46, 53, 55, 62, AND 68

M IS MACH NUMBER DETERMINED FROM P_{S_W}/P_{T_O}

M_δ IS MACH NUMBER AT OUTSIDE EDGE OF BOUNDARY LAYER

SYMBOL	θ_O - IN	δ_O - IN	R_{θ_O}
O	0.0105	0.17	1680
□	0.0160	0.30	2540
△	0.0215	0.33	3420

MACH NUMBER, M OR M_δ

MEASURED M_δ

THEORETICAL M

MEASURED M

DISTANCE FROM CURVED–SURFACE TANGENT POINT, $(X - X_O)$ – IN.

0   5   10   15   20   25   30

LOCAL SURFACE ANGLE, α_S – DEG

67
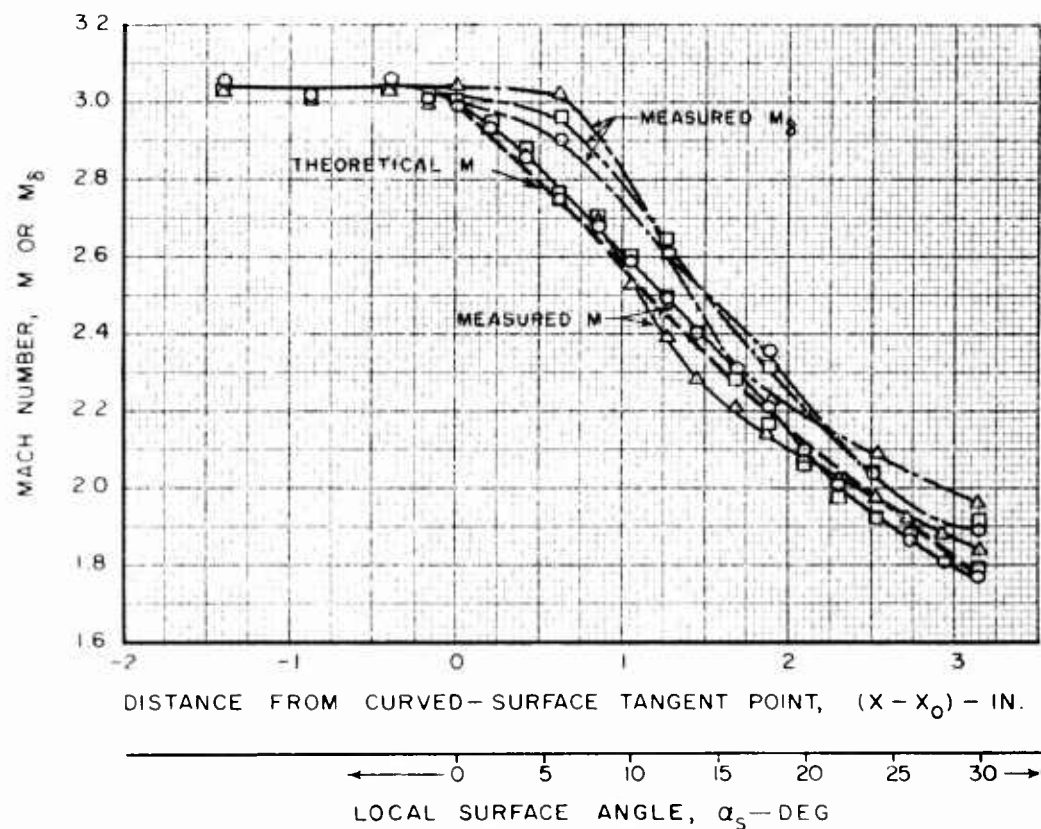
TYPICAL BOUNDARY LAYER VELOCITY PROFILES FOR SINGLE-RADIUS TWO-DIMENSIONAL CURVED-SURFACE MODEL

$M_O = 3.0$ $R = 6$ IN $\alpha_T = 30$ DEG $w_b = 0$

$\theta_O = 0.0160$ IN. $R_{\theta_O} = 2540$

ADDITIONAL DATA FOR THIS MODEL FOUND IN FIGS. 20,21,23,24,46,53,55,62, AND 68

SYMBOL	α_S-DEG	$(x-x_0)$-IN.	θ-IN	δ-IN.	G	M	M_δ
D	0	0	0.0160	0.30	1.08	3.01	3.01
◇	6	0.63	0.0161	0.24	1.15	2.76	3.00
◹	12	1.25	0.0187	0.24	1.15	2.49	2.68
○	18	1.88	0.0200	0.21	1.20	2.17	2.32
□	24	2.51	0.0229	0.24	1.15	1.93	2.04
△	30	3.14	0.0291	0.30	1.12	1.79	1.90

FIG.23
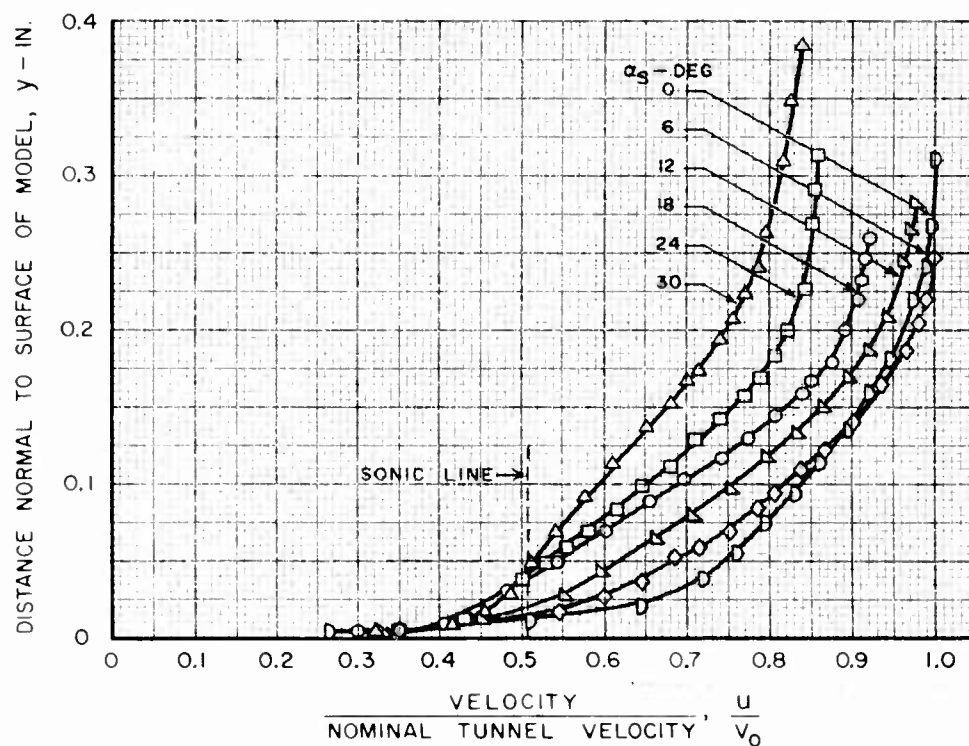
EFFECT OF APPROACH BOUNDARY LAYER THICKNESS ON VELOCITY PROFILES AT DOWNSTREAM END OF ADVERSE PRESSURE GRADIENT FOR SINGLE–RADIUS TWO–DIMENSIONAL CURVED–SURFACE MODEL

$M_O = 3.0$ $R = 6$ IN. $\alpha_S = \alpha_T = 30$ DEG

$W_b = 0$ $X - X_O = 3.14$ IN.

ADDITIONAL DATA FOR THIS MODEL FOUND IN FIGS. 20, 21, 22, 24, 46, 53, 55, 62, AND 68

	CONDITIONS AT STATION O			CONDITIONS AT α_S = 30 DEG			
SYMBOL	δ_O – IN	θ_O – IN.	$R\theta_O$	δ – IN	θ – IN.	G	M
O	0.17	0.0105	1680	0.20	0.0190	1.07	1.76
□	0.30	0.0160	2540	0.30	0.0291	1.12	1.79
△	0.33	0.0215	3420	0.34	0.0380	1.18	1.84
D *	0.37	0.0244	3880	0.31	0.0345	1.25	1.88
▽*	0.43	0.0264	4200	0.33	0.0351	1.28	1.89

*BOUNDARY LAYER SEPARATED NEAR α_S = 15 DEG

SONIC LINE

θ_O – IN.
0.0105
0.0160
0.0215
0.0244
0.0264

DISTANCE NORMAL TO SURFACE OF MODEL, $\frac{y}{\theta}$
BOUNDARY LAYER MOMENTUM THICKNESS

$\frac{\text{VELOCITY}}{\text{NOMINAL TUNNEL VELOCITY}}, \frac{u}{V_O}$
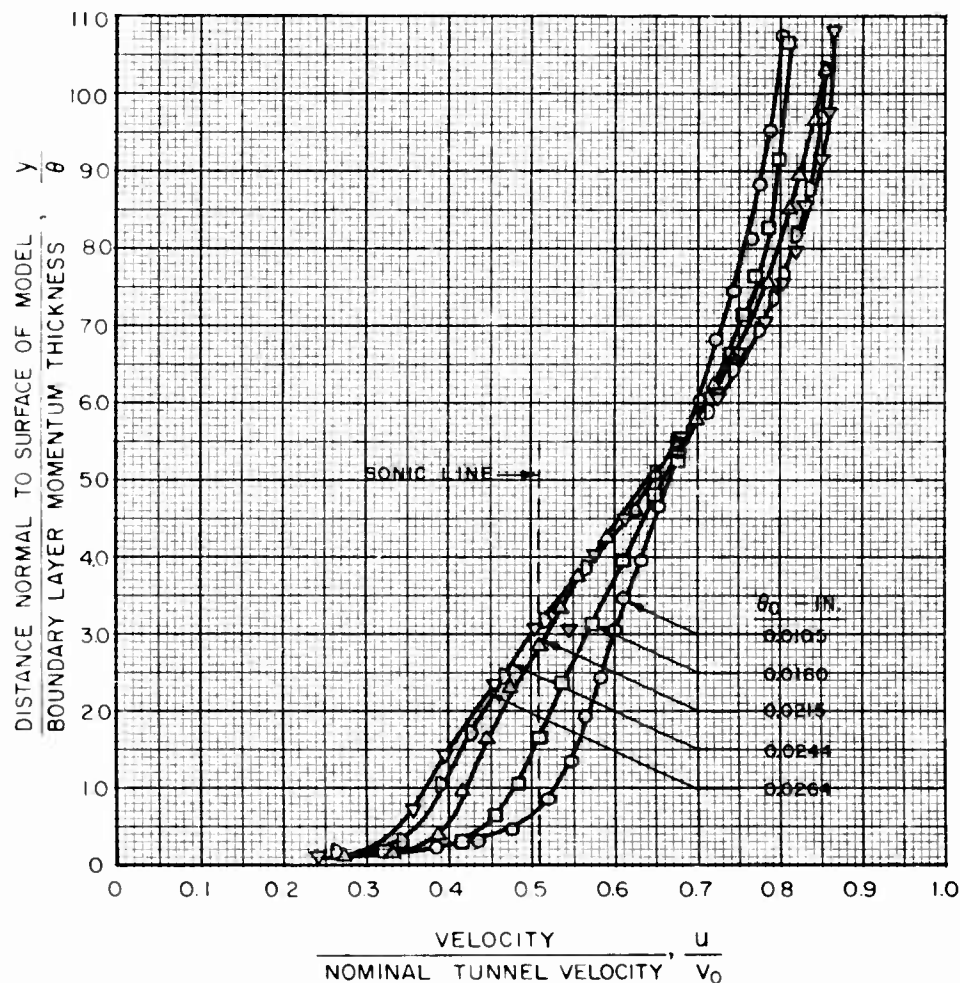
TYPICAL BOUNDARY LAYER CHARACTERISTICS FOR SINGLE-RADIUS TWO-DIMENSIONAL CURVED-SURFACE MODEL

$M_0 = 3.0$ $R = 6$ IN $\alpha_T = 30$ DEG $W_b = 0$

ADDITIONAL DATA FOR THIS MODEL FOUND IN FIGS. 20, 21, 22, 23, 46, 53, 55, 62, AND 68

SYMBOL	θ_0-IN	δ_0-IN	R_{θ_0}
O	0.0105	0.17	1680
□	0.0160	0.30	2540
△	0.0215	0.33	3420
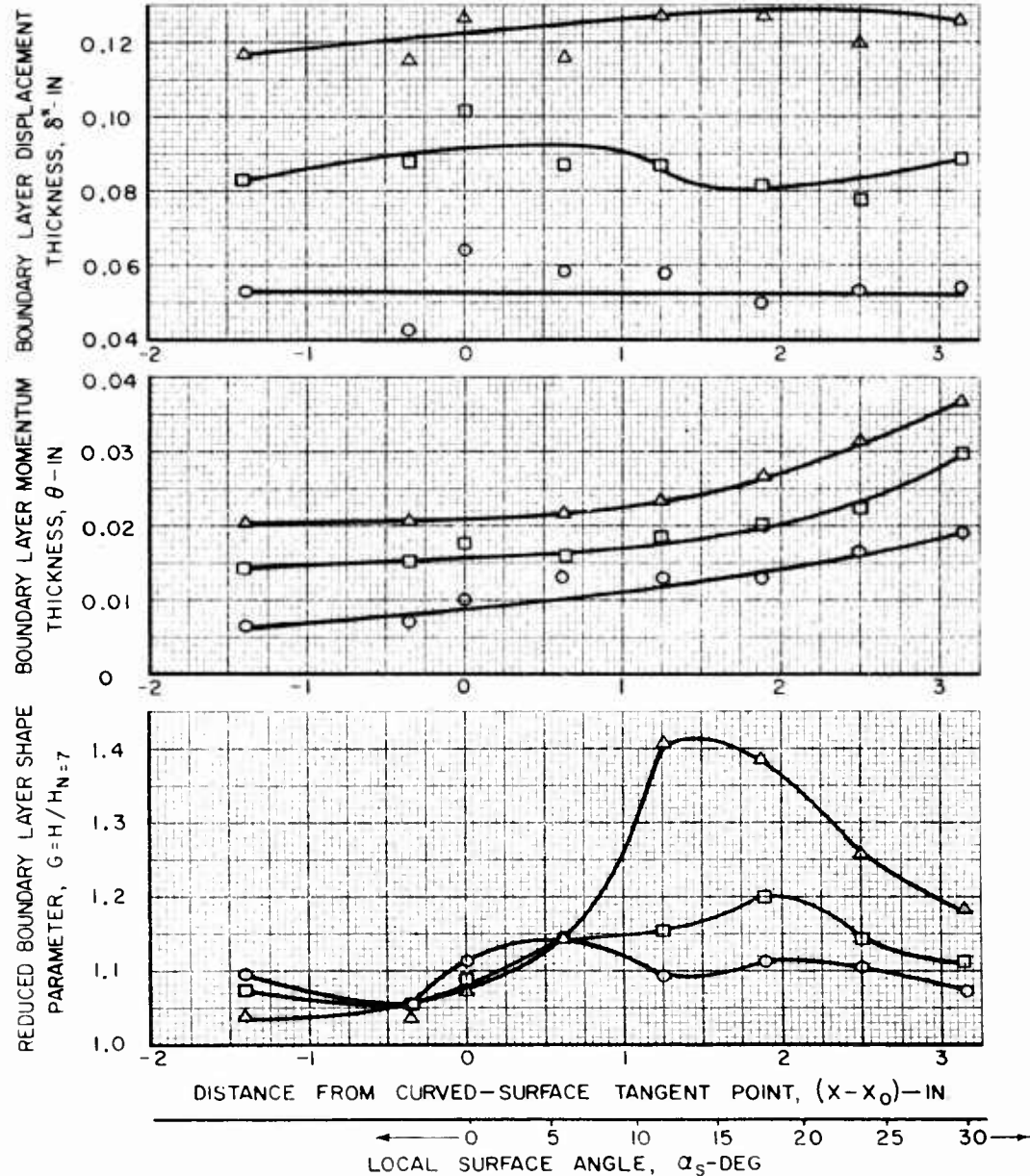
FIG. 25

TYPICAL SCHLIEREN PHOTOGRAPHS OF TWO-RADII TWO-DIMENSIONAL
CURVED-SURFACE MODEL

$M_0 = 3$ $R_1 = 6.0$ IN. $R_2 = 1.5$ IN. $\alpha_1 = 20$ DEG $\alpha_T = 30$ DEG $W_b = 0$
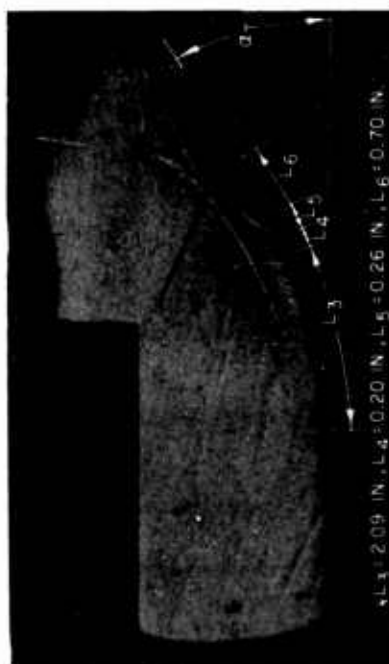
$\theta_0 = 0.0104$ IN. $R_{\theta_0} = 1650$ $\delta_0 = 0.18$ IN.

$\theta_0 = 0.0152$ IN. $R_{\theta_0} = 2420$ $\delta_0 = 0.24$ IN.
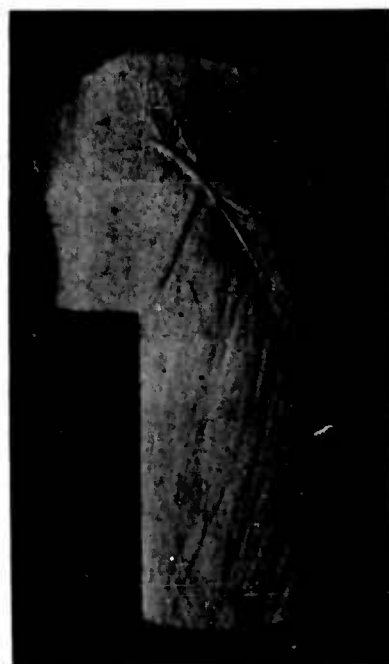
$\theta_0 = 0.0179$ IN. $R_{\theta_0} = 2840$ $\delta_0 = 0.29$ IN.

$\theta_0 = 0.023$ IN. $R_{\theta_0} = 3390$ $\delta_0 = 0.34$ IN.
(INCIPIENT SEPARATION)

FIG. 26

TYPICAL MACH NUMBER AND BOUNDARY LAYER CHARACTERISTICS
FOR TWO-RADII TWO-DIMENSIONAL CURVED-SURFACE MODEL

$M_0 = 3.0$ $R_1 = 6$ IN. $R_2 = 3$ IN. $\alpha_1 = 20$ DEG

$\alpha_T = 35$ DEG $w_b = 0$

ADDITIONAL DATA FOR THIS MODEL FOUND IN FIGS. 57, 63, AND 69

SYMBOL	θ_0 - IN.	R_{θ_0}
○	0.0110	1750
△	0.0180	2840
□	0.0198	3170

DISTANCE FROM CURVED-SURFACE TANGENT POINT, $(X - X_0)$ - IN.

LOCAL SURFACE ANGLE, α_S - DEG

72
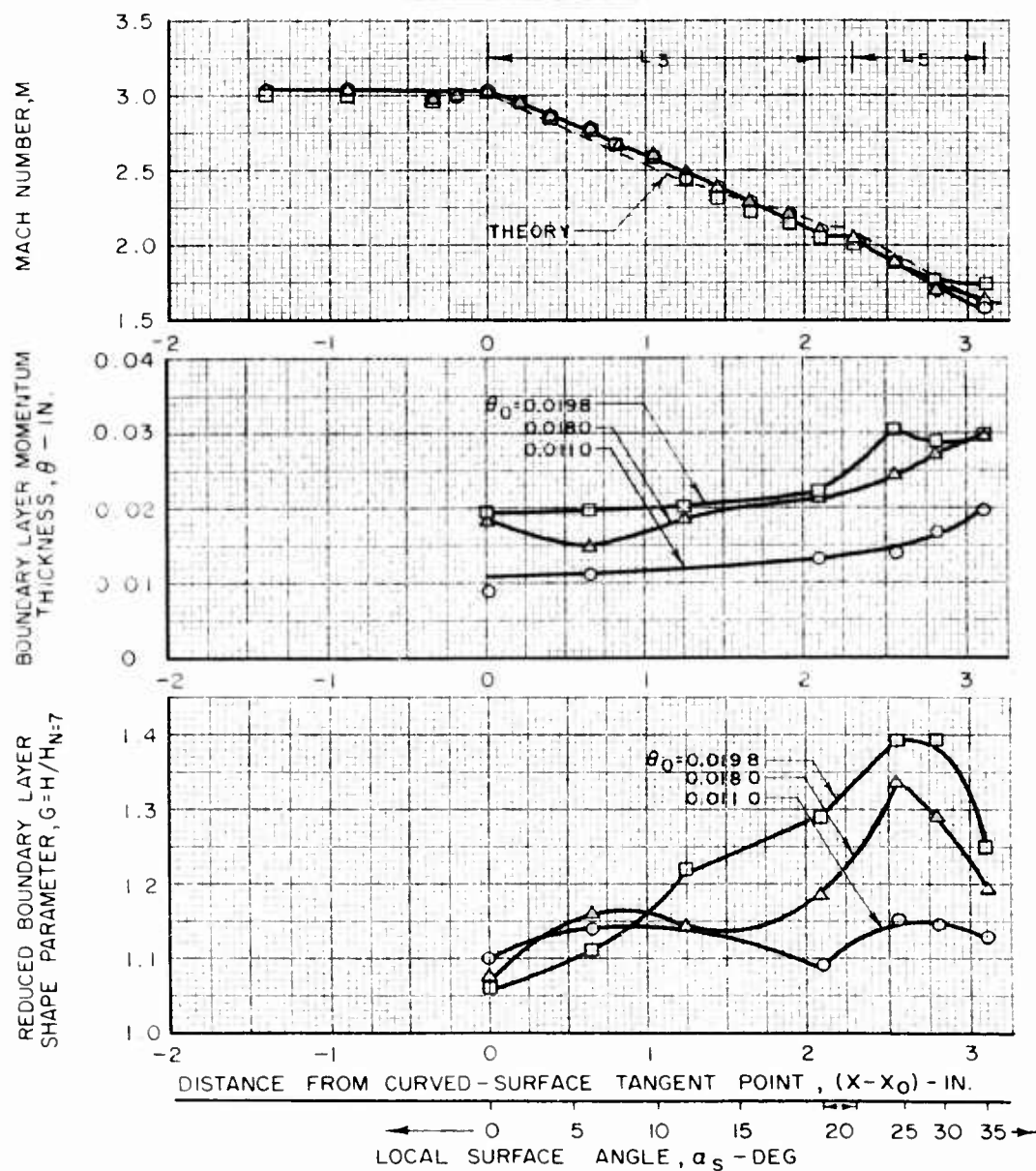
TYPICAL SCHLIEREN PHOTOGRAPH OF AXISYMMETRIC CURVED - SURFACE MODEL

$M_O = 2.5$ $R = 3$ IN. $\alpha_T = 30$ DEG $W_b = 0$

$\theta_O = 0.0072$ IN. $R\theta_O = 1510$ $\delta_O = 0.11$ IN.

FIG. 28

TYPICAL WALL STATIC PRESSURE AND MACH NUMBER
DISTRIBUTIONS ON AXISYMMETRIC CURVED-SURFACE MODEL

$M_O = 3.0$ $\theta_O = 0.0056$ IN. $R = 1.5$ IN. $\alpha_T = 30$ DEG $R_{\theta_O} = 900$ $W_b = 0$

ADDITIONAL DATA FOR THIS MODEL FOUND IN FIGS. 29, 59, 64, AND 70
DIFFERENT SYMBOLS INDICATE DATA OBTAINED ON DIFFERENT DAYS

74

TYPICAL BOUNDARY LAYER CHARACTERISTICS
FOR AXISYMMETRIC CURVED—SURFACE MODEL

$M_O = 3.0$ $R = 1.5$ IN. $\alpha_T = 30$ DEG $w_b = 0$

$\theta_O = 0.0056$ IN. $R_{\theta_O} = 900$

ADDITIONAL DATA FOR THIS MODEL FOUND IN FIGS. 28, 59, 64, AND 70

DIFFERENT SYMBOLS INDICATE DATA OBTAINED ON DIFFERENT DAYS

FIG. 30
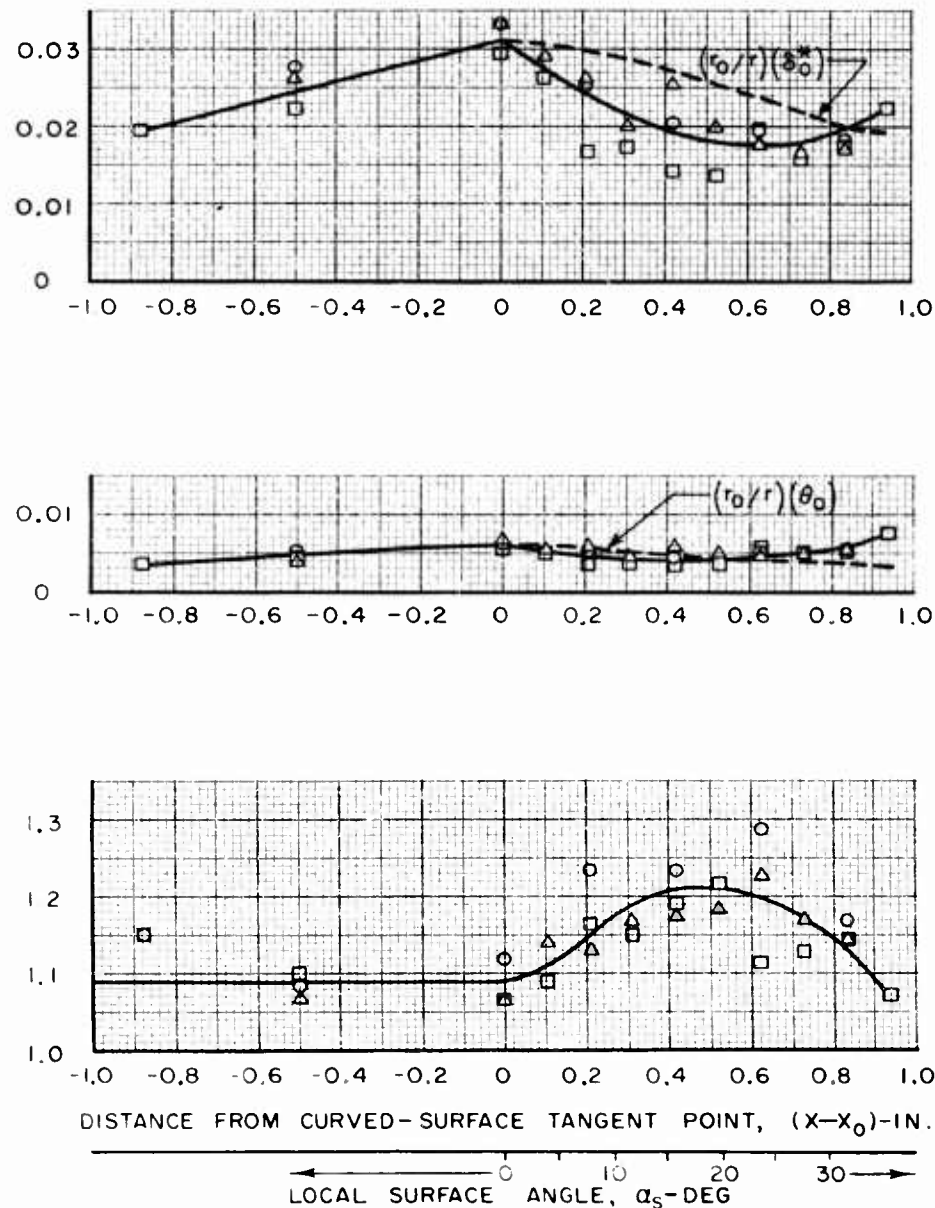
TYPICAL SCHLIEREN PHOTOGRAPHS OF TWO-DIMENSIONAL CURVED-SURFACE
MODEL WITH BOUNDARY LAYER BLEED

$M_0 = 2.5$ $R = 1.5$ IN. $\alpha_T = 30$ DEG $\theta_0 = 0.0152$ IN. $R_{\theta_0} = 3180$

a) SEPARATED BOUNDARY LAYER (NO BLEED, $W_b = 0$)

b) SEPARATED BOUNDARY LAYER (INSUFFICIENT BLEED, $W_b/W_{BL_0} = 0.070$)
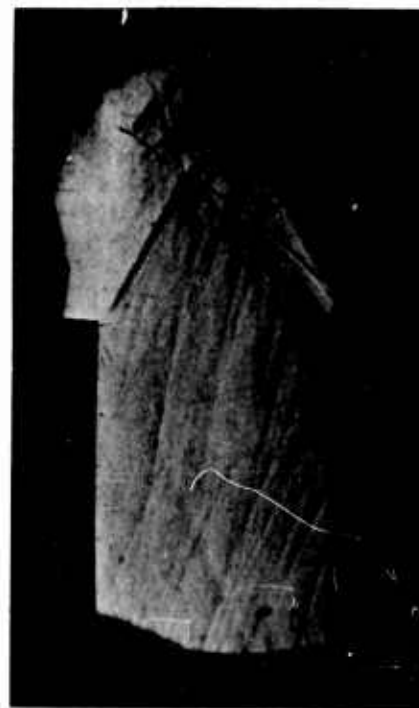
c) INCIPIENT SEPARATION ($W_b/W_{BL_0} = 0.138$)

$L_3 = 0.78$ IN.
$L_6 = 1.00$ IN.

SEPARATED REGION

SCHLIEREN PHOTOGRAPH OF TWO-DIMENSIONAL CURVED-SURFACE
MODEL WITH MORE BOUNDARY LAYER BLEED THAN
THAT REQUIRED TO PREVENT SEPARATION

$M_O = 2.5$ $R = 3$ IN. $\alpha_T = 30$ DEG

$\theta_O = 0.0146$ IN. $R_{\theta_O} = 3050$

77

FIG.32
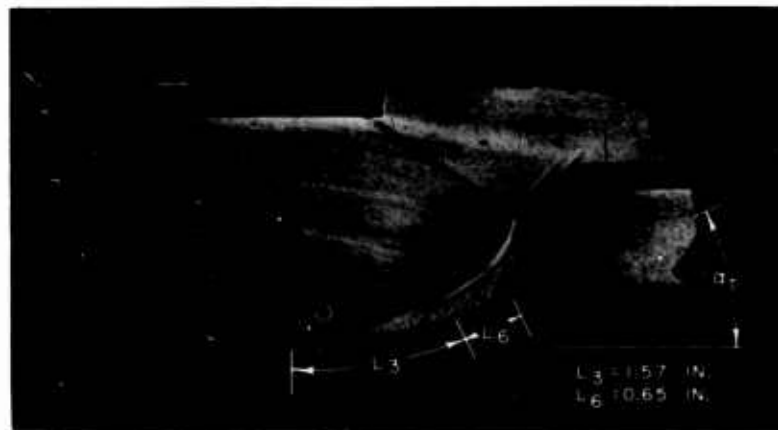
TYPICAL WALL STATIC PRESSURE AND MACH NUMBER DISTRIBUTIONS FOR TWO-DIMENSIONAL CURVED-SURFACE MODEL WITH BOUNDARY LAYER BLEED

$M_0 = 3.0$ $R = 3.0$ IN. $\alpha_T = 30$ DEG $\theta_0 = 0.0228$ IN. $R_{\theta_0} = 3620$

$w_b / w_{BL_0} = 0.134$ ($w_b / w_{BL_0} = 0.078$ AT INCIPIENT SEPARATION)

ADDITIONAL DATA FOR THIS MODEL FOUND IN FIGS. 33 AND 34
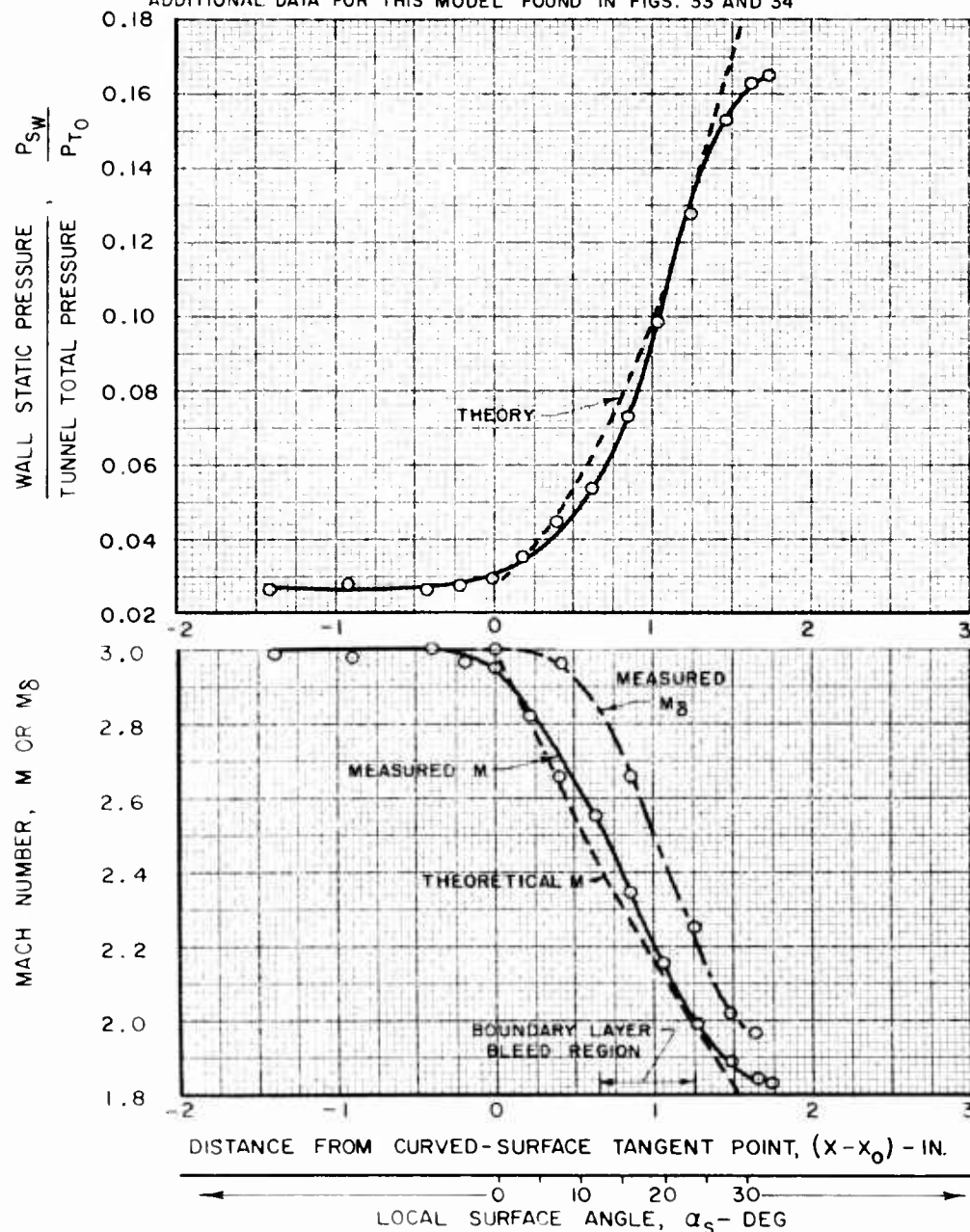
WALL STATIC PRESSURE / TUNNEL TOTAL PRESSURE, $\dfrac{P_{S_W}}{P_{T_0}}$

THEORY

MACH NUMBER, M OR M_δ

MEASURED M_δ

MEASURED M

THEORETICAL M

BOUNDARY LAYER BLEED REGION

DISTANCE FROM CURVED-SURFACE TANGENT POINT, $(X-X_0)$ – IN.

LOCAL SURFACE ANGLE, α_s – DEG

78

TYPICAL BOUNDARY LAYER VELOCITY PROFILES FOR TWO-DIMENSIONAL CURVED-SURFACE MODEL WITH BOUNDARY LAYER BLEED

$M_0 = 3.0$ $R = 3.0$ IN. $\alpha_T = 30$ DEG $\theta_0 = 0.0228$ IN. $R_{\theta_0} = 3620$

$W_b/W_{BL_0} = 0.134$ ($W_b/W_{BL_0} = 0.078$ AT INCIPIENT SEPARATION)

ADDITIONAL DATA FOR THIS MODEL FOUND IN FIGS 32 AND 34

SYMBOL	α_S – DEG	$(x-x_0)$ – IN.	θ – IN.	δ – IN.	G	M	M_δ
D	0	0	0.0228	0.34	1.10	2.95	3.01
◇	8	0.42	0.0220	0.34	1.17	2.66	2.96
○	16	0.84	0.0191	0.23	1.29	2.35	2.66
□	24	1.26	0.0200	0.20	1.40	1.99	2.25
△	30	1.63	0.0267	0.25	1.24	1.84	2.01

BLEED IN REGION OF α_S FROM 12 TO 24 DEG
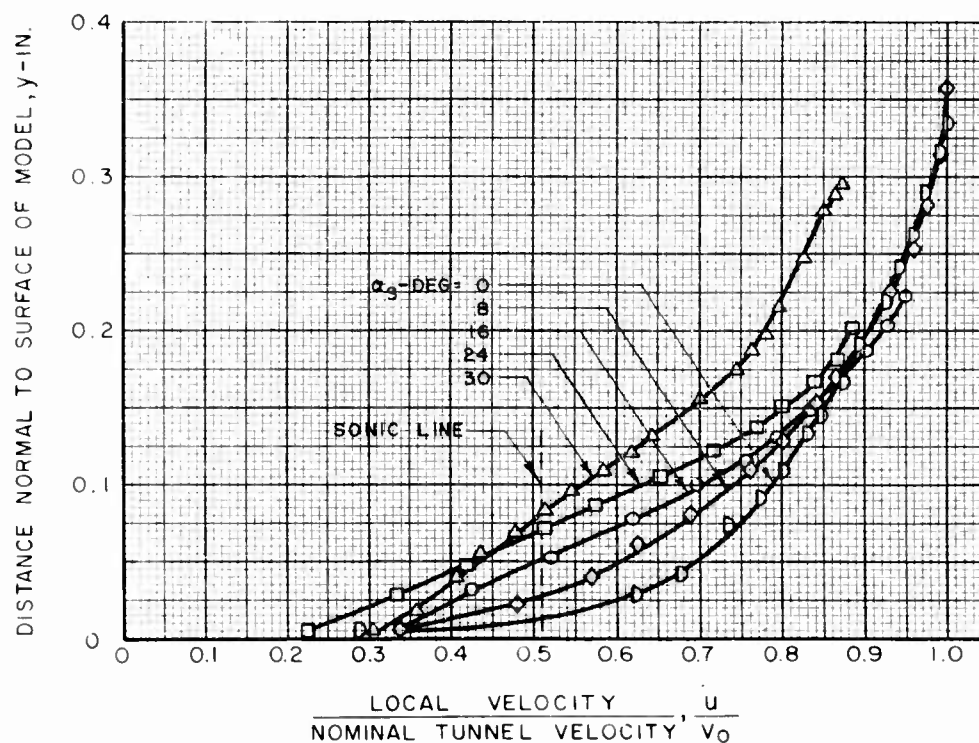
TYPICAL BOUNDARY LAYER CHARACTERISTICS FOR TWO-DIMENSIONAL CURVED-SURFACE MODEL WITH BOUNDARY LAYER BLEED

FIG.35
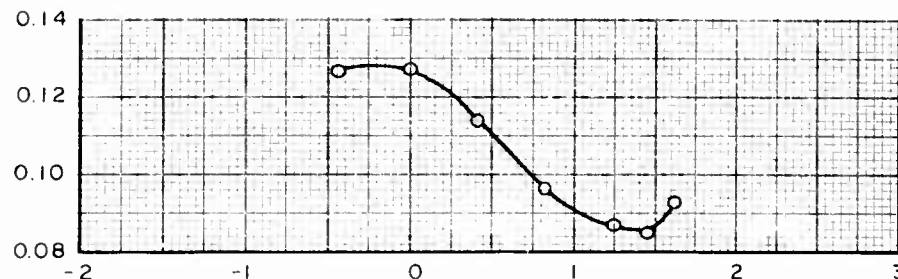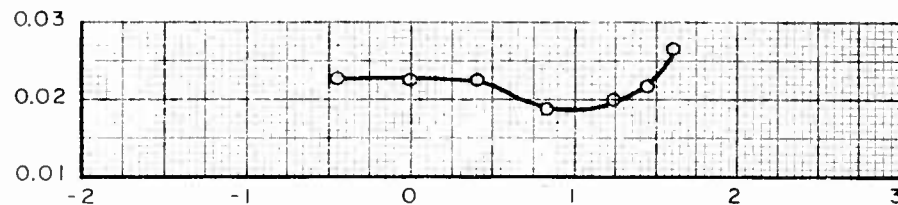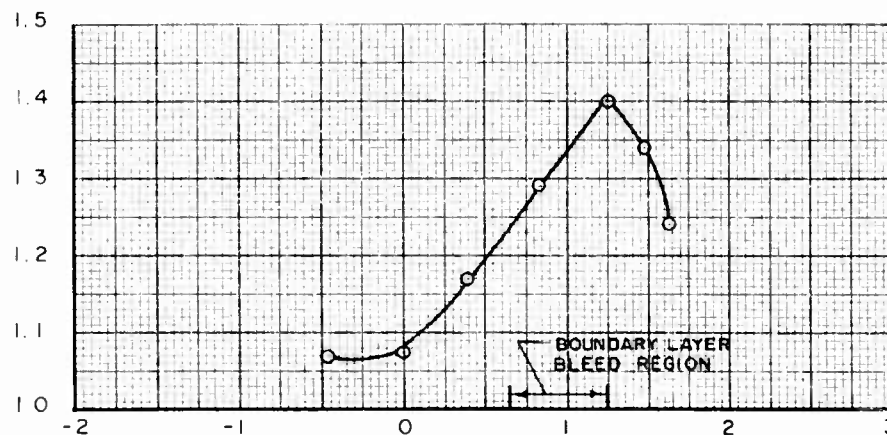
EFFECT OF EXCESSIVE BOUNDARY LAYER BLEED ON VELOCITY PROFILES FOR TWO-DIMENSIONAL CURVED-SURFACE MODEL

$M_O = 3.0$ $R = 3$ IN. $\alpha_T = 30$ DEG $\alpha_S = 24$ DEG

$\theta_O = 0.0228$ IN. $R_{\theta_O} = 3620$ $X - X_O = 1.25$ IN.

SYMBOL	BLEED IN REGION FROM α_S	TO α_S	w_b/w_{BL_O}	θ — IN.	δ — IN.	δ^* — IN.	H	G
O	12	16	0.067	0.0221	0.21	0.0966	4.38	1.47
□	12	18	0.083	0.0210	0.20	0.0886	4.22	1.42
◁	12	20	0.109	0.0196	0.19	0.0831	4.23	1.42
▽	12	22	0.142	0.0168	0.17	0.0684	4.06	1.36

$$\frac{\text{WEIGHT FLOW BLED FROM BOUNDARY LAYER}}{\text{WEIGHT FLOW BLED FROM BOUNDARY LAYER AT INCIPIENT SEPARATION}}$$

1.00
1.24
1.63
2.12

SONIC LINE

DISTANCE NORMAL TO SURFACE OF MODEL, y — IN

$\dfrac{\text{VELOCITY}}{\text{NOMINAL TUNNEL VELOCITY}}$, $\dfrac{u}{V_O}$

81
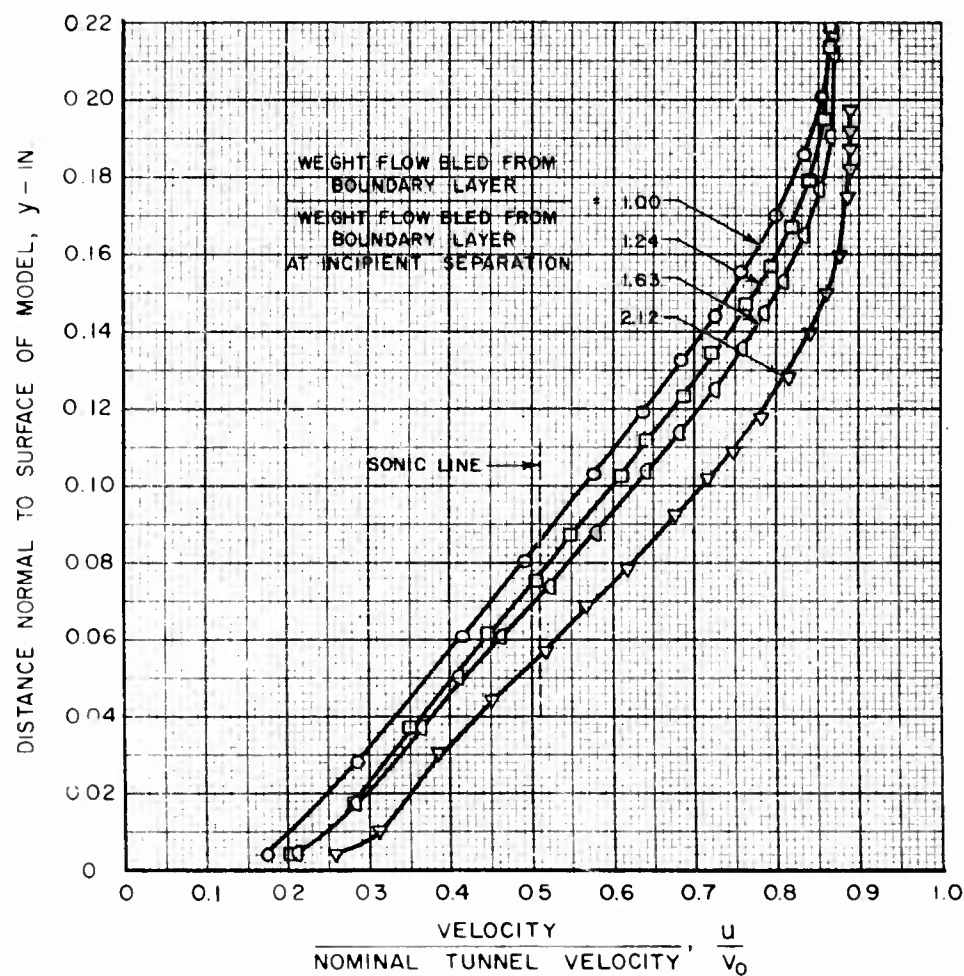
VARIATION OF LOCAL SKIN-FRICTION COEFFICIENT WITH REYNOLDS NUMBER BASED ON BOUNDARY LAYER MOMENTUM THICKNESS

CURVES INTERPOLATED AND EXTRAPOLATED FROM ZERO-PRESSURE-GRADIENT DATA IN REFS. 33 THROUGH 36
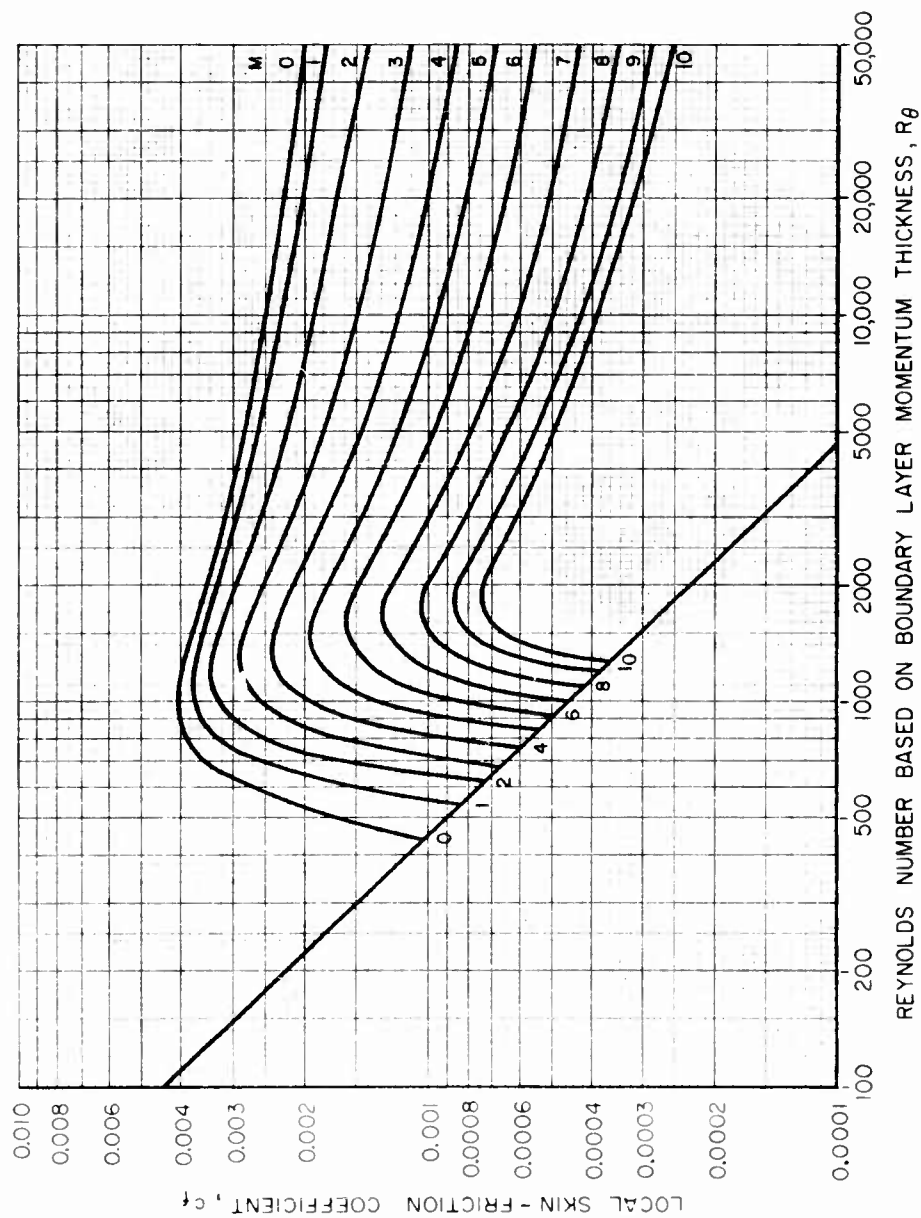
EFFECT OF REDUCED BOUNDARY LAYER SHAPE PARAMETER ON LOCAL SKIN-FRICTION COEFFICIENT

CURVES OBTAINED FROM REFS. 26 AND 37 (SEE TEXT)
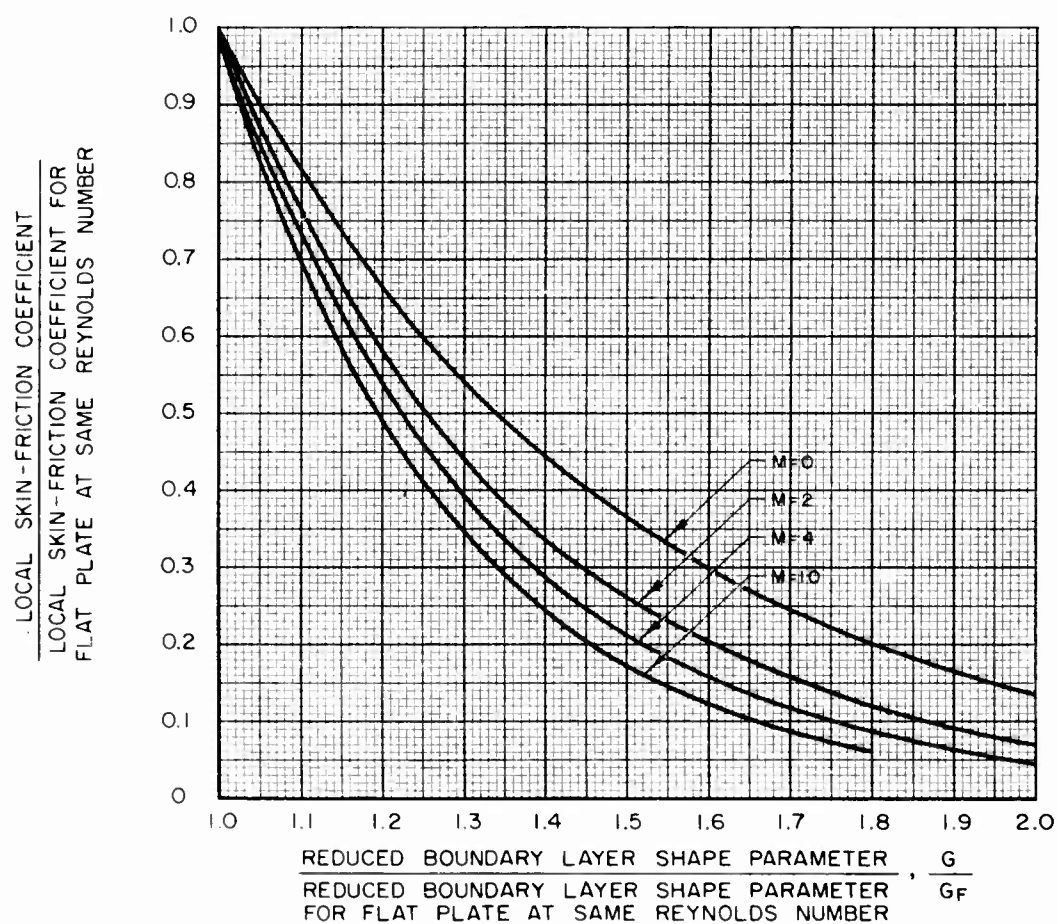
EFFECT OF MACH NUMBER ON BOUNDARY LAYER DECELERATION PARAMETER
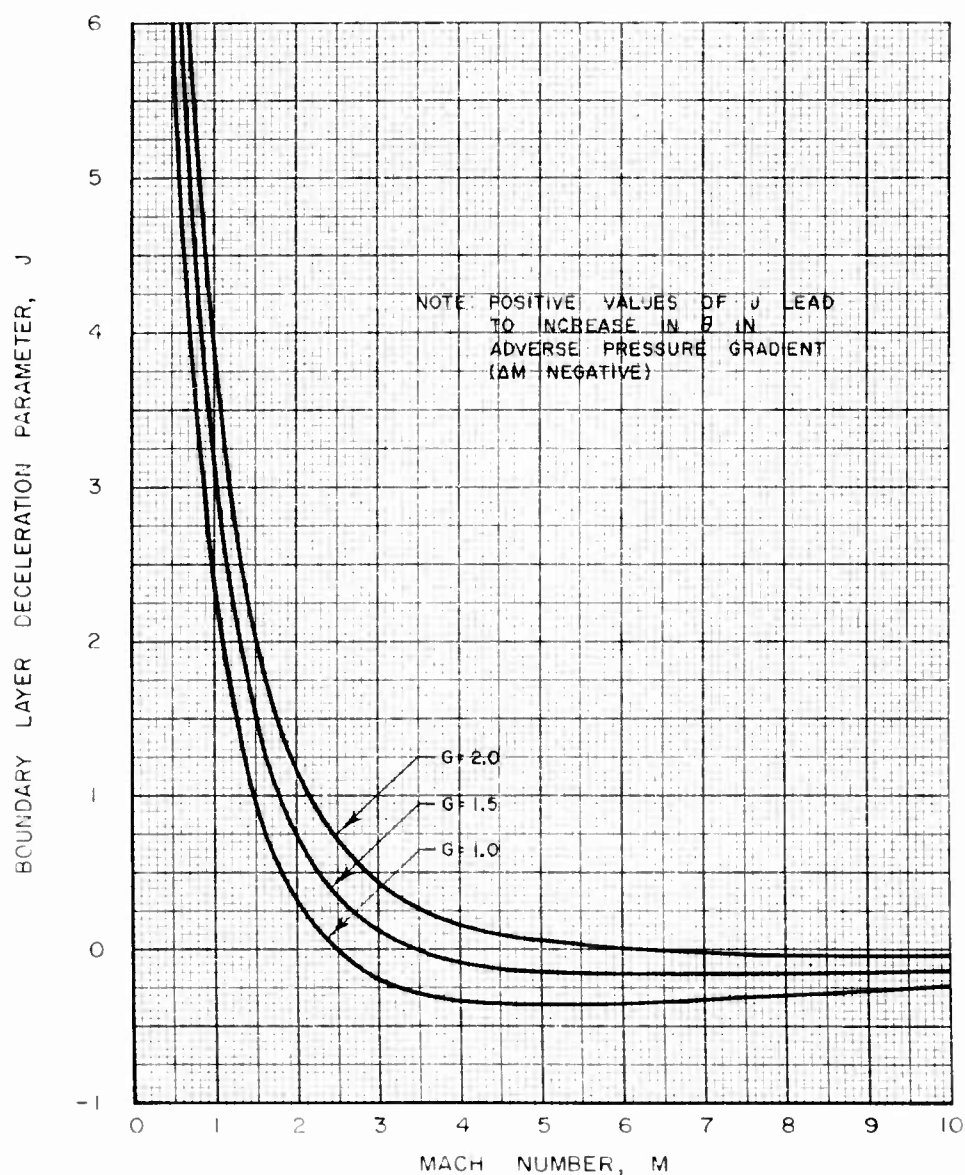
BOUNDARY LAYER DECELERATION PARAMETER
FOR MACH NUMBERS 0.5 TO 1.8

$$J = \left[\frac{dq/q}{dM} + GH_{N=7} \frac{dV/V}{dM} \right]$$

J USED IN FOLLOWING EQUATION (EQ. 12)

$$\Delta\theta = \frac{C_f}{2} \Delta x - \theta J \Delta M$$

85

FIG. 40
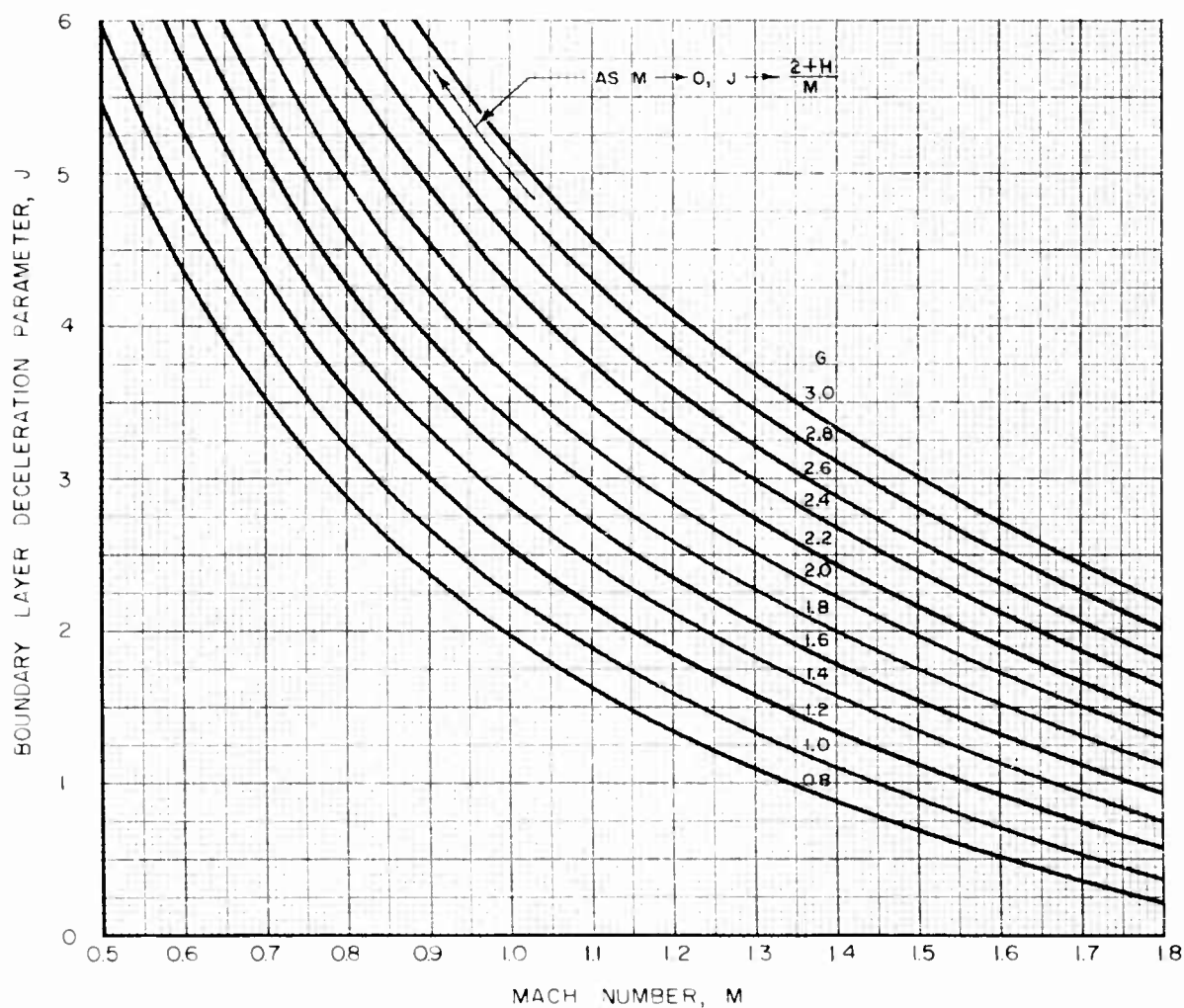
BOUNDARY LAYER DECELERATION PARAMETER
FOR MACH NUMBERS 1.5 TO 3.5

$$J = \left[\frac{dq/q}{dM} + 6H_{N=7}\frac{dV/V}{dM} \right]$$

J USED IN FOLLOWING EQUATION

$$(EQ.12)\ \Delta\theta = \frac{C_f}{2}\Delta X - \theta J\ \Delta M$$

BOUNDARY LAYER DECELERATION PARAMETER, J

MACH NUMBER, M

FIG 41
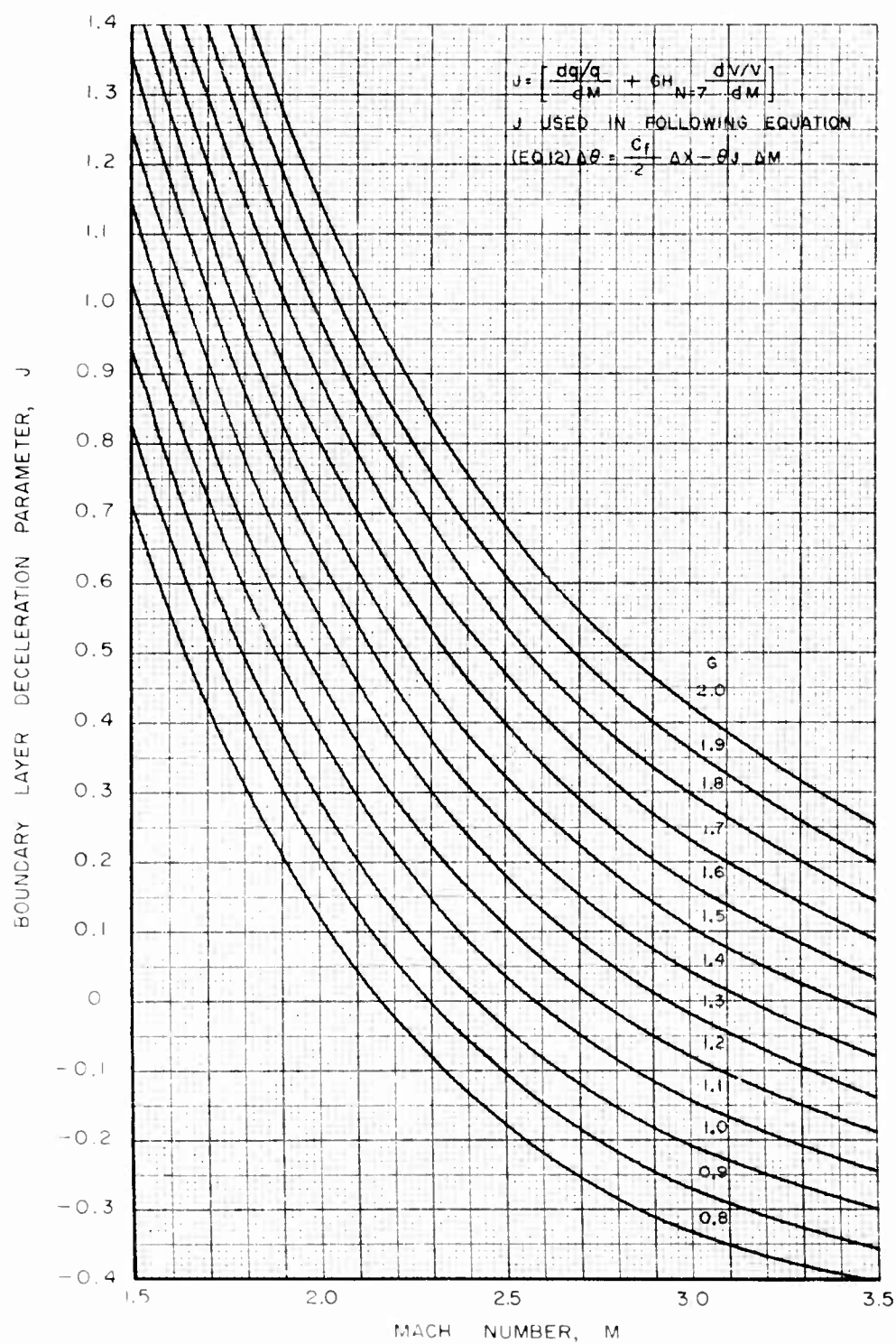
BOUNDARY LAYER DECELERATION PARAMETER
FOR MACH NUMBERS 3.5 TO 10.0

$$J = \left[-\frac{dq/q}{dM} + GH_{N=7} \frac{dV/V}{dM} \right]$$

J USED IN FOLLOWING EQUATION (EQ 12)

$$\Delta\theta = \frac{C_f}{2} \Delta X - \theta J \Delta M$$

MACH NUMBER, M

BOUNDARY LAYER DECELERATION PARAMETER, J
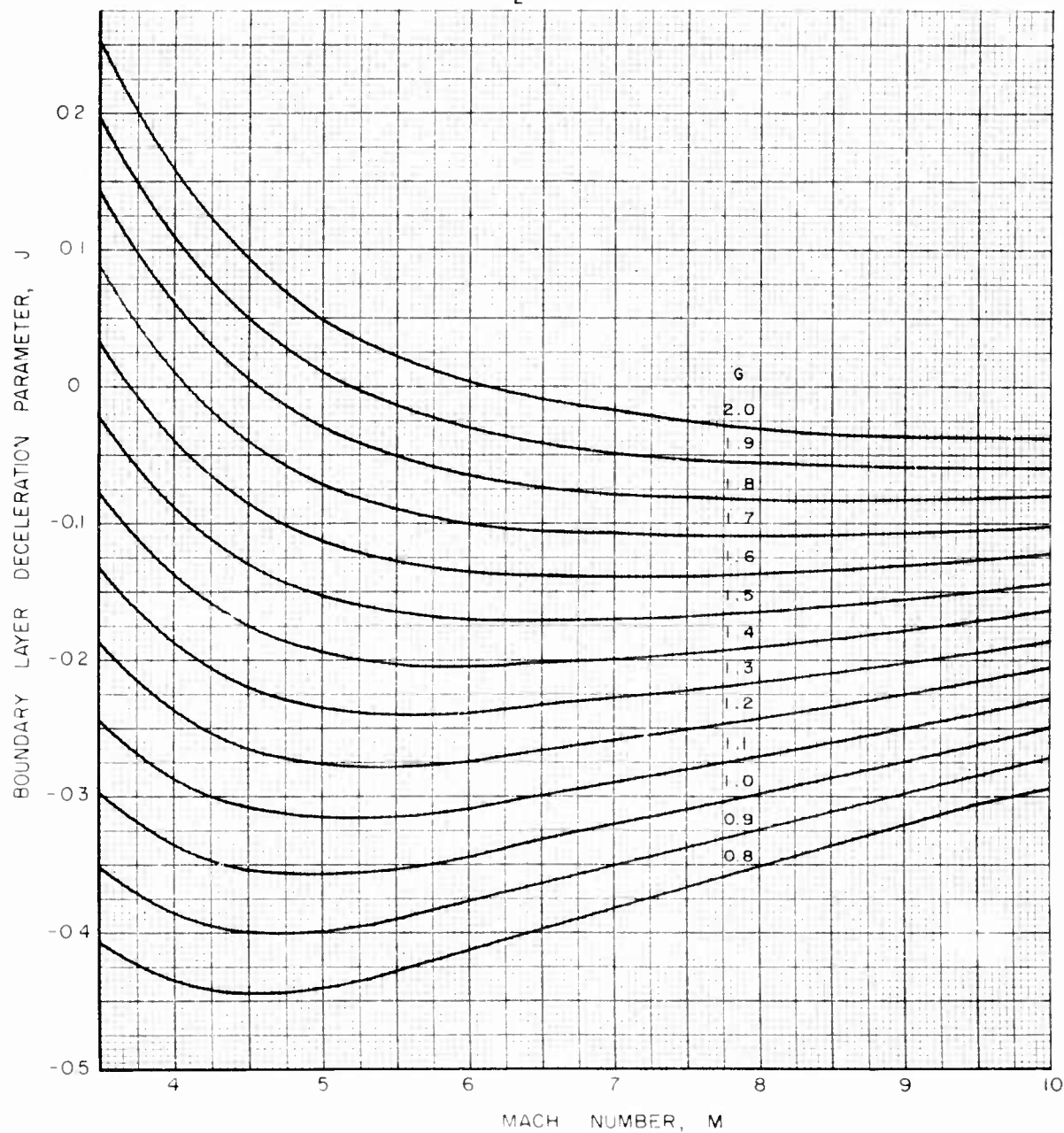
VARIATION OF BOUNDARY LAYER MOMENTUM THICKNESS WITH MACH NUMBER FOR INITIAL MACH NUMBER 3.0

ZERO WALL FRICTION ASSUMED
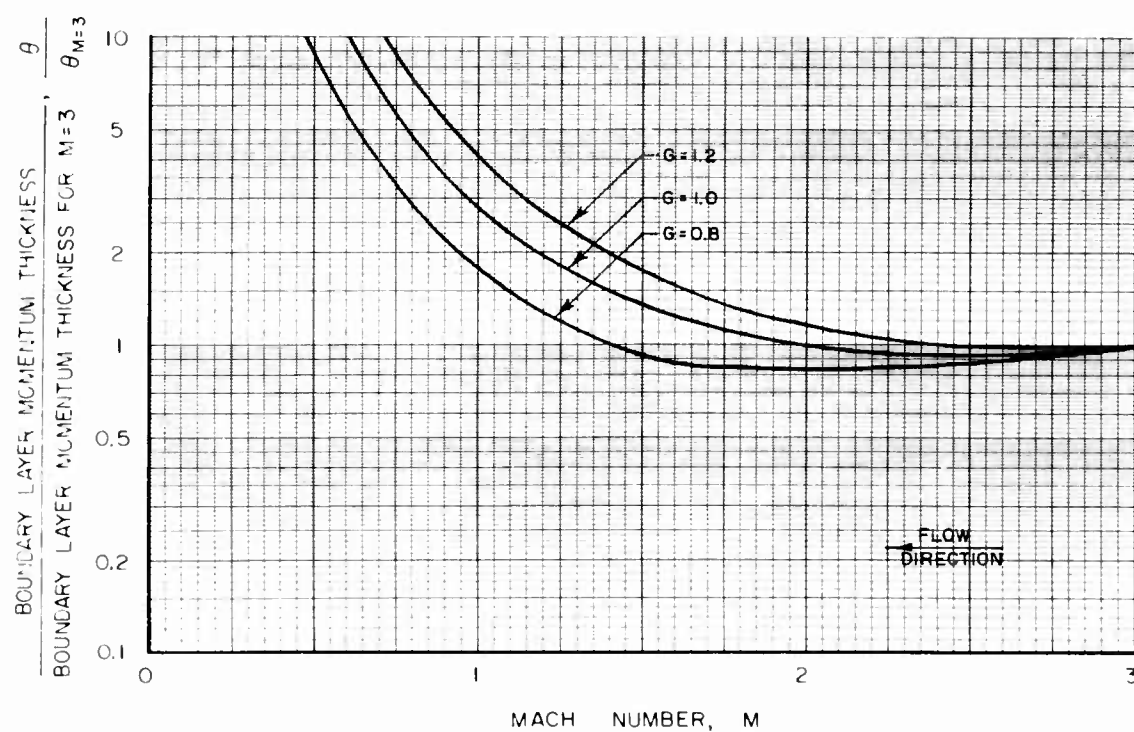
VARIATION OF BOUNDARY LAYER MOMENTUM THICKNESS WITH
MACH NUMBER FOR INITIAL MACH NUMBER 5.0

ZERO WALL FRICTION ASSUMED

MACH NUMBER, M

FIG. 44
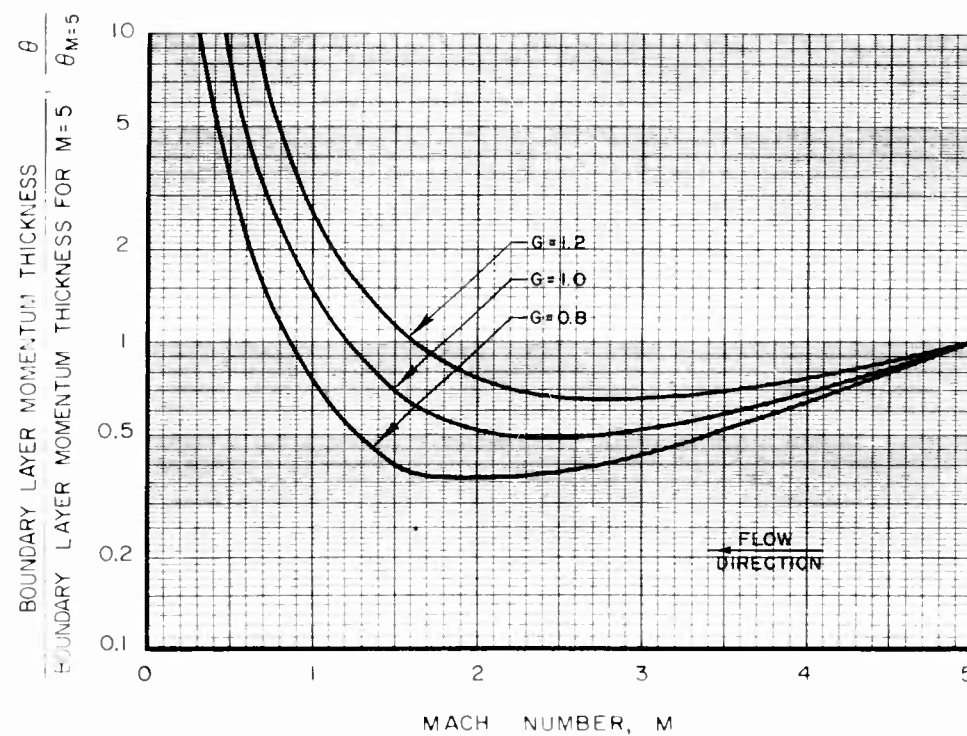
VARIATION OF BOUNDARY LAYER MOMENTUM THICKNESS WITH
MACH NUMBER FOR INITIAL MACH NUMBER 10.0

ZERO WALL FRICTION ASSUMED

FIG 45
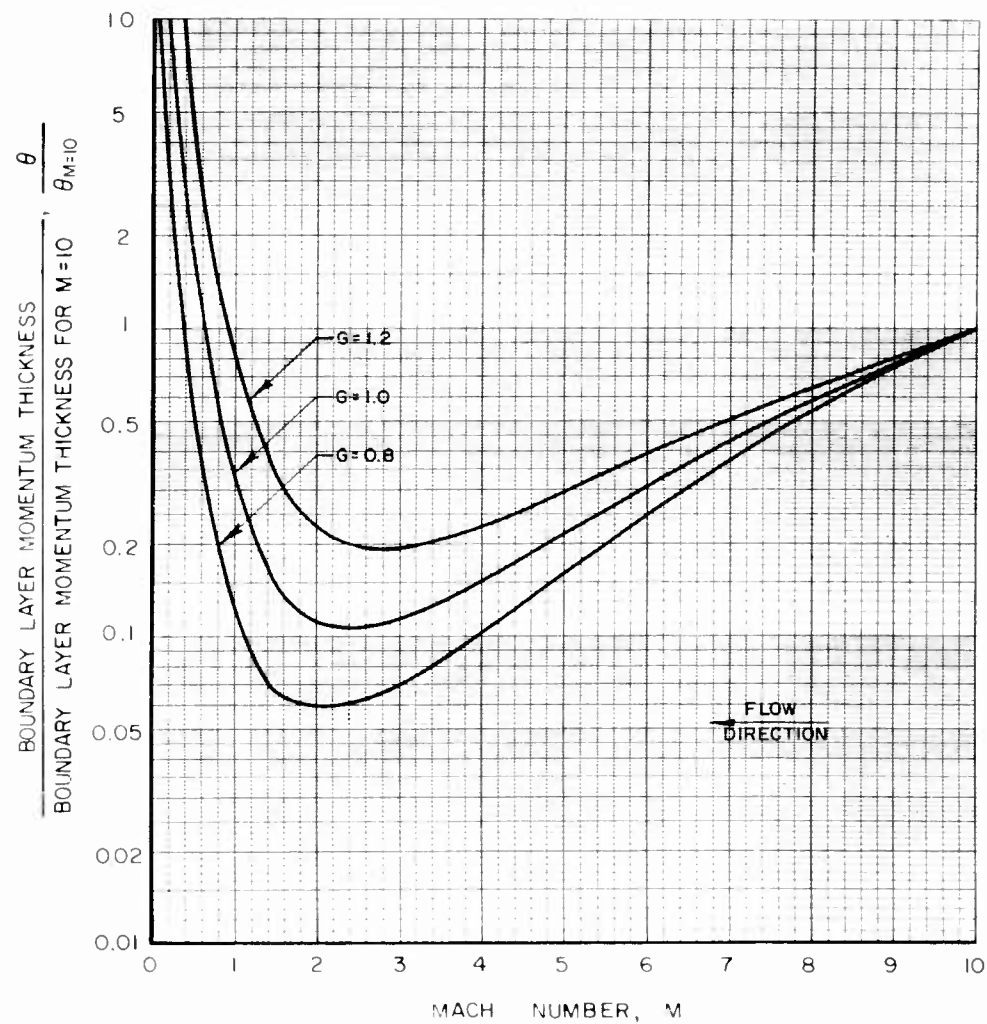
VARIATION OF TOTAL FLOW WITHIN BOUNDARY LAYER WITH MACH NUMBER FOR INITIAL MACH NUMBERS 3.0 , 5.0, AND 10.0

$G = 1.0$

ZERO WALL FRICTION ASSUMED

$\dfrac{W_{BL}}{W_{BLO}} = \dfrac{\int_0^\delta \rho V dy}{\left(\int_0^\delta \rho V dy\right)_{M_C}}$

TOTAL FLOW WITHIN BOUNDARY LAYER
FLOW WITHIN BOUNDARY LAYER AT INITIAL MACH NUMBER

M_O

MACH NUMBER, M

91
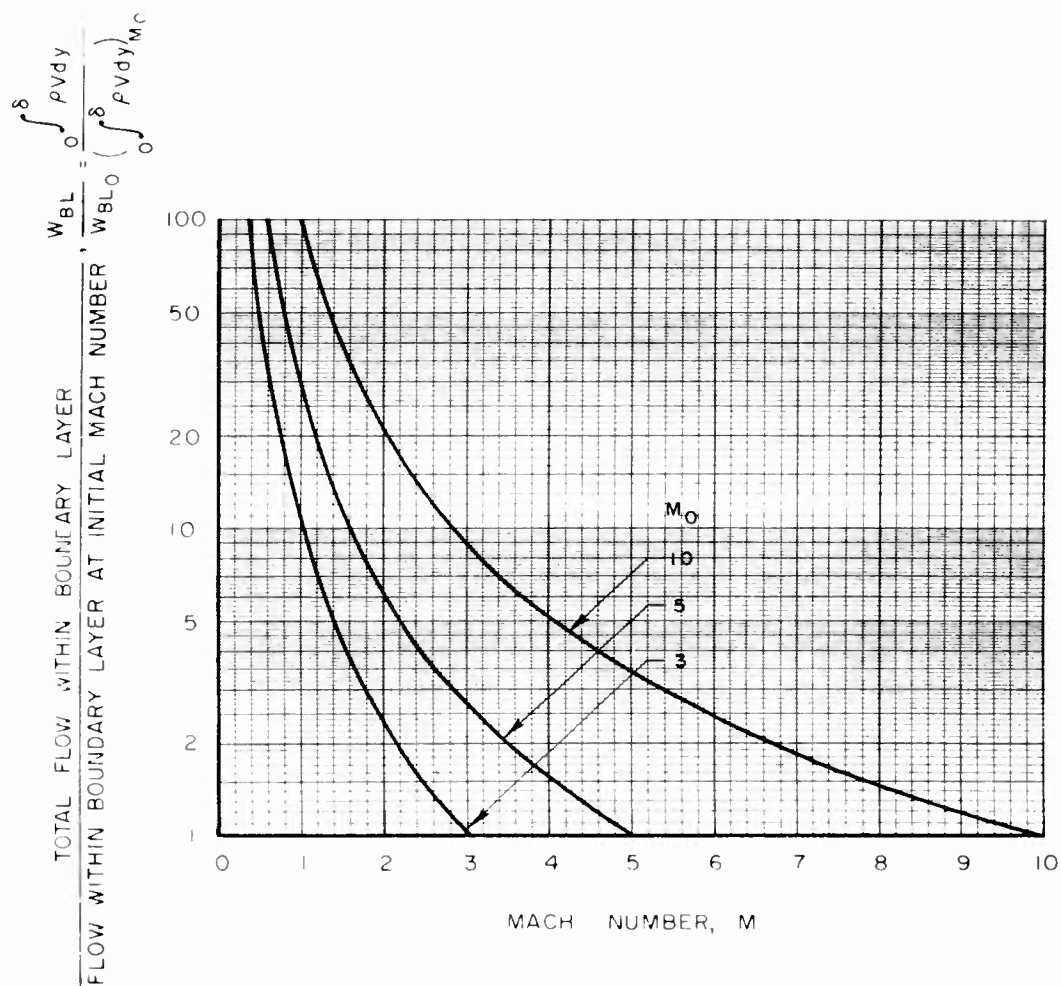
TYPICAL VARIATION OF FLOW WITHIN BOUNDARY LAYER WITH DISTANCE ALONG SINGLE-RADIUS TWO-DIMENSIONAL CURVED-SURFACE MODEL

$M_0 = 3.0$ $R = 6$ IN. $\alpha_T = 30$ DEG $W_b = 0$

$\theta_0 = 0.0215$ IN. $R_{\theta_0} = 3420$

ADDITIONAL DATA FOR THIS MODEL FOUND IN FIGS 20,21,22,23,24,53,55,62, AND 68
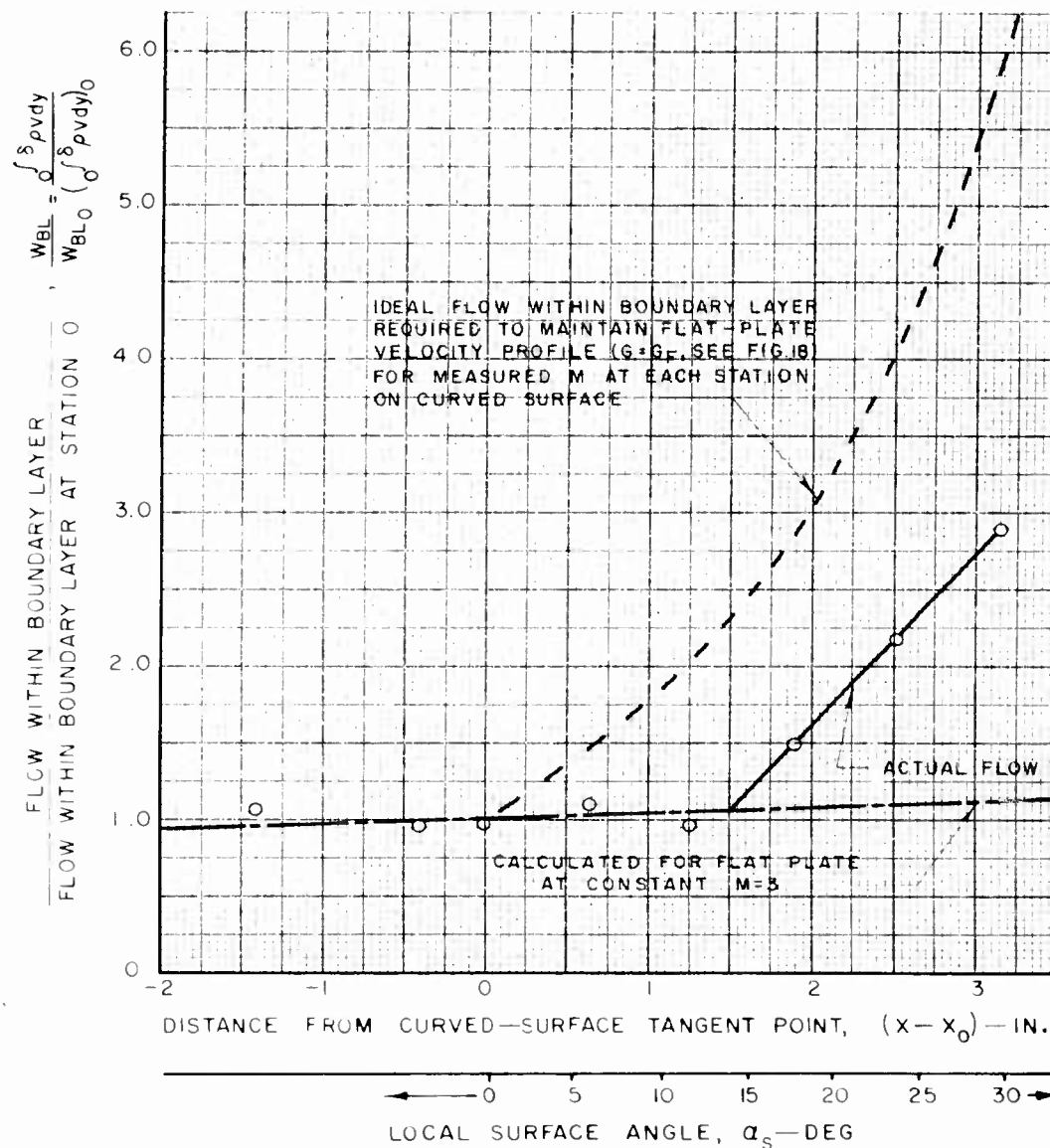
COMPARISON OF EQUIVALENT STEP PROFILE AND
ACTUAL BOUNDARY LAYER PROFILE

ACTUAL   BOUNDARY
LAYER PROFILE

EQUIVALENT   STEP
PROFILE
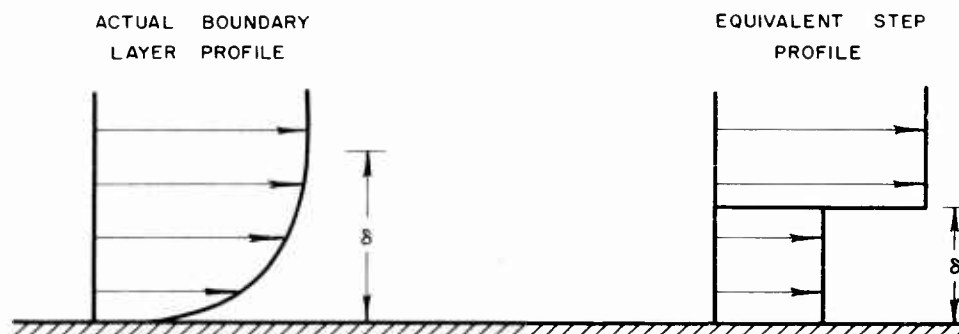
NOTES:

    EQUIVALENT STEP PROFILE AND ACTUAL BOUNDARY LAYER PROFILE
HAVE SAME VALUE OF δ^* AND θ AND, HENCE, H AND G.

    BOUNDARY LAYER THICKNESS, δ, AND FLOW WITHIN BOUNDARY
LAYER, $\int_o^\delta \rho V dY$, ARE LESS FOR EQUIVALENT STEP
PROFILE THAN FOR ACTUAL BOUNDARY LAYER PROFILE.

    LOCAL STATIC PRESSURE IS INDEPENDENT OF DISTANCE NORMAL
TO WALL FOR EQUIVALENT STEP PROFILE.

93

EFFECT OF VELOCITY WITHIN EQUIVALENT STEP PROFILE
ON REDUCED BOUNDARY LAYER SHAPE PARAMETER

FIG. 49
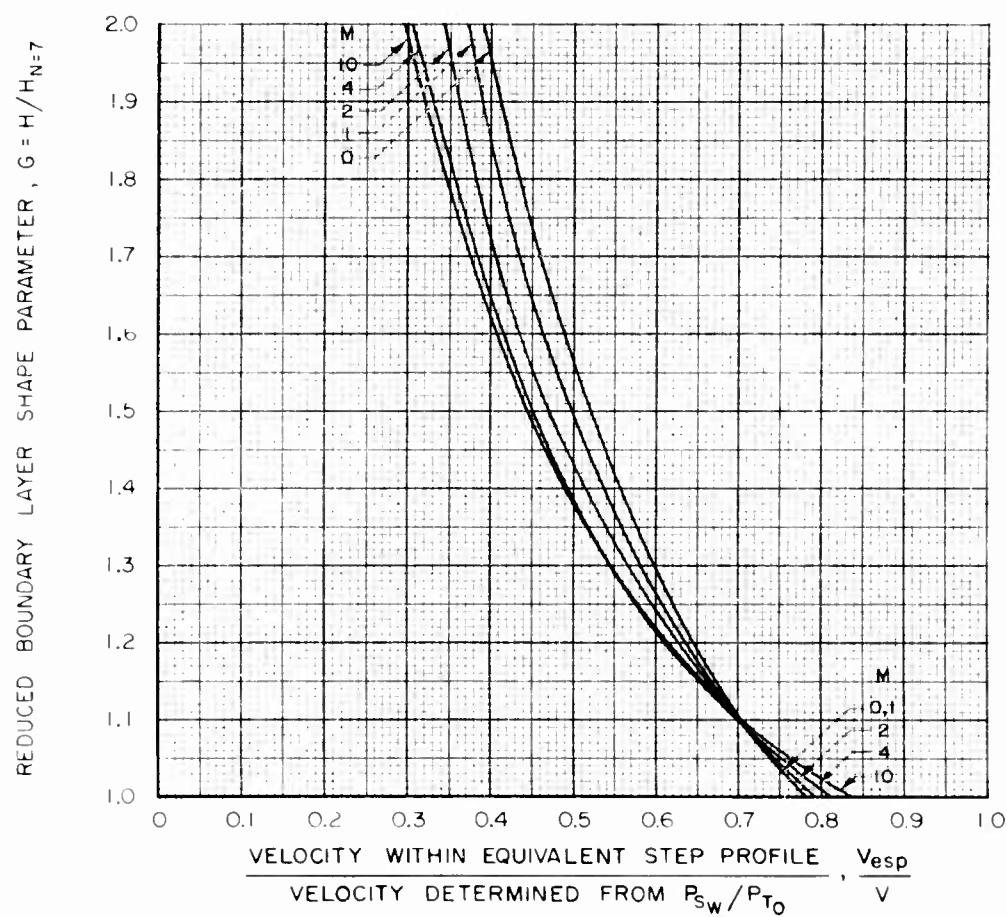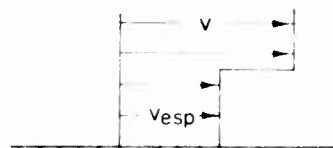
EFFECT OF RAPID DECREASE IN VELOCITY ON BOUNDARY LAYER SHAPE PARAMETERS FOR INCOMPRESSIBLE FLOW

—————— CALCULATED FOR STEP PROFILE (SEE TEXT) NEGLECTING WALL FRICTION AND INFLUX OF FLOW INTO STEP PROFILE

— — — CALCULATED USING FIRST TERM ON RIGHT SIDE OF EQ.15 (EQ. 15 COPIED FROM REF. 27)

— ·· — CALCULATED USING FIRST TERM ON RIGHT SIDE OF EQ. 16 (EQ. 16 COPIED FROM REF. 30)

FRACTIONAL DECREASE IN VELOCITY, $(v_0 - v)/v_0$

95
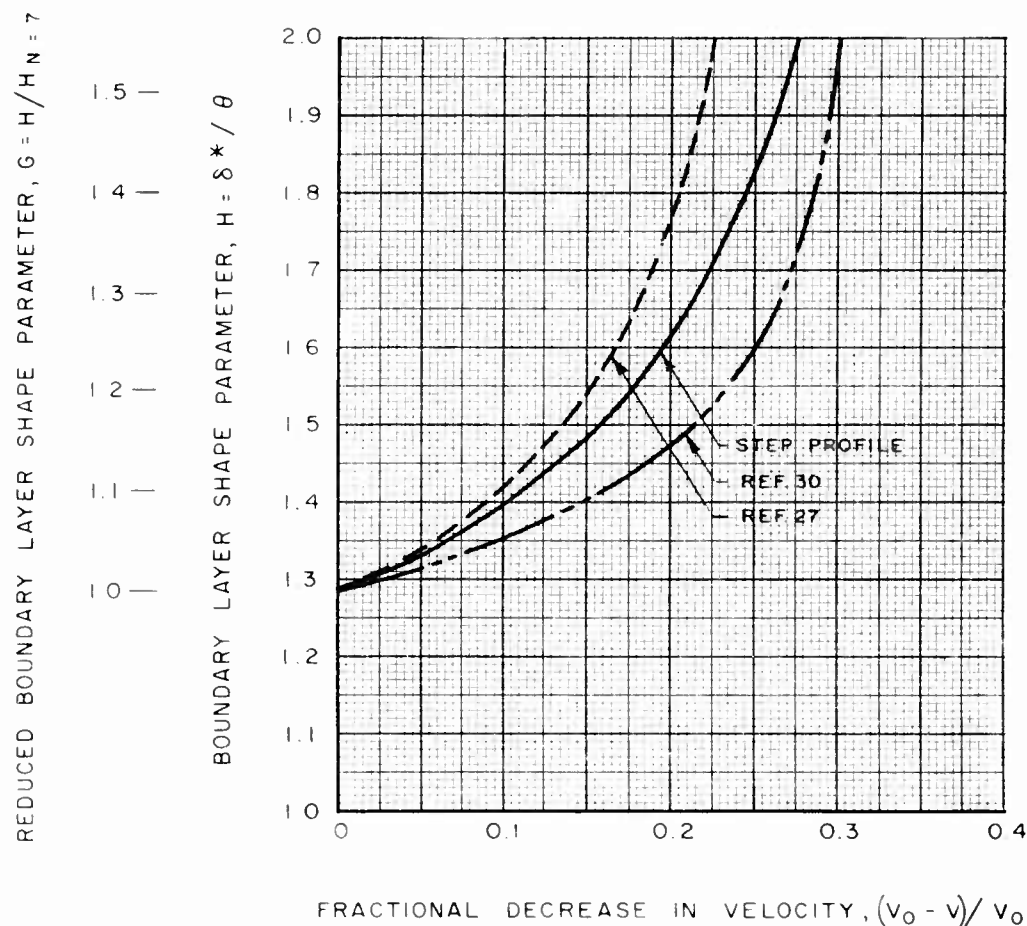
EFFECT OF RAPID DECREASE IN MACH NUMBER ON
REDUCED BOUNDARY LAYER SHAPE PARAMETER
FOR COMPRESSIBLE FLOW

$\gamma = 1.4$

ASSUMPTIONS

1. CONSTANT TOTAL PRESSURE WITHIN
   STEP PROFILE
2. ZERO MIXING FROM OUTSIDE
   BOUNDARY LAYER
3. ZERO WALL FRICTION

REDUCED BOUNDARY LAYER SHAPE PARAMETER, $G = H/H_{N=7}$

FRACTIONAL DECREASE IN MACH NUMBER, $(M_0 - M)/M_0$

96

VARIATION OF DIMENSIONLESS FLOW THICKNESS WITH
REDUCED BOUNDARY LAYER SHAPE PARAMETER
FOR MACH NUMBERS 0.6 TO 4.5

BOUNDARY LAYER FLOW THICKNESS, β, DEFINED AS HEIGHT OF PASSAGE WHICH WILL PASS THE FLOW WITHIN AN EQUIVALENT STEP PROFILE (SEE FIG. 47) AT MACH NUMBER ONE AND FREE-STREAM TOTAL PRESSURE AND TEMPERATURE

$\dfrac{\text{BOUNDARY LAYER FLOW THICKNESS}}{\text{BOUNDARY LAYER MOMENTUM THICKNESS}}, \dfrac{\beta}{\theta}$

REDUCED BOUNDARY LAYER SHAPE PARAMETER, $G = H/H_{N=7}$

FIG 52

VARIATION OF DIMENSIONLESS FLOW THICKNESS WITH REDUCED BOUNDARY LAYER SHAPE PARAMETER FOR MACH NUMBERS 4.5 TO 10.0

BOUNDARY LAYER FLOW THICKNESS, β, DEFINED AS HEIGHT OF PASSAGE WHICH WILL PASS THE FLOW WITHIN AN EQUIVALENT STEP PROFILE (SEE FIG 47) AT MACH NUMBER ONE AND FREE-STREAM TOTAL PRESSURE AND TEMPERATURE

$\dfrac{\text{BOUNDARY LAYER FLOW THICKNESS}}{\text{BOUNDARY LAYER MOMENTUM THICKNESS}}, \dfrac{\beta}{\theta}$

REDUCED BOUNDARY LAYER SHAPE PARAMETER, $G = H/H_{N=7}$

FIG. 53

TYPICAL EXAMPLE OF VARIATIONS OF ACTUAL AND IDEAL BOUNDARY LAYER FLOW THICKNESS AND LAG LENGTH WITH DISTANCE ALONG SINGLE – RADIUS TWO-DIMENSIONAL CURVED-SURFACE MODEL

$M_O = 3.0$ $R = 6$ IN. $\alpha_T = 30$ DEG $W_b = 0$

$\theta_O = 0.0215$ IN. $R_{\theta_O} = 3420$

ADDITIONAL DATA FOR THIS MODEL FOUND IN FIGS. 20, 21, 22, 23, 24, 46, 55, 62, AND 68
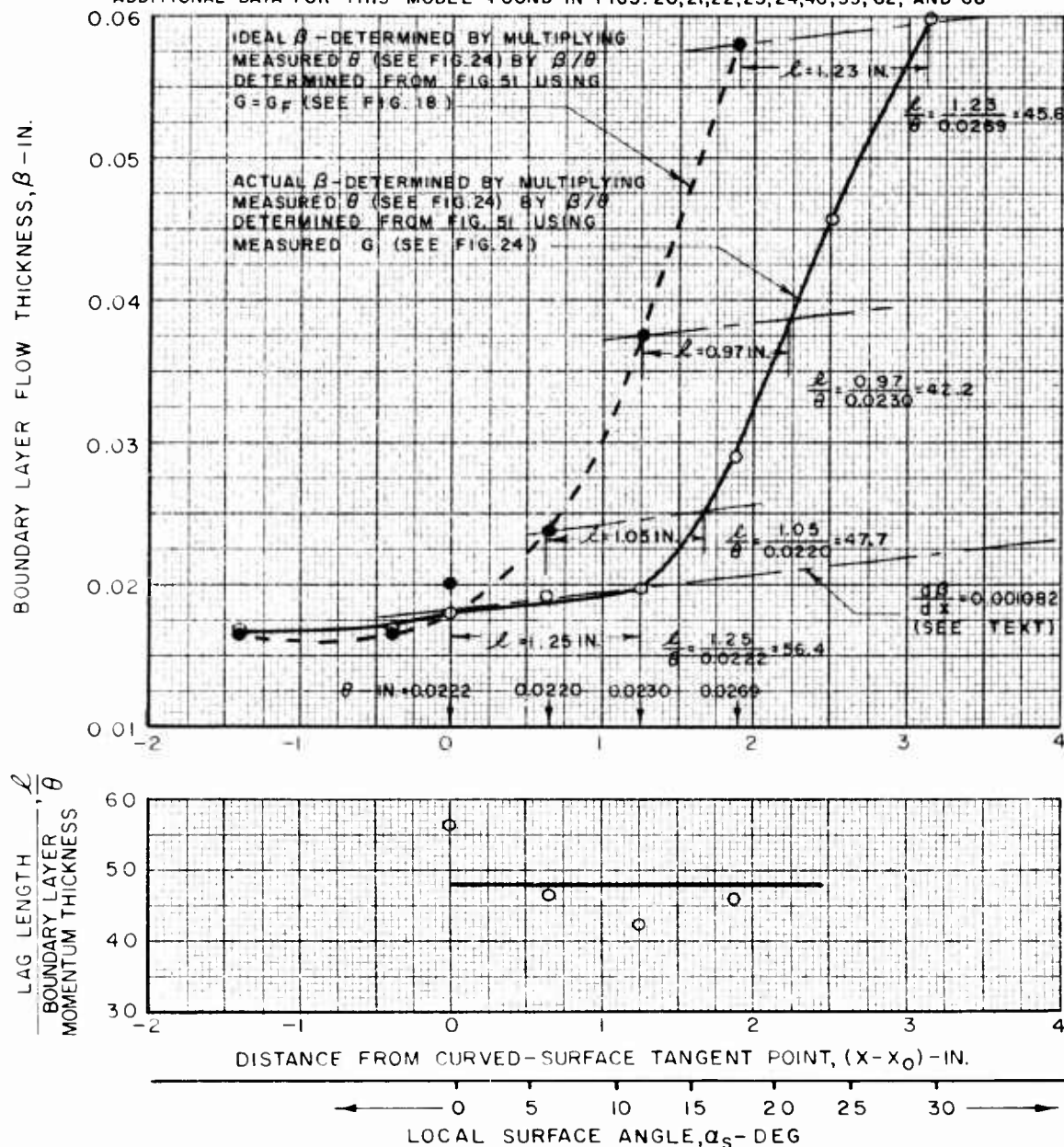
SIMPLIFIED METHOD FOR DETERMINATION OF REDUCED BOUNDARY LAYER SHAPE PARAMETER FOR SMALL ADVERSE MACH NUMBER GRADIENTS

DETERMINATION OF EFFECTIVE VALUE OF $M_O - M$

EFFECTIVE VALUE OF $M_O - M = (dM/dx)(\ell)$

$\ell = (\ell/\theta)(\theta)$

IDEAL β

ACTUAL β

DISTANCE

DETERMINATION OF G FROM EFFECTIVE VALUE OF $M_O - M$
(SEE FIG. 50)

$$\frac{M_O - M}{M_O} = \frac{dM}{dx} \frac{\ell}{\theta} \frac{\theta}{M_O}$$

FRACTIONAL DECREASE IN MACH NUMBER, $(M_O - M)/M_O$

100
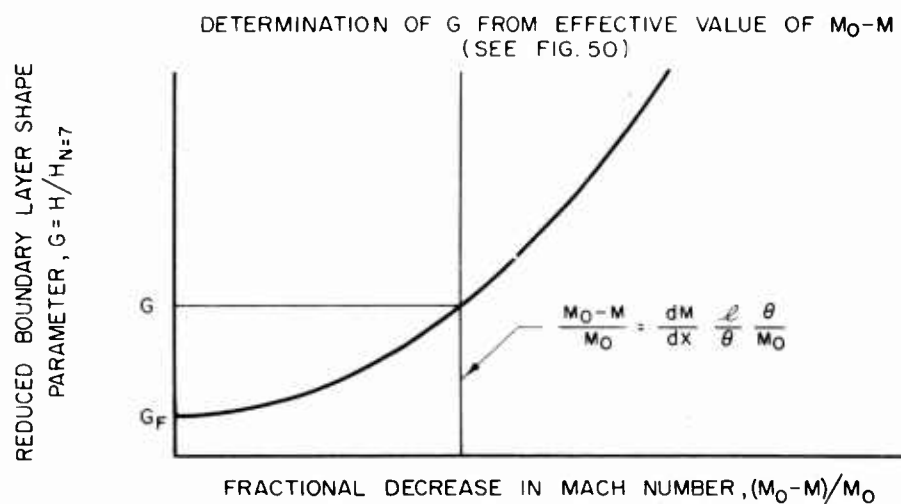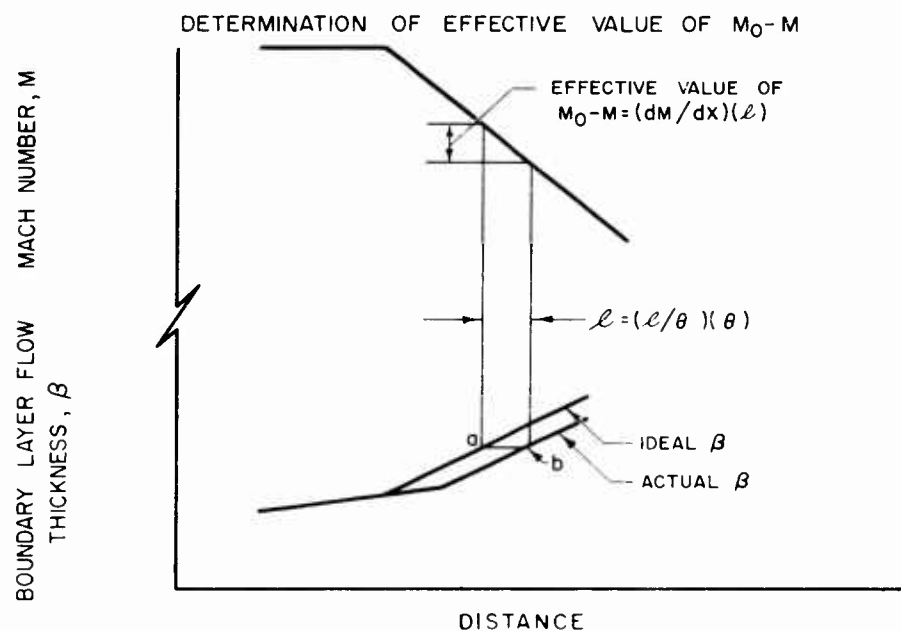
TYPICAL VALUES OF BOUNDARY LAYER FLOW THICKNESS FOR SINGLE-RADIUS TWO-DIMENSIONAL CURVED-SURFACE MODEL

$M_O = 3.0$ $R = 6$ IN. $\alpha_T = 30$ DEG $W_b = 0$

ADDITIONAL DATA FOR THIS MODEL FOUND IN FIGS. 20,21,22,23,24,46,53,62, AND 68

ARROWS ($\downarrow$) INDICATE STATIONS AT WHICH VALUES OF ℓ/θ GIVEN IN FIG. 56 WERE DETERMINED
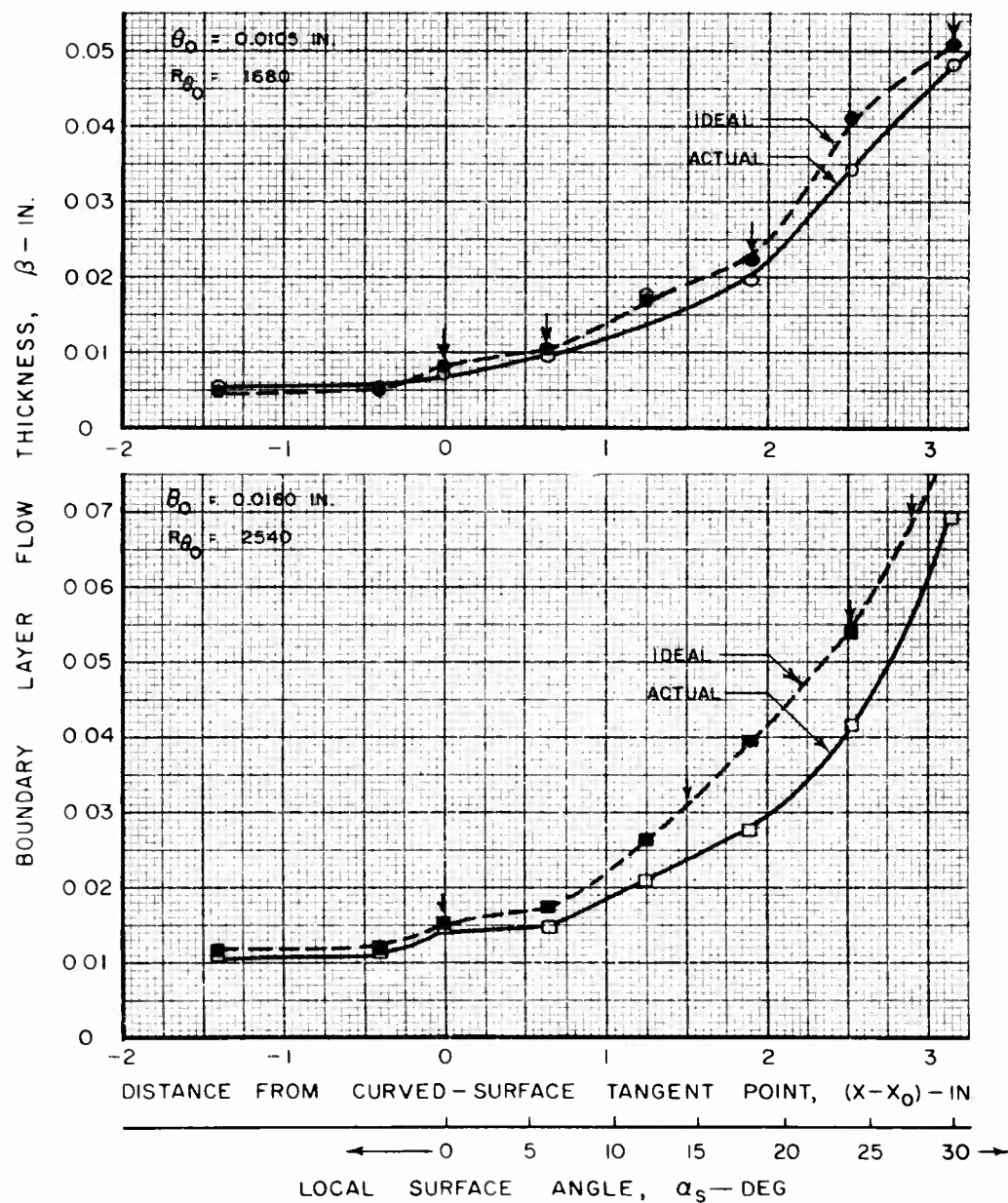
TYPICAL VALUES OF LAG LENGTH FOR SINGLE-RADIUS
TWO-DIMENSIONAL CURVED-SURFACE MODEL

$M_0 = 3.0$ $R = 6$ IN. $\alpha_T = 30$ DEG $W_b = 0$

SYMBOL	θ_0 — IN.	R_{θ_0}
⎯⎯○⎯⎯	0.0105	1680
⎯ ⎯□⎯ ⎯	0.0160	2540
⎯ ⎯△⎯ ⎯	0.0215	3420

LAG LENGTH / BOUNDARY LAYER MOMENTUM THICKNESS, $\frac{\ell}{\theta}$

$R_{\theta_0} = 3420$

$R_{\theta_0} = 2540$

$R_{\theta_0} = 1680$

REYNOLDS NUMBER BASED ON BOUNDARY LAYER MOMENTUM THICKNESS, R_θ

FIG. 57
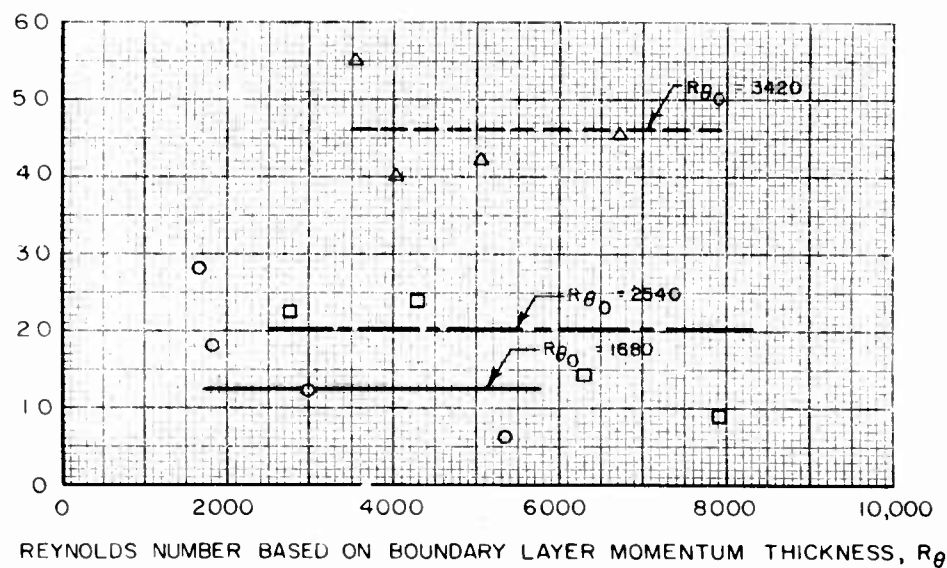
TYPICAL VALUES OF BOUNDARY LAYER FLOW THICKNESS
FOR TWO-RADII TWO-DIMENSIONAL CURVED-SURFACE MODEL

$M_0 = 3.0$ $R_1 = 6$ IN. $R_2 = 3$ IN. $\alpha_1 = 20$ DEG $\alpha_T = 35$ DEG $W_b = 0$

ADDITIONAL DATA FOR THIS MODEL FOUND IN FIGS. 26, 63, AND 69

ARROWS (↑) INDICATE STATIONS AT WHICH VALUES OF ℓ/θ GIVEN IN FIG. 58 WERE DETERMINED

BOUNDARY LAYER FLOW THICKNESS, β – IN.

DISTANCE FROM CURVED-SURFACE TANGENT POINT, $(x-x_0)$-IN.

LOCAL SURFACE ANGLE, α_s–DEG

103
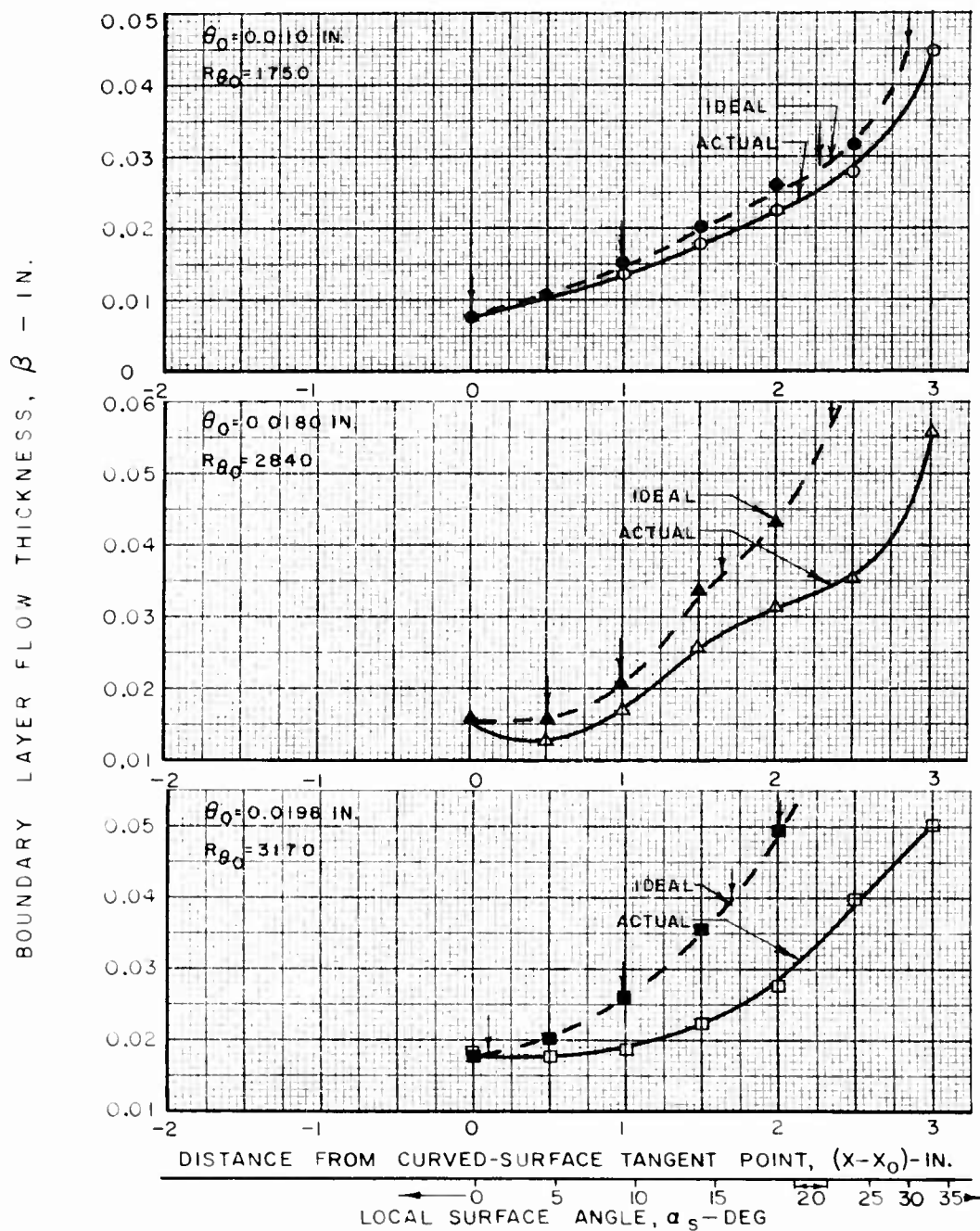
TYPICAL VALUES OF LAG LENGTH FOR TWO-RADII
TWO-DIMENSIONAL CURVED-SURFACE MODEL

$M_0 = 3.0$ $R_1 = 6$ IN. $R_2 = 3$ IN. $\alpha_1 = 20$ DEG

$\alpha_T = 35$ DEG $W_b = 0$

SYMBOL	θ_0 -IN.	R_{θ_0}
——○——	0.0110	1750
——△——	0.0180	2840
——□——	0.0198	3170

REYNOLDS NUMBER BASED ON BOUNDARY LAYER MOMENTUM THICKNESS, R_θ

104
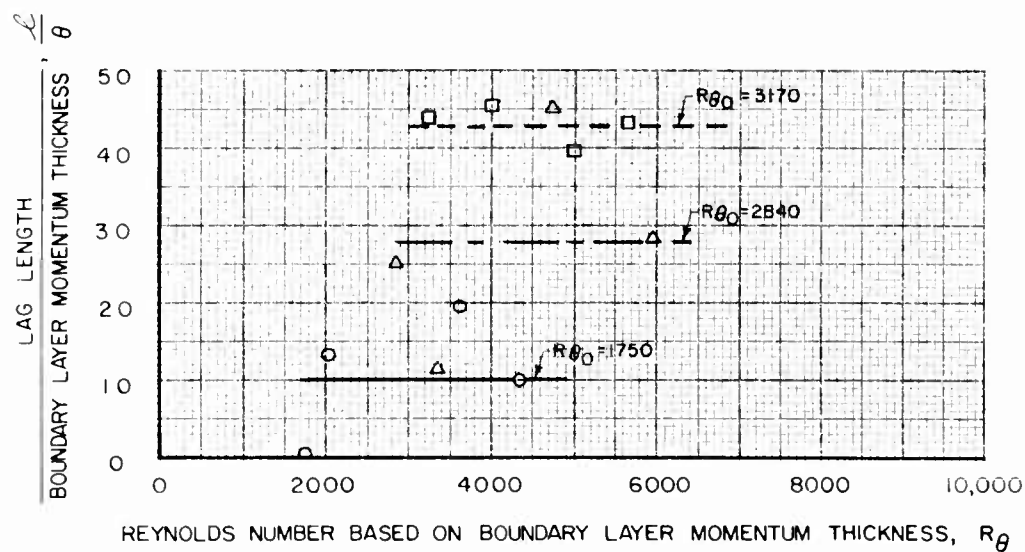
TYPICAL VALUES OF BOUNDARY LAYER FLOW THICKNESS AND LAG LENGTH FOR AXISYMMETRIC CURVED-SURFACE MODEL

$M_0 = 3.0$ $R = 1.5$ IN $\alpha_T = 30$ DEG $w_b = 0$

$\theta_0 = 0.0056$ IN. $R_{\theta_0} = 900$

ADDITIONAL DATA FOR THIS MODEL FOUND IN FIGS. 28, 29, 64, AND 70

ARROWS ($\downarrow$) INDICATE STATIONS AT WHICH VALUES OF ℓ/θ WERE DETERMINED

DISTANCE FROM CURVED-SURFACE TANGENT POINT, $(X - X_0)$-IN.

LOCAL SURFACE ANGLE, α_S-DEG

REYNOLDS NUMBER BASED ON BOUNDARY LAYER MOMENTUM THICKNESS, R_θ

FIG.60
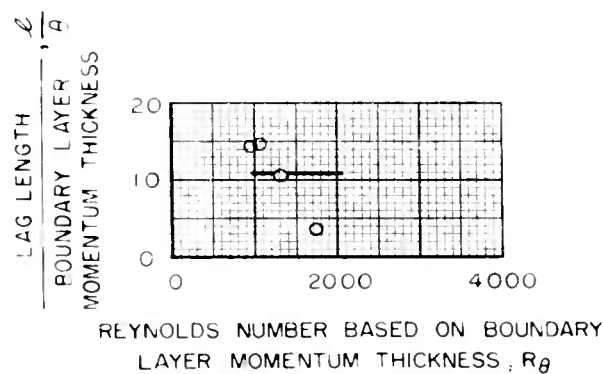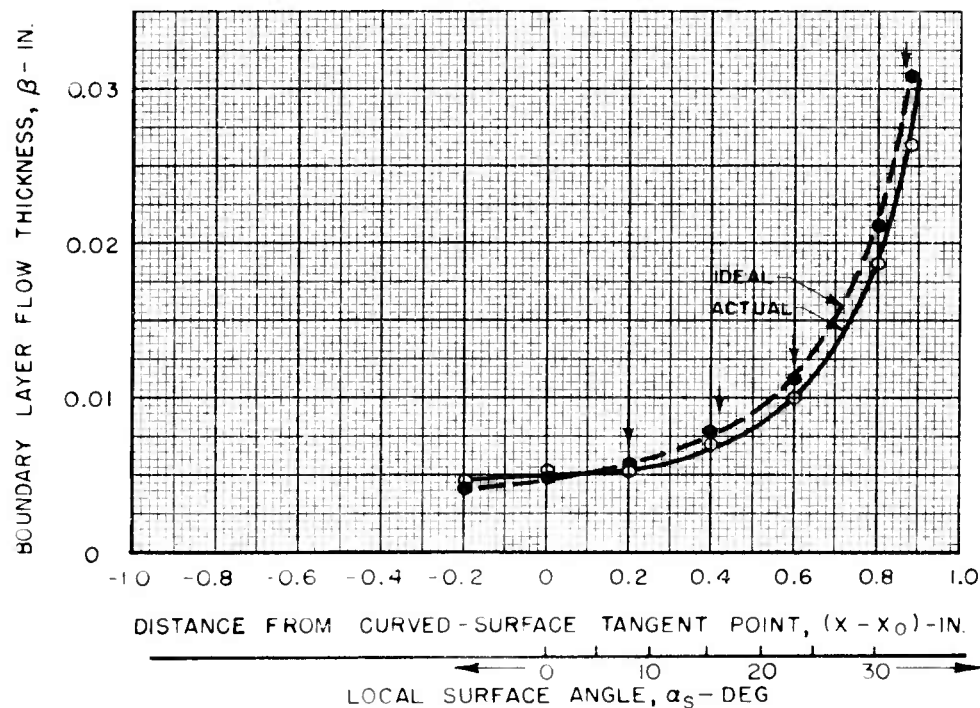
PLOT OF CURVE FITTED THROUGH LAG—LENGTH DATA

$$\ell/\theta = -22.5 + 49.7 \left[\left(\frac{R_{\theta_Q}}{1000} - 1 \right)^{0.2} \left(\frac{1}{1 + \left(\frac{R_\theta - R_{\theta_Q}}{1000} \right)} \right)^{0.5} + \left(\frac{R_\theta}{1000} - 1 \right)^{0.2} \left(1 - \left(\frac{1}{1 + \left(\frac{R_\theta - R_{\theta_Q}}{1000} \right)} \right)^{0.5} \right) \right]$$
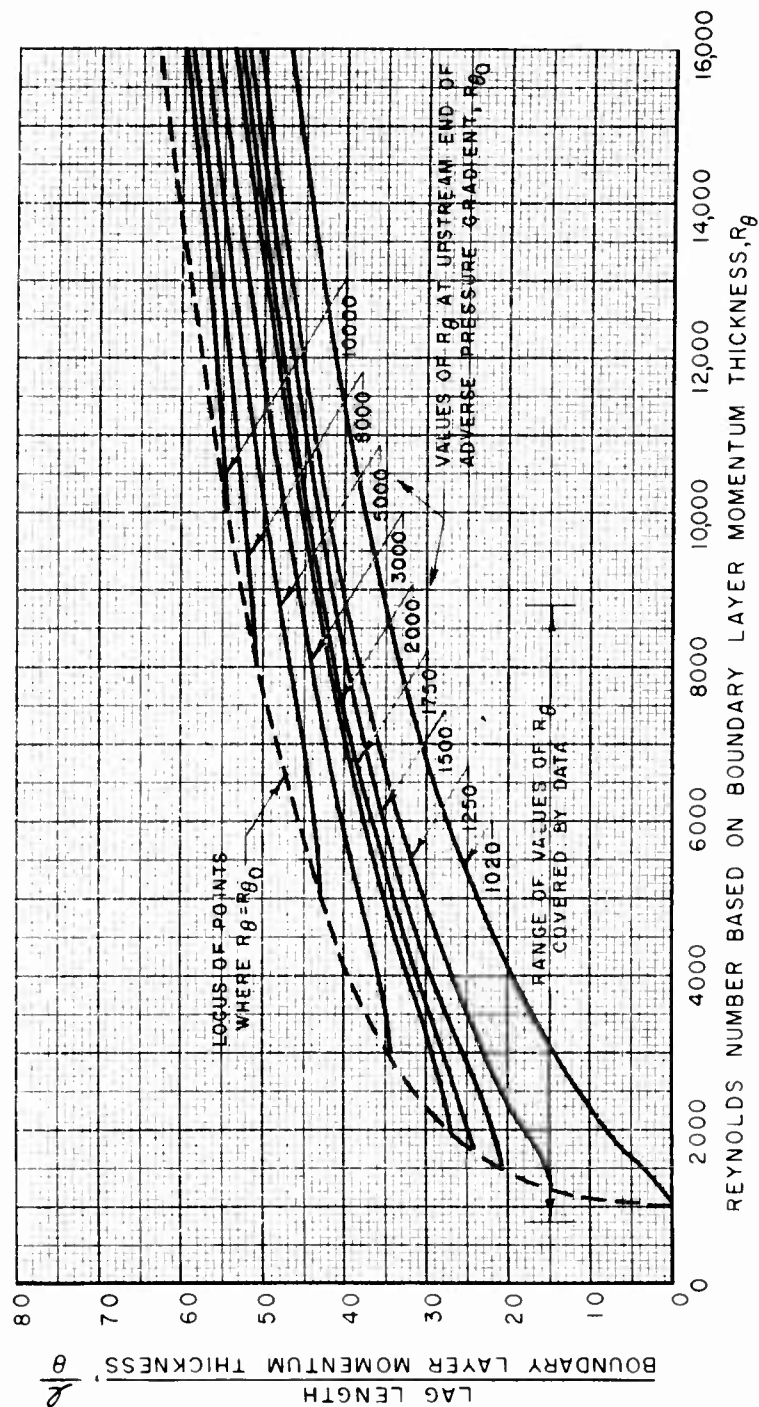
(EQ. 19)

COMPARISON OF LAG LENGTHS FROM DATA
AND FROM FITTED CURVES

AVERAGE VALUE = 0

ROOT - MEAN - SQUARE SCATTER = 15.8

SYMBOL	M_O
△	2.0
○	2.5
●	3.0
×	3.5
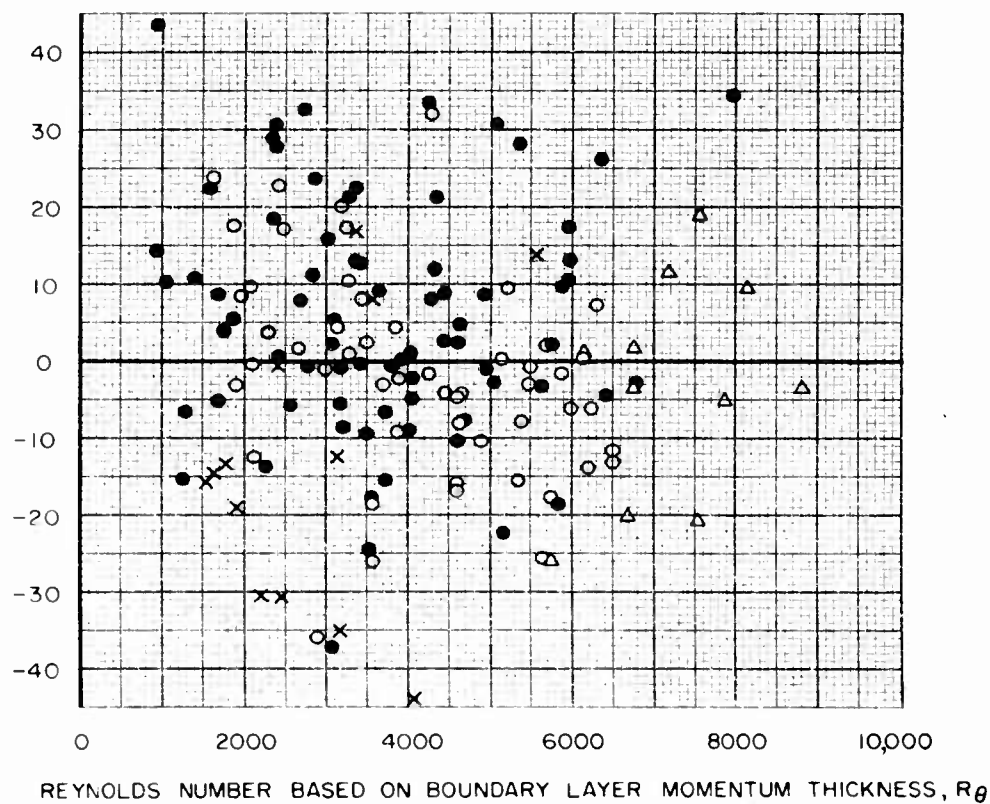
TYPICAL COMPARISON OF CALCULATED AND MEASURED VALUES OF REDUCED BOUNDARY LAYER SHAPE PARAMETER FOR SINGLE-RADIUS TWO-DIMENSIONAL CURVED-SURFACE MODEL

$M_O = 3.0$ $R = 6$ IN. $\alpha_T = 30$ DEG

ADDITIONAL DATA FOR THIS MODEL FOUND IN FIGS. 20, 21, 22, 23, 24, 46, 53, 55, AND 68
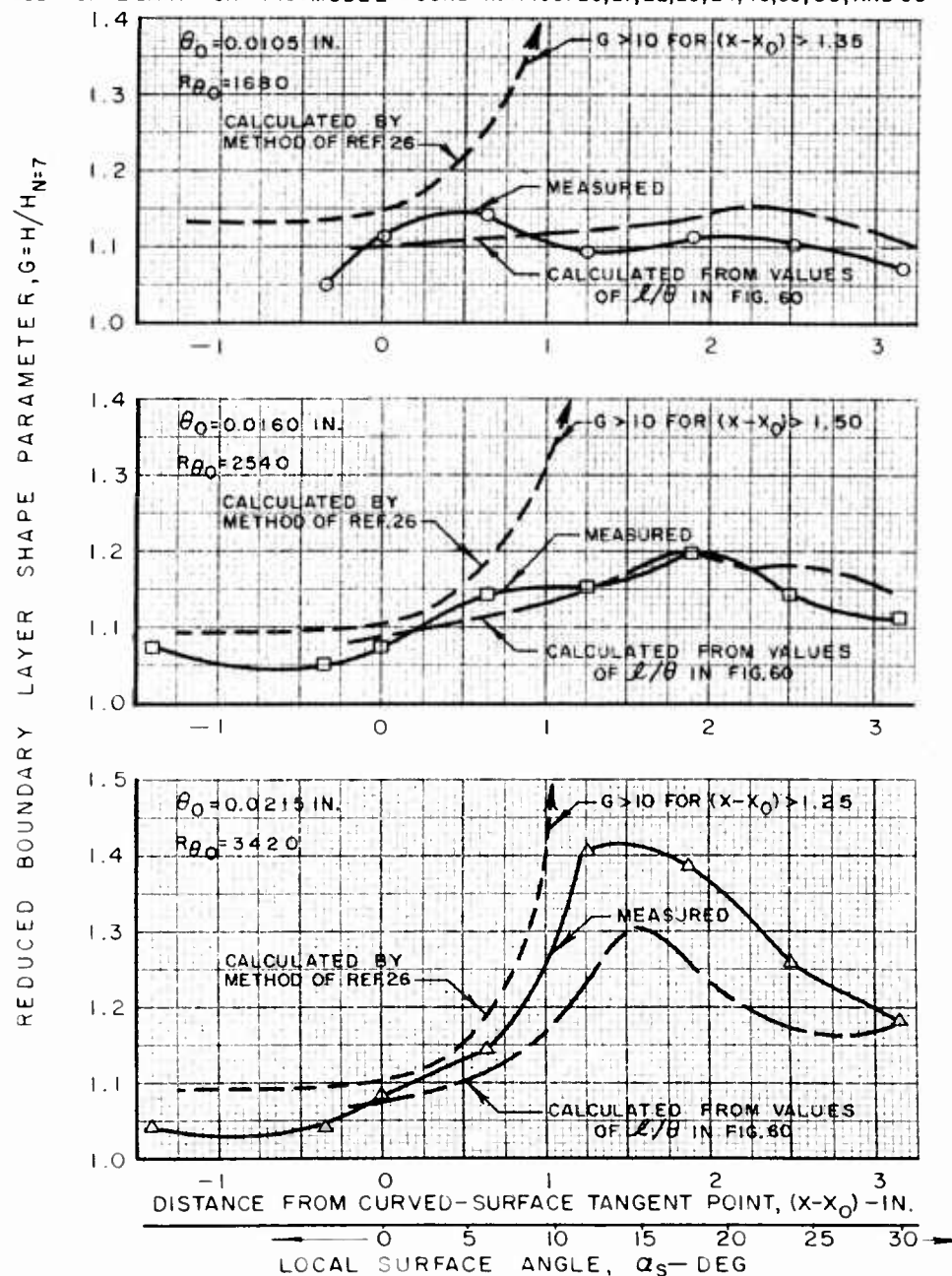
FIG. 63

TYPICAL COMPARISON OF CALCULATED AND MEASURED VALUES OF REDUCED BOUNDARY LAYER SHAPE PARAMETER FOR TWO-RADII TWO-DIMENSIONAL CURVED-SURFACE MODEL

$M_O = 3.0$ $R_1 = 6$ IN. $R_2 = 3$ IN. $\alpha_1 = 20$ DEG $\alpha_T = 35$ DEG $W_b = 0$

ADDITIONAL DATA FOR THIS MODEL FOUND IN FIGS. 26, 57, AND 69
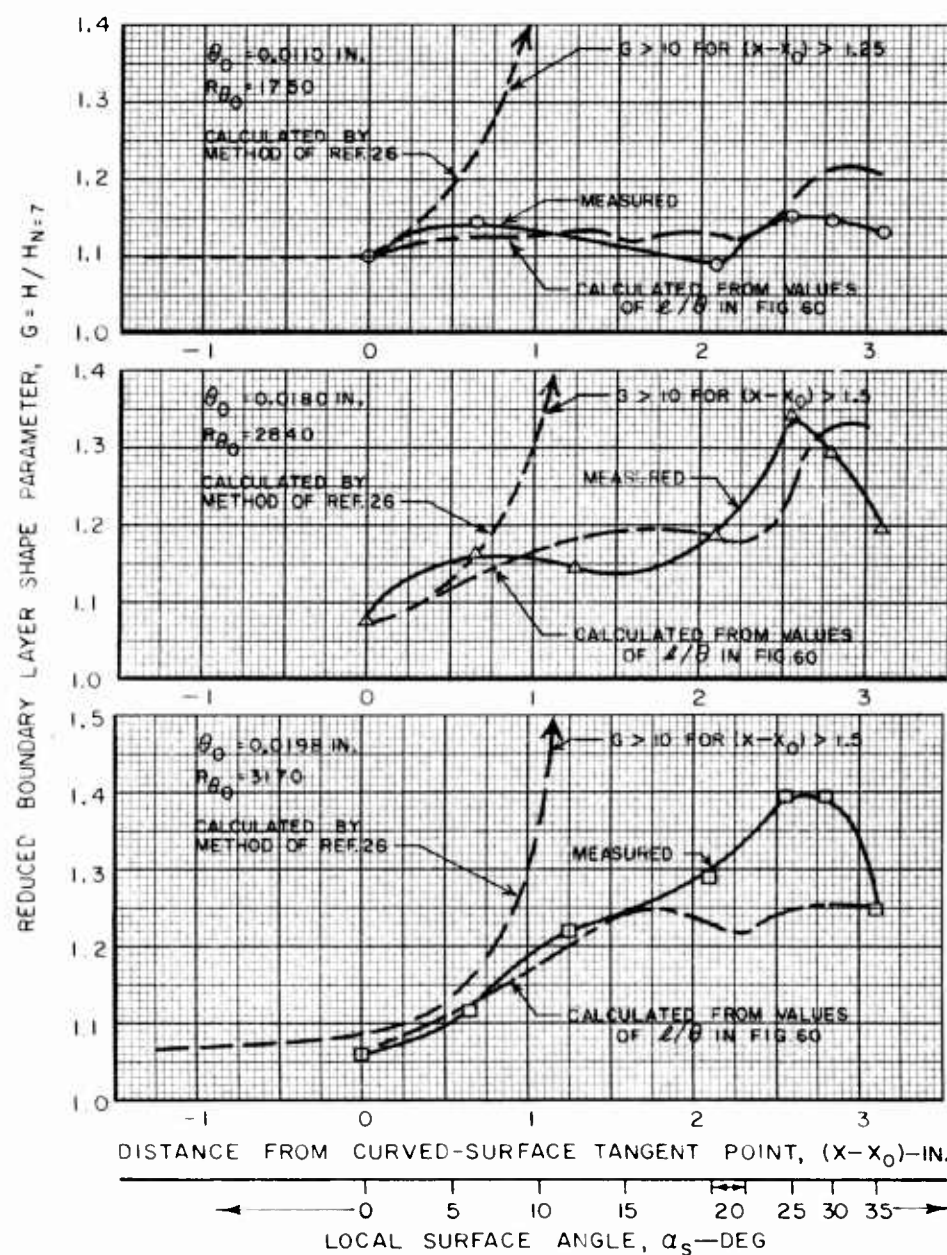
DISTANCE FROM CURVED-SURFACE TANGENT POINT, $(X-X_O)$—IN.

LOCAL SURFACE ANGLE, α_S—DEG

TYPICAL COMPARISON OF CALCULATED AND MEASURED VALUES OF REDUCED BOUNDARY LAYER SHAPE PARAMETER FOR AXISYMMETRIC CURVED-SURFACE MODEL

$M_O = 3.0$ $R = 1.5$ IN. $\alpha_T = 30$ DEG

$\theta_O = 0.0056$ IN. $R_{\theta_O} = 900$

ADDITIONAL DATA FOR THIS MODEL FOUND IN FIGS. 28, 29, 59, AND 70
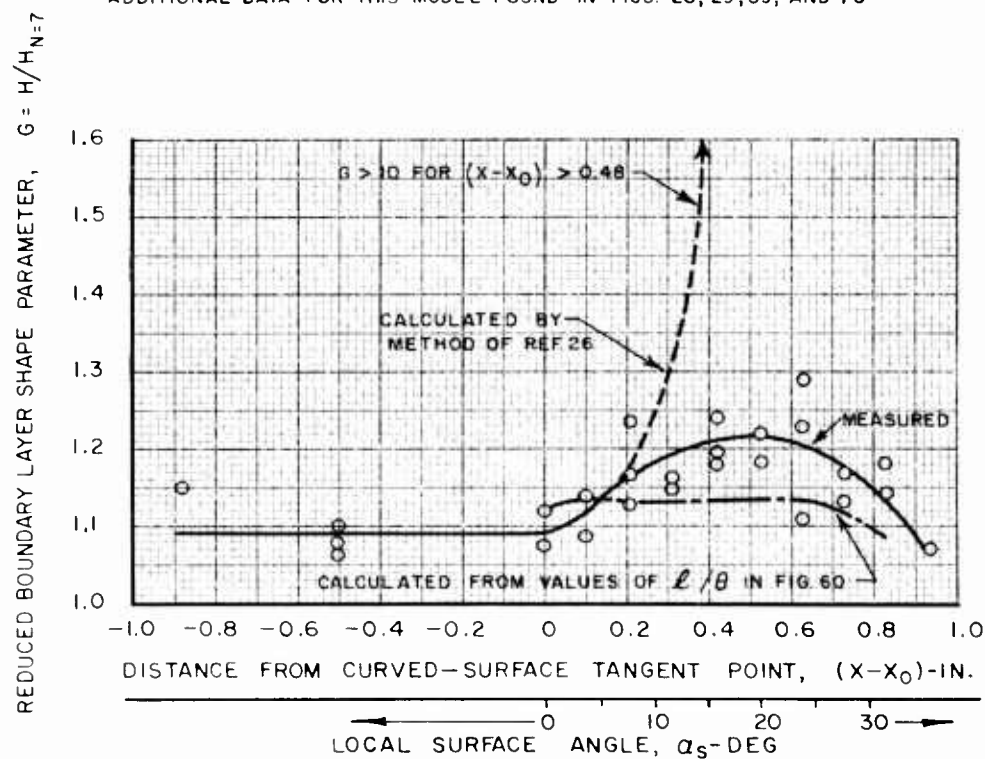
SUMMARY OF DATA ON DIFFERENCE BETWEEN CALCULATED AND MEASURED MAXIMUM VALUES OF REDUCED BOUNDARY LAYER SHAPE PARAMETER

$w_b = 0$

SYMBOL	M_O
△	2.0
○	2.5
●	3.0
×	3.5

AVERAGE VALUE = 0.044
ROOT-MEAN-SQUARE
SCATTER = 0.094

REYNOLDS NUMBER BASED ON BOUNDARY LAYER MOMENTUM THICKNESS AT STATION O, R_{θ_0}

(MAXIMUM MEASURED G) − (MAXIMUM G CALCULATED FROM VALUES OF ℓ/θ IN FIG. 60)
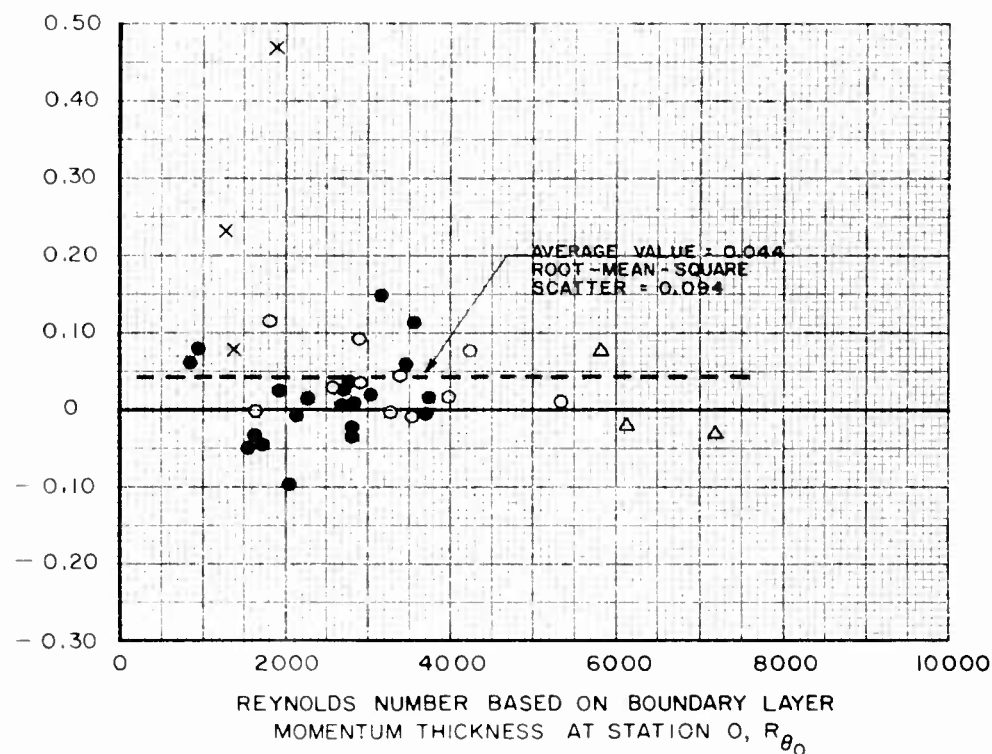
EFFECT OF SMALL CHANGES IN MACH NUMBER DISTRIBUTION ON CALCULATED VALUES OF REDUCED BOUNDARY LAYER SHAPE PARAMETER FOR SINGLE-RADIUS TWO-DIMENSIONAL CURVED-SURFACE MODEL

$M_O = 3.0$ $\quad\quad$ $R = 6$ IN. $\quad\quad$ $\alpha_T = 30$ DEG $\quad\quad$ $W_b = 0$

$\theta_O = 0.0215$ IN. $\quad\quad\quad\quad\quad\quad\quad\quad$ $R_{\theta_O} = 3420$
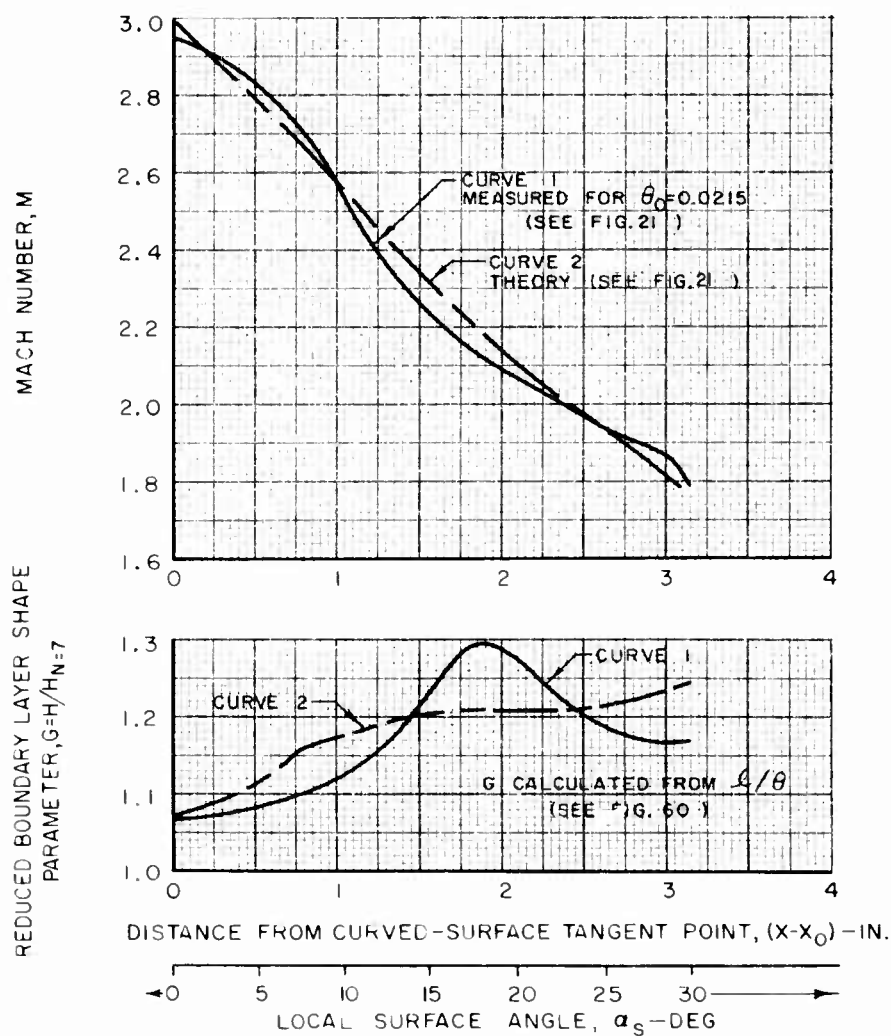
ASSUMPTIONS EMPLOYED IN CALCULATING BOUNDARY LAYER MOMENTUM THICKNESS GROWTH ON CURVED – SURFACE MODELS

CURVE IDENTIFICATION	G USED IN CALCULATION	C_f USED IN CALCULATION
a	G_F , FIG. 18	O
b	MEASURED	O
c	MEASURED	FROM FIGS. 36 AND 37
d	MEASURED	FROM FIG. 36
e	CALCULATED FROM ℓ/θ IN FIG. 60	FROM FIGS. 36 AND 37

BOUNDARY LAYER MOMENTUM THICKNESS, θ

DISTANCE FROM CURVED – SURFACE TANGENT POINT, $(X-X_O)$
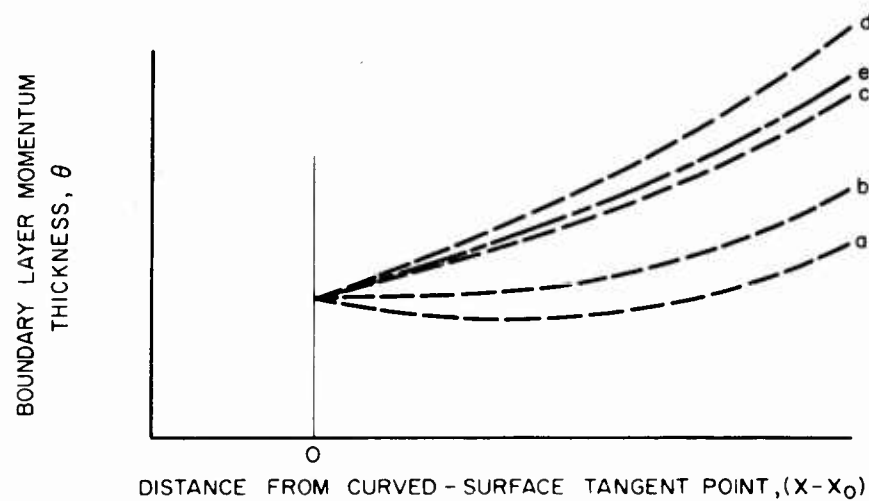
$\theta_b - \theta_a$ CAUSED BY FACT THAT ACTUAL G IN ADVERSE PRESSURE GRADIENT IS GREATER THAN G THAT WOULD EXIST ON FLAT PLATE AT SAME R_θ

$\theta_c - \theta_b$ CAUSED BY WALL FRICTION

$\theta_d - \theta_c$ CAUSED BY FACT THAT FRICTION IN ADVERSE PRESSURE GRADIENT IS LESS THAN FRICTION ON FLAT PLATE BECAUSE OF REDUCED VELOCITY GRADIENT AT WALL

$\theta_e - \theta_c$ CAUSED BY FACT THAT VALUES OF G CALCULATED BY LAG-LENGTH PROCEDURE ARE NOT EXACTLY EQUAL TO MEASURED VALUES OF G
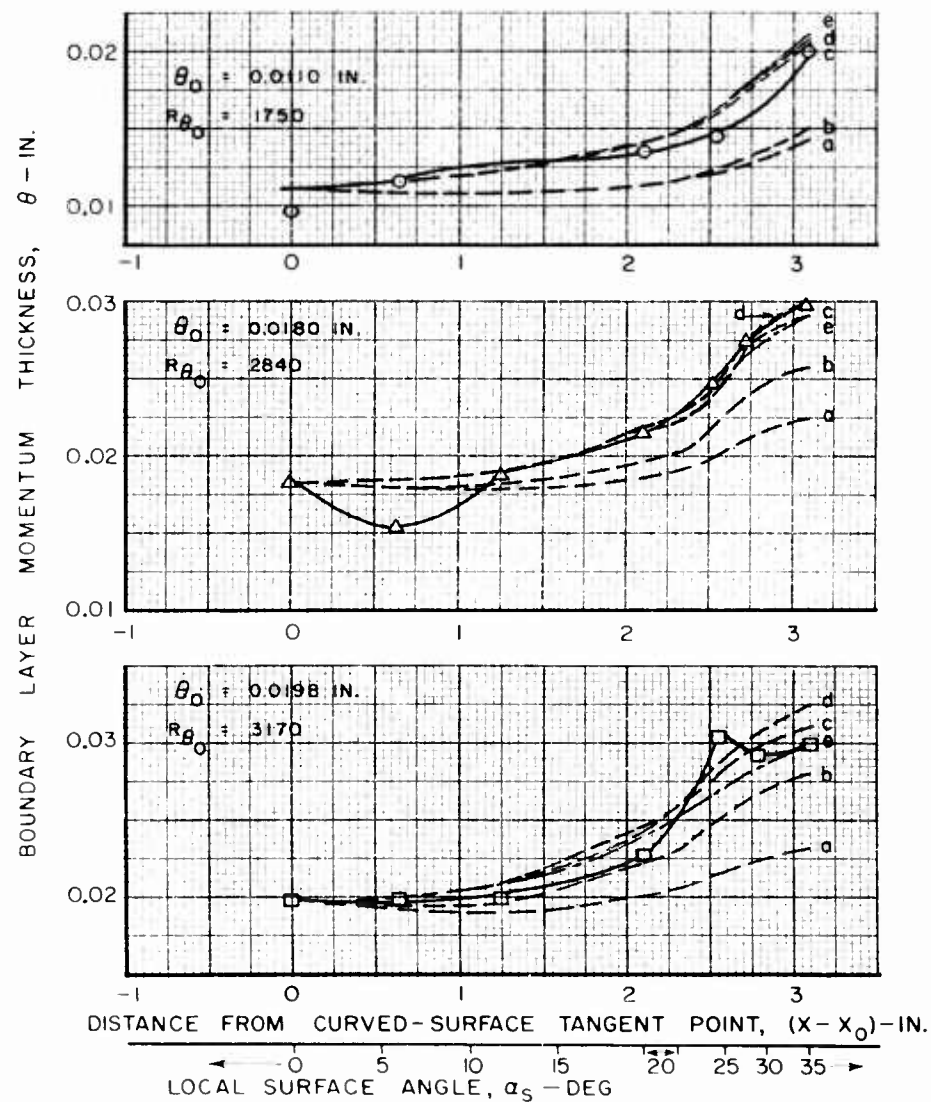
113

TYPICAL COMPARISON OF CALCULATED AND MEASURED VALUES OF
BOUNDARY LAYER MOMENTUM THICKNESS FOR SINGLE-RADIUS
TWO-DIMENSIONAL CURVED-SURFACE MODEL

$M_O = 3.0$ $R = 6$ IN. $\alpha_T = 30$ DEG $W_b = 0$

ADDITIONAL DATA FOR THIS MODEL FOUND IN FIGS. 20,21,22,23,24,46,53,55,AND 62
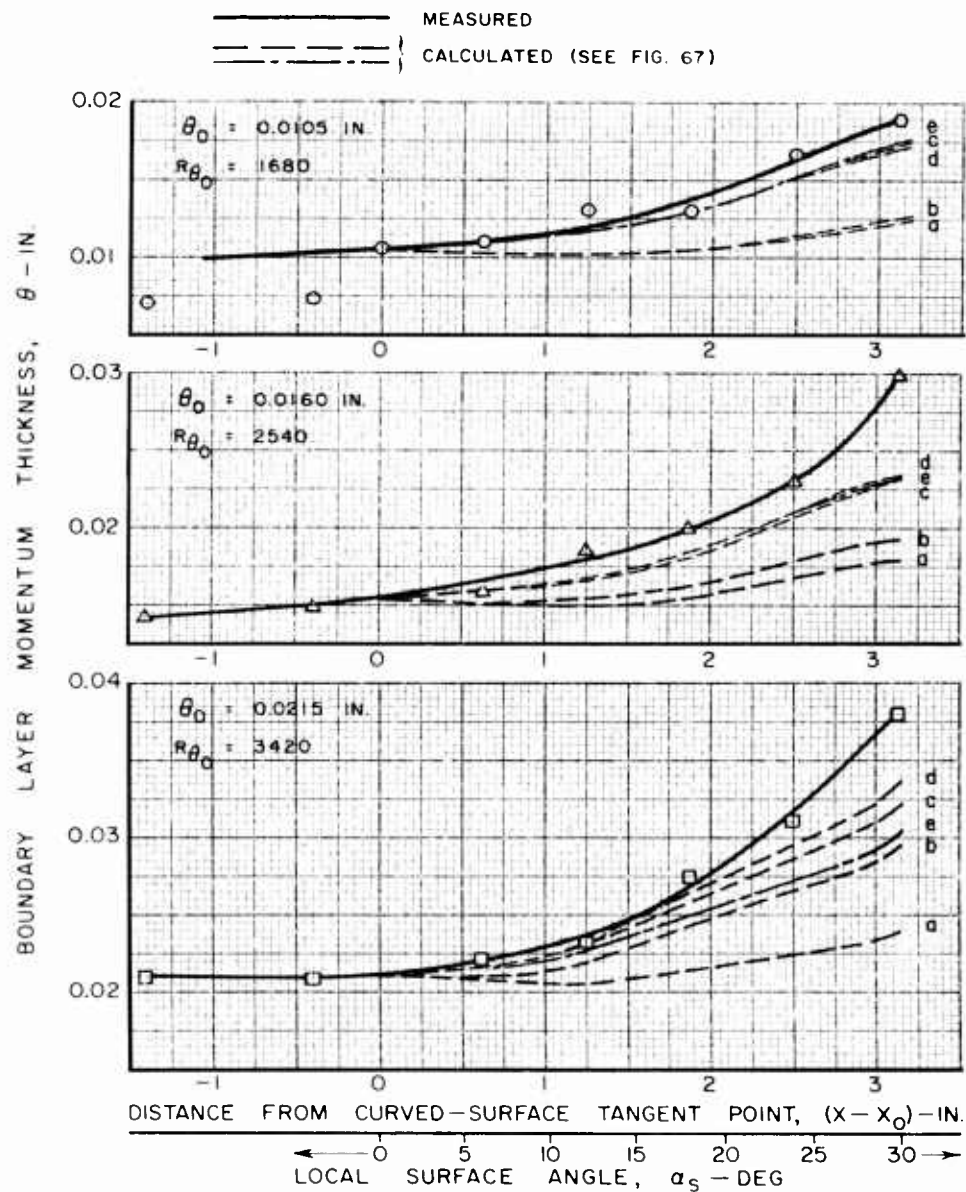
TYPICAL COMPARISON OF CALCULATED AND MEASURED VALUES OF BOUNDARY LAYER MOMENTUM THICKNESS FOR TWO-RADII TWO-DIMENSIONAL CURVED-SURFACE MODEL

$M_0 = 3.0$ $R_1 = 6$ IN. $R_2 = 3$ IN. $\alpha_1 = 20$ DEG $\alpha_T = 35$ DEG $W_b = 0$
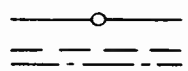
ADDITIONAL DATA FOR THIS MODEL FOUND IN FIGS. 26, 57, AND 63

————————— MEASURED

— — — · — · — } CALCULATED (SEE FIG. 67)

TYPICAL COMPARISON OF CALCULATED AND MEASURED VALUES OF
BOUNDARY LAYER MOMENTUM THICKNESS FOR AXISYMMETRIC
CURVED-SURFACE MODEL

$M_O = 3.0$ $R = 1.5$ IN. $\alpha_T = 30$ DEG $w_b = 0$

MEASURED

CALCULATED (SEE FIG. 67)
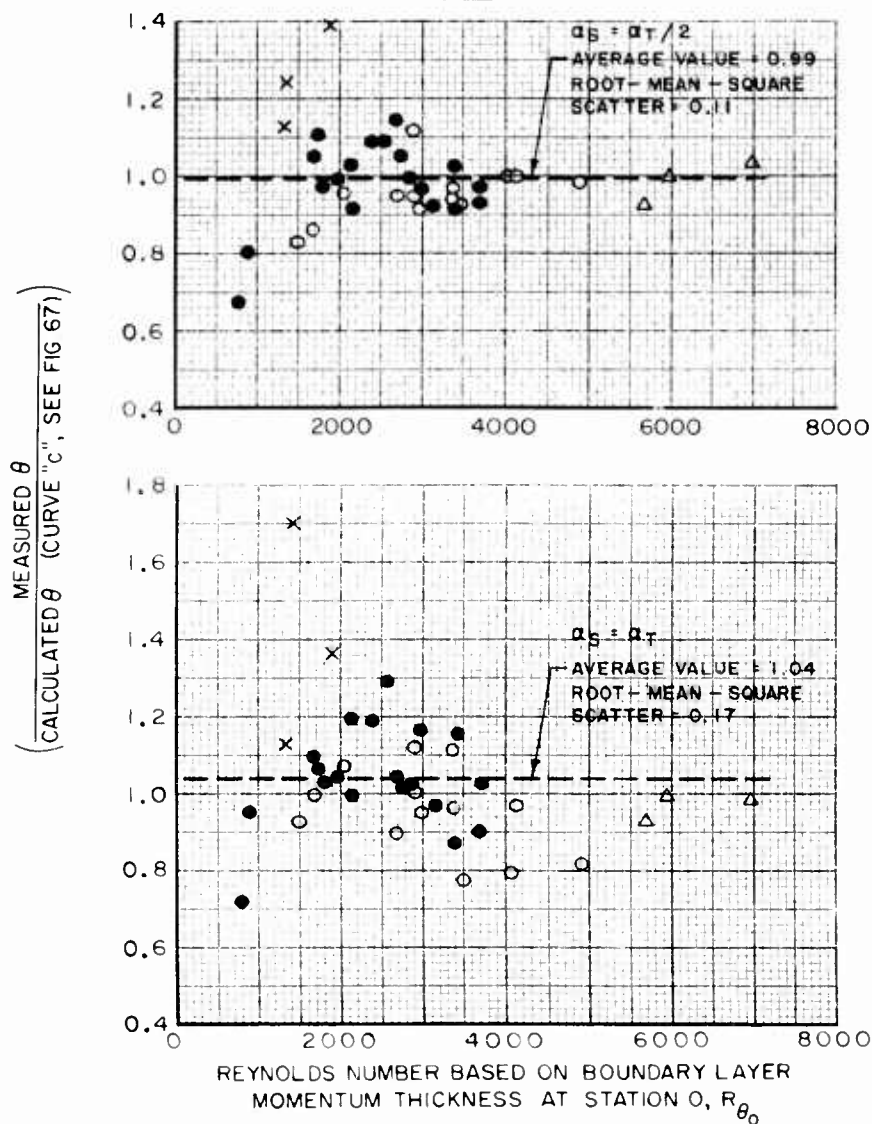
ADDITIONAL DATA FOR THIS MODEL FOUND IN FIGS. 28, 29, 59, AND 64

$\theta_0 = 0.0056$ IN.

$R_{\theta_0} = 900$

BOUNDARY LAYER MOMENTUM THICKNESS, θ - IN.

DISTANCE FROM CURVED-SURFACE TANGENT POINT, $(x - x_0)$ - IN.

LOCAL SURFACE ANGLE, α_s - DEG
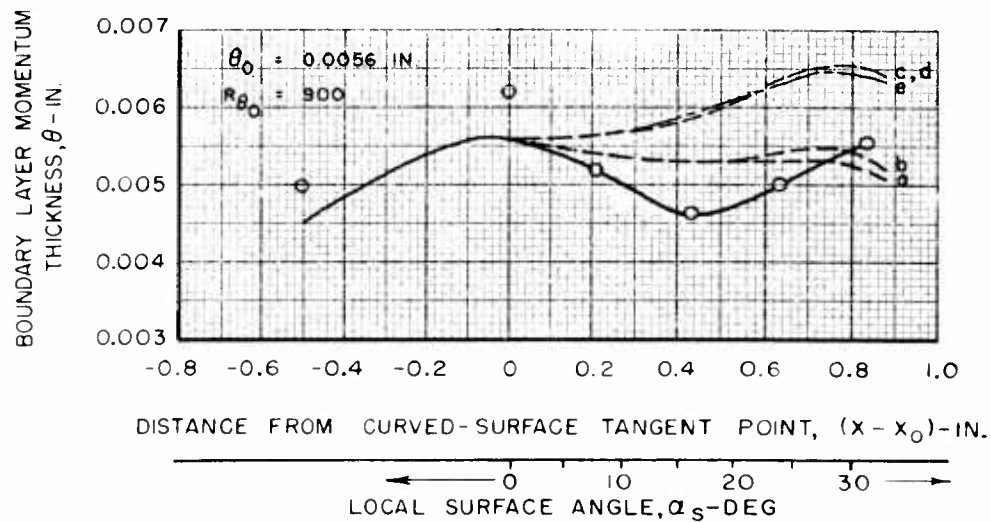
COMPARISON OF CALCULATED AND MEASURED VALUES
OF BOUNDARY LAYER MOMENTUM THICKNESS

$$w_b = 0$$

SYMBOL	M_0
△	2.0
○	2.5
●	3.0
×	3.5

$\alpha_S = \alpha_T/2$
AVERAGE VALUE = 0.99
ROOT-MEAN-SQUARE
SCATTER = 0.11

$\alpha_S = \alpha_T$
AVERAGE VALUE = 1.04
ROOT-MEAN-SQUARE
SCATTER = 0.17

$\dfrac{\text{MEASURED } \theta}{\text{CALCULATED } \theta} \left(\text{CURVE "C", SEE FIG 67} \right)$

REYNOLDS NUMBER BASED ON BOUNDARY LAYER
MOMENTUM THICKNESS AT STATION O, R_{θ_0}

117

FIG. 72

EFFECT OF BOUNDARY LAYER BLEED ON GROWTH OF BOUNDARY LAYER MOMENTUM THICKNESS
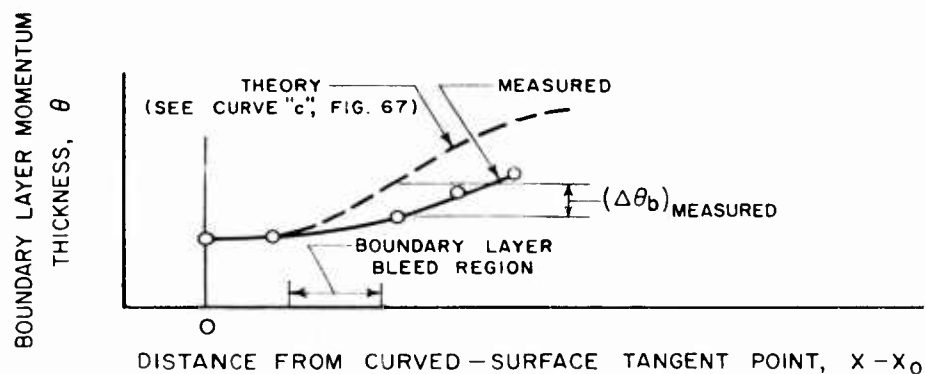
SYMBOL	M_0	R — IN.	α_T—DEG
O	2.5	3.0	30
●	3.0	3.0	30
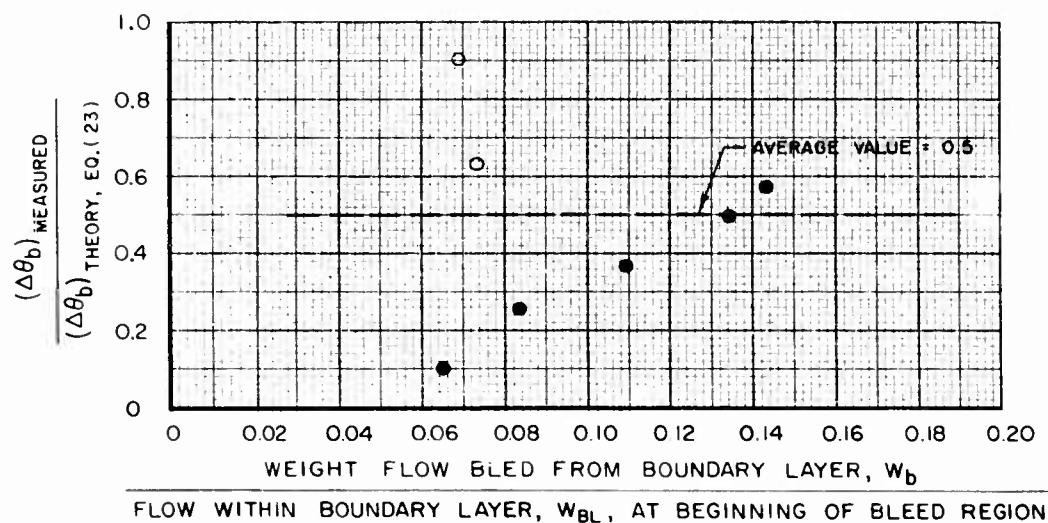
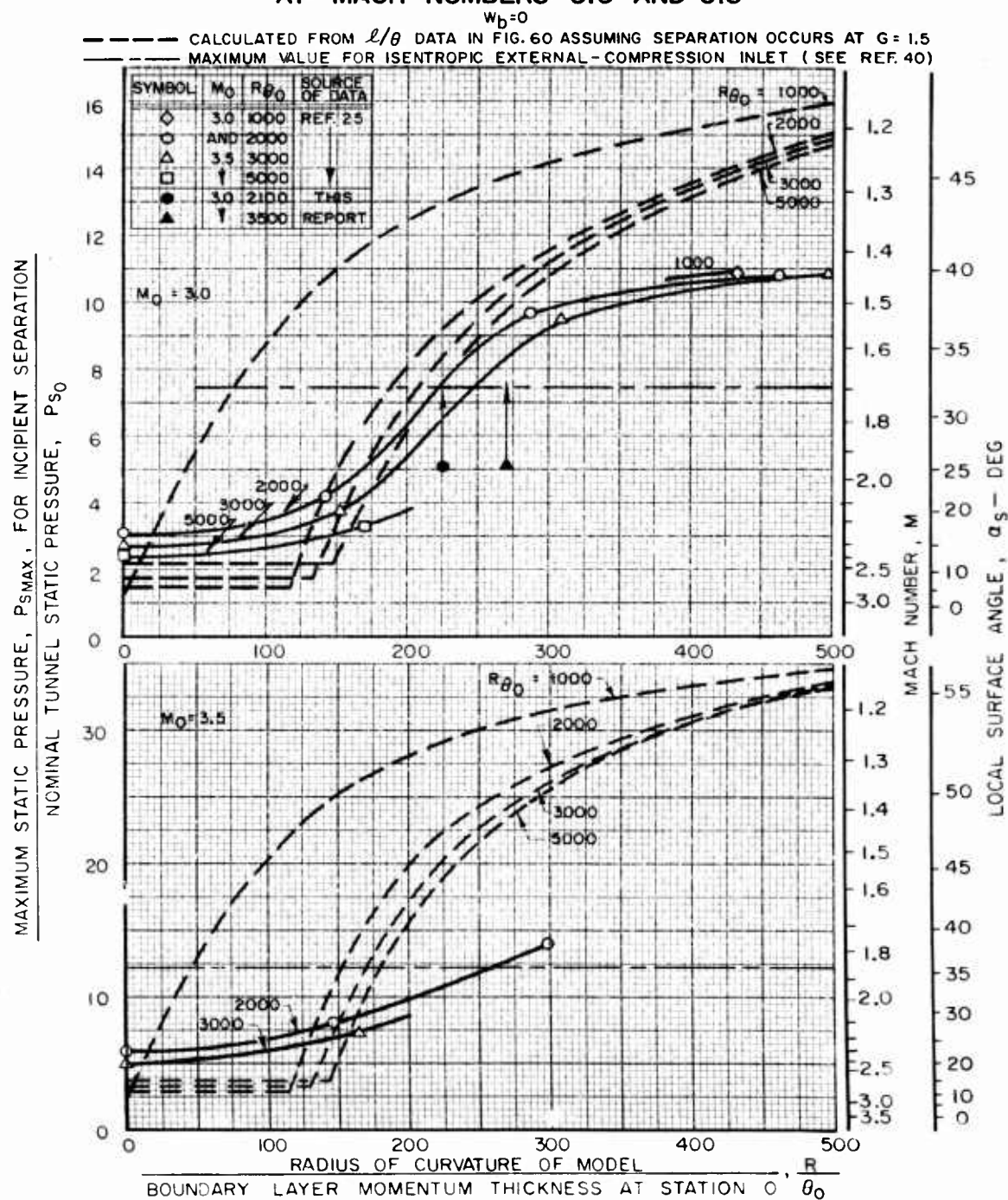# PRESSURE RATIO FOR INCIPIENT SEPARATION ON SINGLE-RADIUS TWO-DIMENSIONAL CURVED-SURFACE MODEL AT MACH NUMBERS 2.0 AND 2.5
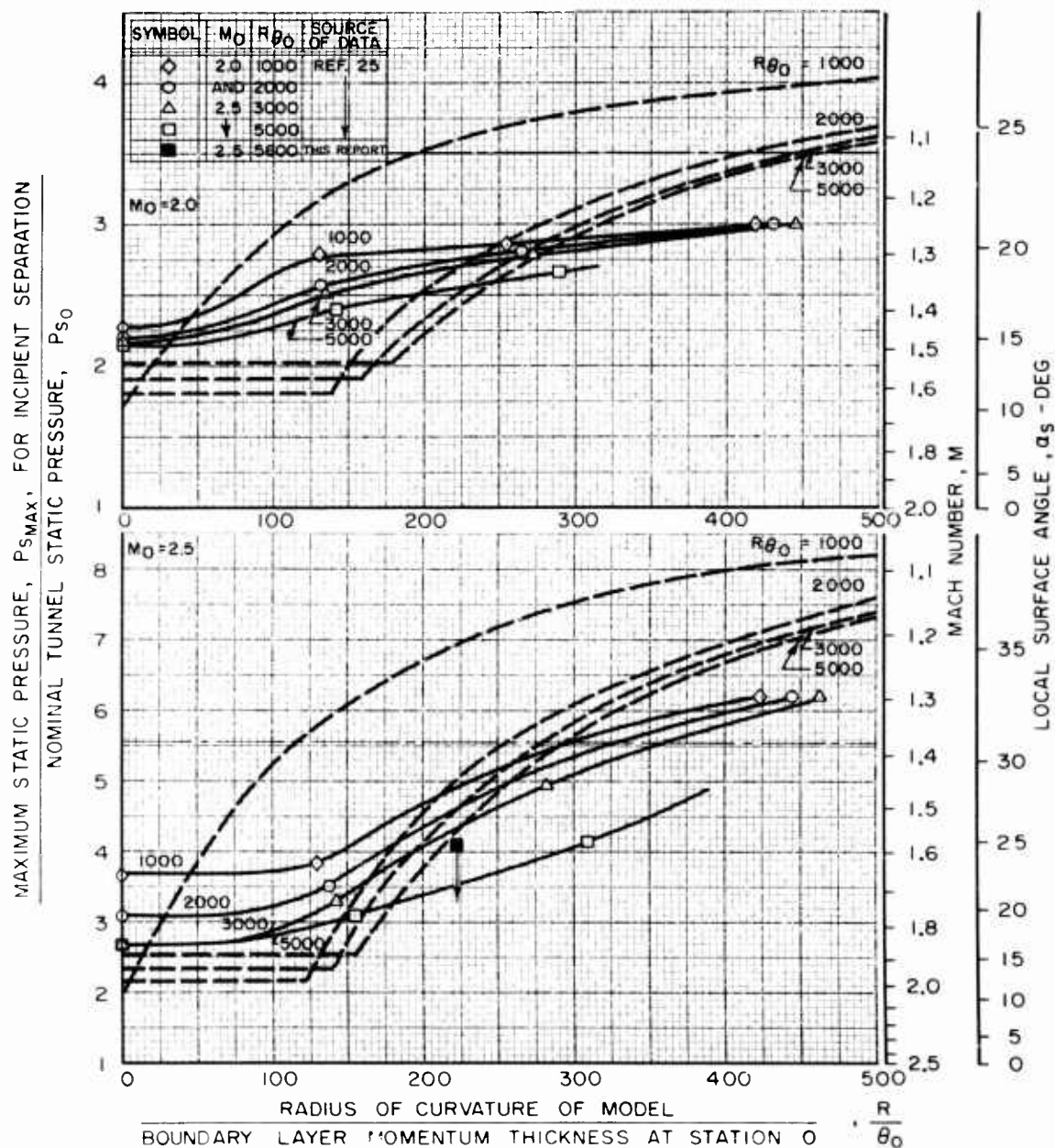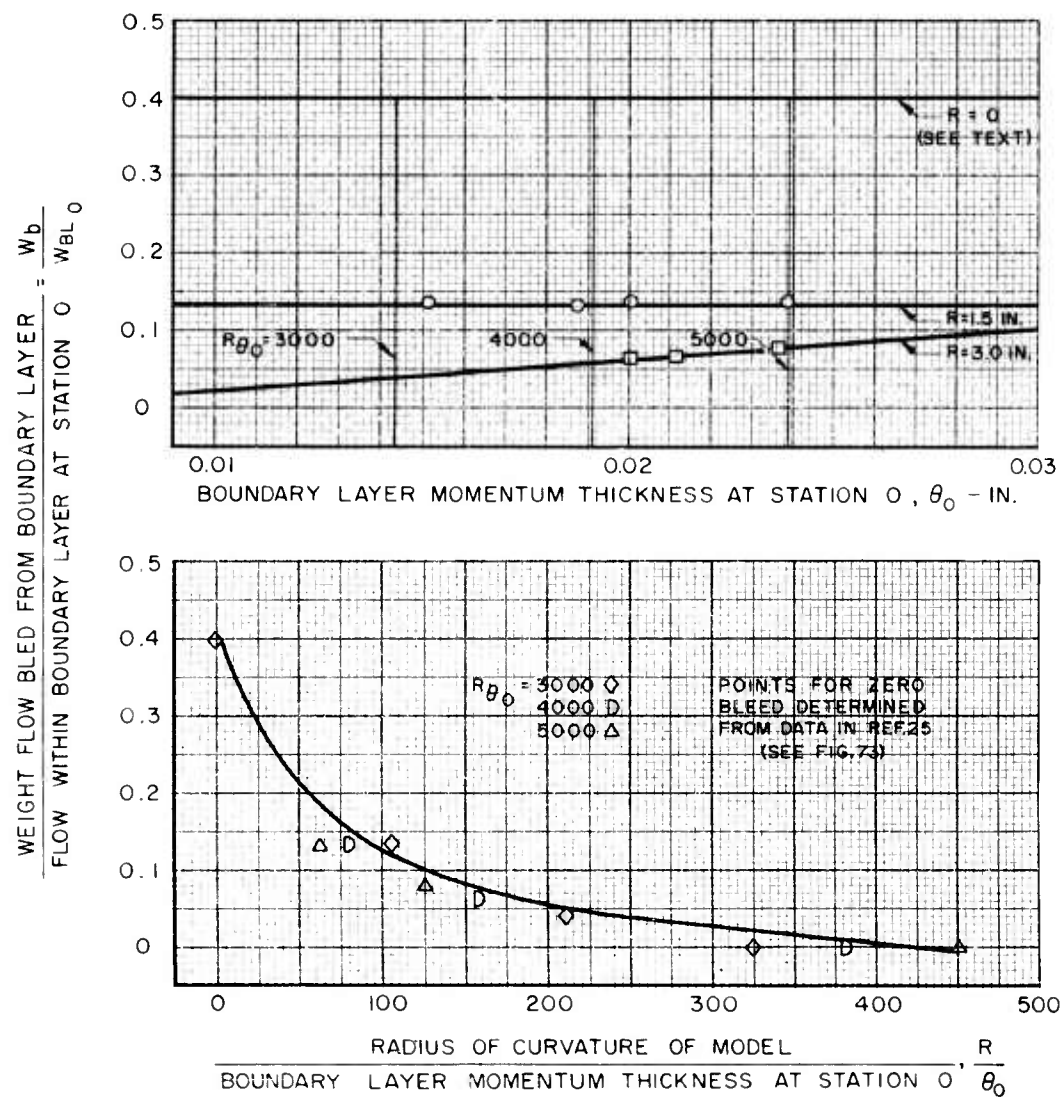
PRESSURE RATIO FOR INCIPIENT SEPARATION ON SINGLE-RADIUS TWO-DIMENSIONAL CURVED-SURFACE MODEL AT MACH NUMBERS 3.0 AND 3.5

BOUNDARY LAYER BLEED REQUIRED TO PREVENT SEPARATION
ON SINGLE-RADIUS TWO-DIMENSIONAL CURVED-SURFACE
MODEL AT MACH NUMBER 2.5

$\alpha_T = 30$ DEG

FLOW BLED BETWEEN $\alpha_S = 12$ AND 25 DEG

BOUNDARY LAYER BLEED REQUIRED TO PREVENT SEPARATION ON SINGLE-RADIUS TWO-DIMENSIONAL CURVED-SURFACE MODEL AT MACH NUMBER 3.0

$\alpha_T = 30$ DEG

FLOW BLED BETWEEN $\alpha_S = 12$ AND 25 DEG
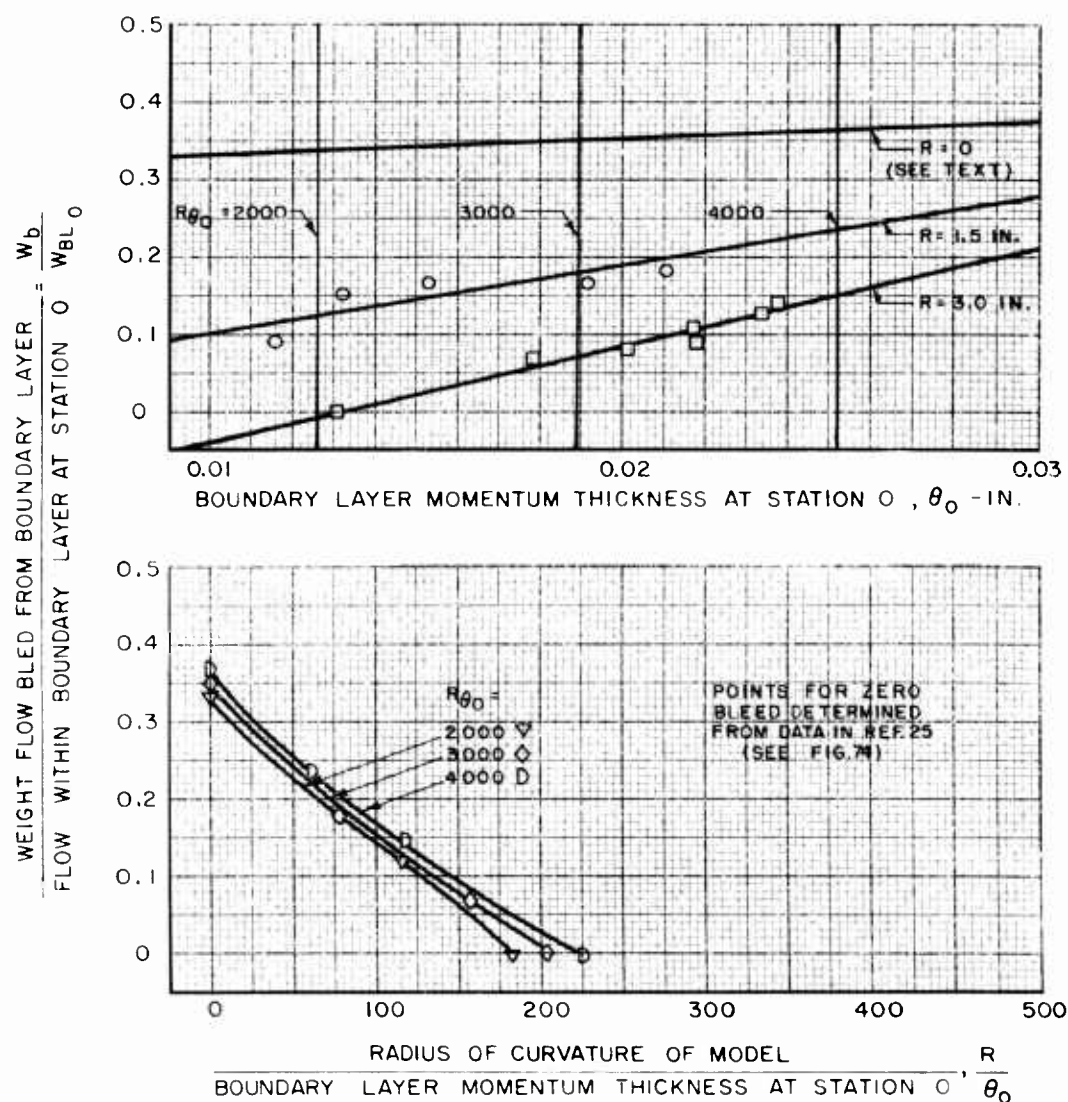
EFFECT OF WALL TEMPERATURE ON
LOCAL SKIN-FRICTION COEFFICIENT

$R_\theta = 13,500$
ZERO PRESSURE GRADIENT

CURVES OBTAINED FROM REF. 32

LOCAL SKIN-FRICTION COEFFICIENT

$$\frac{\text{LOCAL SKIN-FRICTION COEFFICIENT}}{\text{LOCAL SKIN-FRICTION COEFFICIENT FOR INSULATED WALL}}$$

$$\frac{\text{WALL TEMPERATURE}}{\text{INSULATED-WALL TEMPERATURE}}$$
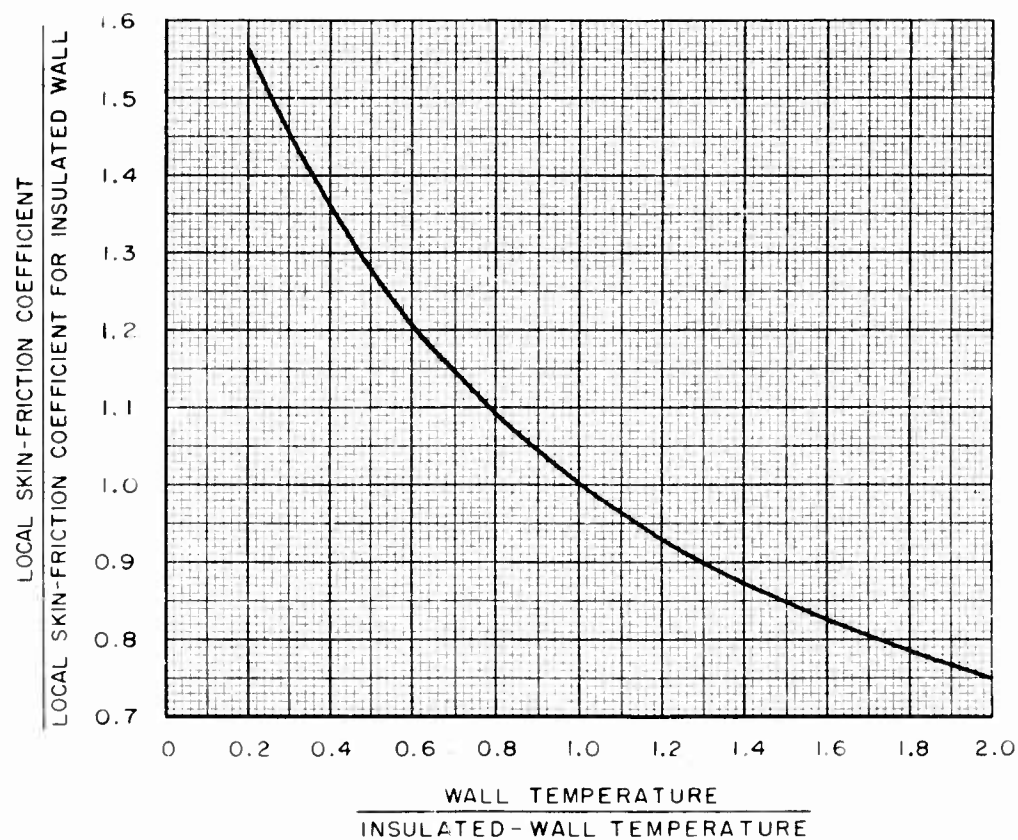
EFFECT OF WALL TEMPERATURE ON REDUCED
BOUNDARY LAYER SHAPE PARAMETER

N = 7

CURVES OBTAINED FROM TABLES OF REF. 41